Earth-Science Reviews 283 (2026) 105687

Contents lists available at ScienceDirect

Earth-Science Reviews

journal homepage: www.elsevier.com/locate/earscirev

Review Article

Deciphering spatiotemporal river-borne sediment signals at the eastern China margin since the last glaciation: Clay mineralogy insights from the Oujiang Delta and regional data synthesis

Yuhao Chen [a], Xing Jian [a,*], Pan Wang [b], Haowei Mei [a], Ling Wang [a,c], Hanjing Fu [a,d]

[a] State Key Laboratory of Marine Environmental Science, College of Ocean and Earth Sciences, Xiamen University, Xiamen 361102, PR China
[b] Institute of Hydrogeology and Environmental Geology, Chinese Academy of Geological Sciences, Xiamen 361024, PR China
[c] State Key Laboratory of Marine Geology, Tongji University, Shanghai 200092, PR China
[d] Xiamen Ocean Vocational College, Xiamen 361102, PR China

ARTICLE INFO

Keywords::
Eastern China
Holocene transgression
Last glaciation
Clay minerals
Climate proxy
Sediment source-to-sink system

ABSTRACT

Sedimentary records in dynamic land-sea transition zones are complicated by the interplays between terrestrial and marine processes. On the East Asian continental margin, the glacial–interglacial climate fluctuations have profoundly shaped sediment source-to-sink patterns by modulating sea level, monsoon intensity, and terrestrial output. Questions remain on the sediment source-to-sink system of the eastern China marginal seas since the last glacial period, with several key issues focusing on river-derived sediment contributions and the role of oceanic dynamics in sediment dispersal. To decode how the river-borne fine-grained sediment signals have evolved across these cycles, this study, from a clay mineralogy perspective, integrates a new drilling core from the Oujiang River delta with a comprehensive database of surface and core sediments from the eastern China marginal seas. Kaolinite/illite ratios and illite chemical indices indicate that clay mineral assemblages of the marginal sea sediments are primarily inherited and weathered minerals from sedimentary rocks. Crucially, we demonstrate that fluvial signals are not constant across glacial–interglacial timescales, recommending that modern fluvial sediments may be inappropriate analogues for ancient marine sediment provenance studies and for reliable paleoclimate reconstructions. During the middle-late Holocene high sea-level period, the increasing kaolinite/illite values among cores from the inner East China Sea shelf mud belt suggest an amplified signal from the Zhejiang-Fujian rivers, driven by attenuated coastal currents. Our findings emphasize an evident decoupling between clay-mineral-based weathering indication and local climate at continental margins. This contribution, based on an integrated database analysis of clay mineral and geochemical records, facilitates a better understanding of sedimentary processes in a unique marginal sea and offers significant implications for both modern and deep-time source-to-sink system investigations worldwide.

Contents

* Corresponding author.
E-mail address: xjian@xmu.edu.cn (X. Jian).

https://doi.org/10.1016/j.earscirev.2026.105687
Received 1 January 2026; Received in revised form 8 September 2026; Accepted 14 September 2026
Available online 20 September 2026

1. Introduction

The land-sea transition zone on the Earth's surface provides environmental and socio-economic services (Barbier et al., 2011; Barceló et al., 2023; Pittman and Armitage, 2016) and also represents the frontline of climate change and sea-level fluctuations (Barbier, 2015; Seibert et al., 2020). Its high sensitivity to natural and anthropogenic activities underscores the necessity to clarify the processes connecting land and sea, which is essential for a better understanding of material cycles at the Earth's surface and their controlling mechanisms (Barbier, 2015; Pittman and Armitage, 2016; Zielinski et al., 2022). From a sedimentological perspective, the coastal area is a critical pathway for terrestrial sediment transfer to the sea. Hydrodynamics—such as waves, tides, alongshore currents, and river plumes—shape sedimentary environments and coastal landforms (Grotzinger and Jordan, 2014). It remains a challenge to conduct long-term observations on the land and sea simultaneously in such volatile conditions (Weymer et al., 2022). Nevertheless, sedimentary records in coastal zones retain key paleoenvironmental information, enabling reconstructions of past climate, paleo-hydrology, and sediment provenance characteristics. It is well known that sedimentary sequences across river deltas, coastal plains and shelves were strongly influenced by sea level changes during the late Quaternary glacial–interglacial cycles (Grotzinger and Jordan, 2014; Wang et al., 2022b). Over the past ~500 ka, global sea level oscillated between ~120 m below present during glacial maxima and about 5–10 m above during interglacial periods, following a ~100-ka eccentricity cyclicity (Grant et al., 2014). The rapid transgression over the past 20 ka has led to progressive migration of the land-sea transition zone, with significant changes in coastal sedimentary records (Lambeck, 2004; Lambeck et al., 2014; Lewis et al., 2013; Li et al., 2014a).

The East Asian continental margin is characterized by a broad and flat shelf with water depths below 150 m across most of the area. The continental shelf has witnessed a gradual fall of sea level reaching ~135 m until the Last Glacial Maximum (LGM), followed by a rapid rise during the Last Glacial Termination (Denton et al., 2010; Lambeck, 2004; Lambeck and Chappell, 2001; Rohling et al., 2014). Most areas of the epicontinental seas in the East Asian margin today were exposed during the low sea level periods (Qiao et al., 2017; Wang et al., 2022b). The eastern China marginal seas (ECMS), as the most representative region of the East Asian continental margin, are the waters on the continental shelf surrounding the eastern China mainland, covering an area over 122×10^4 km^2 (Fig. 1). Large rivers originating from the Tibetan Plateau and mountainous small rivers located in southeastern China have supplied abundant terrigenous sediment to the area since the late Quaternary (Cao et al., 2023; Liu et al., 2024; Qiao et al., 2017; Xu et al., 2009). As a typical river-dominated continental margin, the ECMS represents a critical window for deciphering how river-borne sediment signals have evolved and for understanding the varying dynamics of the sediment source-to-sink systems under such sea-level fluctuations (Gao, 2013; Jin et al., 2023; Shi et al., 2024; Yang et al., 2015).

The ECMS can be divided into four regions from north to south: the Bohai Sea (BS), the Yellow Sea (YS), the East China Sea (ECS) and the Taiwan Strait. The elongated Okinawa Trough embraces the ECMS at the eastern edge of continental shelf, which is considered as one of the major ultimate sinks of terrigenous materials from the continent (Li et al., 2019). To the south, the South China Sea (SCS) connects to the ECMS via the Taiwan Strait. Under the influence of the ocean currents and the seafloor topography, several fine-grained sediment depocenters have formed in the marginal seas around eastern China, including the muddy belts along the Zhejiang-Fujian coast (the inner shelf of the ECS), the Bohai Sea, the Shandong Peninsula, the southwestern Cheju Island, and the Central Yellow Sea (Li et al., 2014a; Qiao et al., 2017; Zhang and Chu, 2018; Liang et al., 2015). Despite numerous studies that have investigated the sedimentary systems of the ECMS since the Late Pleistocene, key questions remain regarding their source-to-sink dynamics, particularly concerning the river-borne sediment outputs and the role of

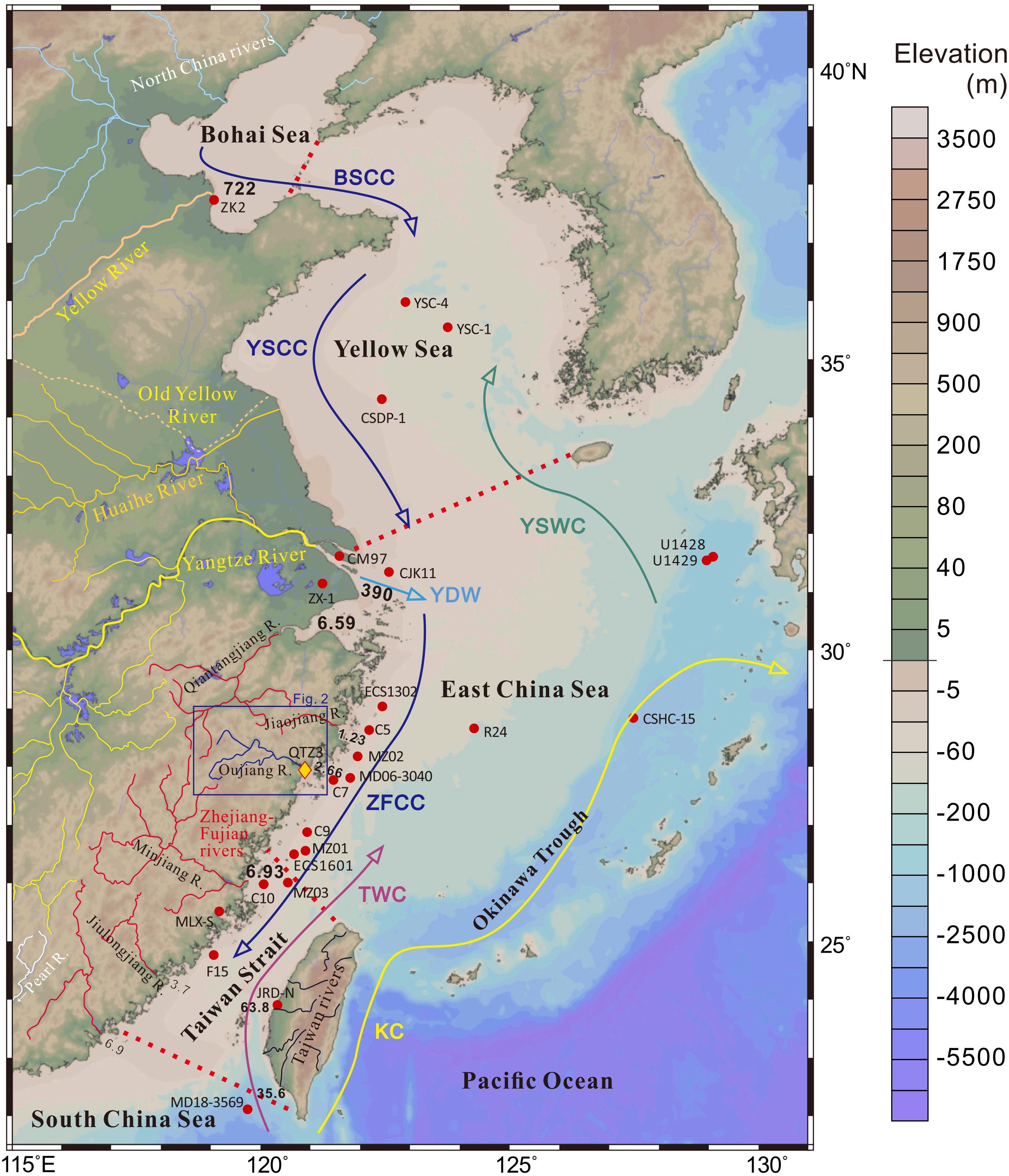

Fig. 1. Topographic map showing major river systems (including the Yangtze River, Yellow River, Huaihe River, Pearl River, Zhejiang-Fujian rivers, and Taiwan rivers) and major oceanic currents in eastern China. Numbers around the river estuaries indicate the annual sediment load (Mt/yr) (modified after Jian et al., 2020b; Zhang et al., 2022c; Zhao et al., 2018a). TWC: Taiwan Warm Current; KC: Kuroshio Current; ZFCC: Zhejiang-Fujian Coastal Current; YDW: Yangtze River Diluted Water; YSCC: Yellow Sea Coastal Current; YSWC: Yellow Sea Warm Current; BSCC: Bohai Sea Coastal Current. Locations of sediment core samples used in this study are shown in a yellow diamond (core QTZ3) and red dots (from previous studies).

marine processes in the formation and evolution of these fine-grained sediment depocenters.

2. Key issues and debates on the sediment source-to-sink system of the ECMS since the last glaciation

River systems in eastern China can be categorized into three types: large river systems (e.g., the Yangtze and Yellow Rivers), small mountainous rivers in tectonically active regions (e.g., Taiwan), and tidal-influenced mountainous rivers in subtropical SE China (Jian et al., 2020b; Li et al., 2025; Yang et al., 2014). One of the key issues in recent sedimentological investigations in eastern China is the discrimination of terrigenous sediment compositions and fluxes to the marginal seas, especially for those small-to-medium-scale mountainous river systems. It is widely believed that the Yangtze-derived fine-grained sediment has primarily contributed to the East China Sea (Jia et al., 2021; Liu et al., 2018a; Xu et al., 2012) and interacted with SE China's mountainous river estuaries (Gao, 2013; Guang et al., 2025; Qiu et al., 2024). Challenges remain in tracing sediment from mountainous rivers, whose output signals are highly varied under the influence of monsoon precipitation and typhoons (Bi et al., 2015; Jian et al., 2020b; Jian et al., 2020a; Su et al., 2018). Except for the seasonal and interannual variation of river discharge that regulating the sediment composition and flux, the increasing human activities since the late Holocene dramatically impacts on the sediment source-to-sink process (Li et al., 2018a; Lu et al., 2023; Zhang et al., 2022a). Furthermore, the shifts between terrestrial and marine sedimentary environments during glacial–interglacial cycles lead to the complexity of river-borne sediment preservation (Li et al., 2014a; Liu et al., 2023a; Xu et al., 2022). The modulation of ocean current intensity, tidal effects, and monsoon variations, on the sedimentary characteristics from the marginal seas is commonly underestimated (Qiao et al., 2017; Zhao et al., 2018c; Xue et al., 2018b). Whether and how the terrigenous sediment composition and flux have changed since the last glacial period remain controversial. The Oujiang River is an ideal window to reveal these issues as one of the mountainous rivers in SE China (Fig. 1). The Oujiang Delta, located about 400 km south to the Yangtze Delta, preserves a valuable sedimentary archive to identify the Oujiang-derived and Yangtze-derived provenance and weathering signals, and to clarify how these signals have evolved since the last glacial period.

The marine sedimentary processes in the ECMS are also controversial because of the spatial heterogeneity of the monsoon system (Chandana et al., 2018; Liu et al., 2017; Yu et al., 2017) and the poorly constrained evolution of regional ocean current circulation (Li et al., 2009; Yang et al., 2014; Yao et al., 2017). Specifically, how the interplay between ocean current intensity, monsoon dynamics, and global climate changes during the deglacial and post-glacial periods modulated the sedimentary characteristics of these marginal seas remains underestimated. Recent studies have fueled debates on three specific aspects: 1) the dispersion of Yangtze-derived sediments into small mountainous river catchments along the SE China coast, with controversial understandings on the fine-grained sediment transport mechanism (e.g., Guang et al., 2025; Li et al., 2025; Wang et al., 2024); 2) the formation of the mud belts in the ECMS, which mainly includes the views from contemporaneous large river discharges (Yangtze and Yellow River) or shelf sediments reworking (e.g., Gao and Collins, 2014; Xu et al., 2023a; Shi et al., 2021); and 3) the timing of the coastal current system establishment and its intensity evolution with the East Asian monsoon climate (e.g., Chen et al., 2017a; Shan et al., 2023; Zhao et al., 2018a).

As major detrital components in fine-grained terrestrial sediments, clay minerals have been widely utilized as a proxy to reveal fine-grained sediment provenance and to decode sediment source-to-sink systems (Dianto et al., 2019; Gingele et al., 2001; Liu et al., 2016a; Wang et al., 2020; Xu et al., 2012). Clay mineral assemblages in fine-grained sediments are indicators for silicate weathering (Fu et al., 2023; Li et al., 2020; Warr et al., 2024), but factors in parent rock lithology, transport pathway, and sediment reworking may distort the weathering intensity interpretations (Fagel, 2024; An et al., 2020). The independent selection of reference values of source clay mineral proxies in previous studies introduces contradictions when reconstructing regional sediment transport pathways (Liu et al., 2014, 2024; Mi et al., 2017). It is essential to unravel the variation and controlling factors of clay mineral proxies in sediments from various sedimentary environments across the ECMS, specifically concerning weathering intensity, sediment provenance, and distribution mechanisms from a broader spatial perspective.

In this contribution, we compile new and previously published clay mineral data (involving 5489 samples in total) from 19 sediment cores (2930 samples, including 59 samples from a new sediment core at the Oujiang Delta in SE China) and surface sediment samples (458 modern river sediment samples and 2101 marginal sea sediment samples) from the marginal seas along the eastern China. Additional elemental and Sr-Nd isotopic data from 8 sediment cores in this region are involved for comparative discussion with clay mineral proxies. The aims of this study are: 1) to review the temporal and spatial variation in clay minerals in sediments from the rivers and marginal seas within the eastern China region, 2) to investigate the controlling mechanisms of fine-grained sediment distribution and evolution in diverse sedimentary environments over the last glacial–interglacial cycle, and 3) to discuss the applicability of clay mineral proxies for indicating environmental signals in land-sea interaction zones.

3. Geological settings

3.1. Epicontinental seas in eastern China

Asia has the largest and highest continent on the modern planet. It collides with the Indian Plate on the southwest and is subducted by the Pacific Plate from the east. The shallow continental shelf around eastern China situates at the West Pacific Continental Margin and occupies most areas of the present-day ECMS region. The continental shelf has experienced complex deformation during the Cenozoic and exhibits an east-tilting topography that transformed the pre-Cenozoic highland into a continental margin basin (Suo et al., 2015). During the last glacial period, most of this area was exposed as coastal plains, allowing terrigenous sediments to be transported by rivers across the exposed shelf and delivered either to the shelf edge or directly into the Okinawa Trough (Li et al., 2014a; Shi et al., 2024).

The hydrodynamic framework of the ECMS is integrated by the monsoon, oceanic currents, tides, river runoff, and submarine topography. The currents of the ECMS show obvious variation in seasons (Liu et al., 2021b). Here, we simplify the circulation system in the ECMS into 1) currents along the coast of continent and 2) currents from the open ocean (Fig. 1). The northwesterly winter monsoon drives coastal currents to the south, which include the Bohai Sea Coastal Current (BSCC) in the Bohai Sea, the Yellow Sea Coastal Current (YSCC) in the Yellow Sea, the Zhejiang-Fujian Coastal Current (ZFCC) in the East China Sea (Liu et al., 2021b; Yang et al., 2014; Zhao et al., 2018a). The coastal currents flow along the coast of China from north to south in winter and weaken or even reverse in summer (Xu et al., 2023a; Zhang et al., 2022c). Input of fresh water from large rivers can also contribute to coastal currents, in which the most notable one is the Yangtze River Diluted Water (YDW, also named Changjiang Diluted Water) (Chen et al., 2017b; Yang et al., 2014). From the open ocean, the Kuroshio Current (KC) flows northward on the edge of the outer continental shelf, which forms the Taiwan Warm Current (TWC) on the western side of Taiwan Island. The Yellow Sea Warm Current (YSWC) flows into the Yellow Sea from the east and intrudes into the northern part during winter (Liu et al., 2018b). In general, the coastal currents flow southwards and the open-ocean currents flow northwards. The modern current system in the ECMS was formed after the sea level reached close to the present situation about 7–8 ka ago. The coastal currents are highly influenced by the intensity of the East Asian monsoon and the KC (Jian et al., 2000; Liu et al., 2016a; Zhao et al., 2018a). Some studies suggested that the ZFCC declined in the late Holocene (ca. ~4 ka) as the East Asian winter monsoon weakened (Chen et al., 2017a; Xiao et al., 2005). The ECMS is mostly controlled by semi-diurnal tides with high tidal ranges exceeding 4 m (Larsen et al., 1985; Liu et al., 2010a; Uehara and Saito, 2003). Modern tidal sand ridges are distributed widely within 30 m depth on the bottom of ECMS (Berné et al., 2002; Li et al., 2014a; Liu et al., 2007).

3.2. Modern sediment sources and river systems around the ECMS

The modern East Asia presents an east-tilting topography with major rivers flowing from west to east into the marginal seas (Wang, 2004). The Yangtze River (Changjiang River) and Yellow River (Huanghe River) are major contributors that transport terrigenous sediments to the ECMS (Gao, 2013; Qiao et al., 2017). The Yangtze River originates on the Tibet Plateau and extends 6300 km eastward to the ECMS, with annual discharges at 900 km^3 (Milliman and Farnsworth, 2011). The Yangtze River delivers 390 Mt of sediment to the ECS annually, of which about 50% deposits accumulate within the estuarine area (Qiao et al., 2017). In the upper reach, the drainage is covered by Mesozoic rocks with subordinate upper Paleozoic carbonate rocks and Cenozoic strata. The middle and lower reaches are mainly covered by Paleozoic carbonate rocks, Mesozoic intermediate-acidic igneous rocks, and Quaternary sedimentary rocks, together with metamorphic rocks (Bi et al., 2017; Liu et al., 2018c). The current water discharge and sediment fluxes are highly influenced by monsoonal climate and human activities (Wang et al., 2008). The deltaic sediments formed in glaciation are left on the East China Sea Shelf and retransported by strong tidal currents.

Although the runoff volume and discharge area of the Yellow River are lower than those of the Yangtze River, the sediment content of the Yellow River reaches the highest in the world. The Yellow River delivers 722 Mt/yr of sediment into the BS, which has decreased significantly (260 Mt/yr for 1996–2000 average, Liu et al., 2012a) since the second half of the 20th century due to the runoff yield and precipitation decrease, vegetation preservation and water conservation (Li et al., 2017; Qiao et al., 2017; Tian et al., 2021). The drainage mainly consists of Archean metamorphic rocks, Paleozoic carbonates, and Cenozoic clastic rocks (Pang et al., 2018). Both the modern and ancient Yellow River have similar catchment lithology and over 90% of sediment loads from the Loess Plateau (Huang et al., 2019). Due to the high sediment loads and the high sedimentation rates at the lower reach of the Yellow River, the channel and the estuary have changed frequently throughout history (Zhang et al., 2018). The continuous diversion of the Yellow River at its lower reach provides considerable terrestrial materials to the BS and the YS regions.

The drainage of the Huaihe River is located between the Yangtze and Yellow Rivers (Fig. 1). Its main channel marks the boundary between the northern and southern climates of China (Zhang et al., 2011; Zhang et al., 2016). The Archean to Paleozoic rocks are exposed in the mountainous areas of the western and southern parts of the basin, including various igneous rocks and metamorphic rocks. Neogene and Quaternary sediments are distributed over the large plains in the eastern part of the watershed (Zhang et al., 2011b). Climate changes and human activities caused changes in sediment provenance from the downstream Huaihe River and in the YS (An et al., 2020; Zhang et al., 2018). The ancient Yellow River flows into the southern YS by taking the channel of the Huaihe River during 1128–1855 AD, resulting in rapid sedimentation at the coastal plain of northern Jiangsu Province in the late Holocene (Chen et al., 2012; Gao, 2013). Today, artificial irrigation canals are built on the coastal plain to bear a portion of the water volume. The natural channel of the Huaihe River integrates into the Yangtze River and eventually flows into the ECS (Zhang et al., 2011).

Mountainous rivers around the coast of Zhejiang and Fujian Provinces (e.g., the Qiantangjiang, Oujiang, Minjiang, Jiulongjiang Rivers, etc.) are located in tectonically stable settings in the hilly areas of southeastern China under the influence of the East Asian monsoon. In comparison to the Yangtze, Yellow, and Huaihe Rivers, the runoff and sediment discharge of the Zhejiang-Fujian (also called Zhe-Min) rivers are much lower (Milliman and Farnsworth, 2011). Yanshanian volcanic-sedimentary strata are widely distributed in the Zhejiang-Fujian region, which are located in the eastern part of the Cathaysia Block. The proportion of volcanic-volcaniclastic rocks decreases and intrusive rocks increase southward (Yang et al., 2021; Zhou et al., 2006). Mesozoic and older sedimentary strata are scattered in the area and can be dominant in the basins of particular small rivers or tributaries (Wang et al., 2024). Sediment from the small and medium-sized Zhejiang-Fujian rivers is distributed in a limited area close to the coast (Xu et al., 2023b; Xue et al., 2018a). The Zhejiang-Fujian rivers are sensitive to human activities (dam construction, agricultural plantations, urbanization, etc.) due to their small catchment and undulating topography (Chen et al., 2017b). In addition, the intensity of sediment input by the Zhejiang-Fujian rivers remains controversial due to seasonal changes caused by monsoon climate and frequent typhoons (Jian et al., 2020a; Su et al., 2018; Wu et al., 2023). Although the river basins are small, the Zhejiang-Fujian region has large number of rivers and shows significant

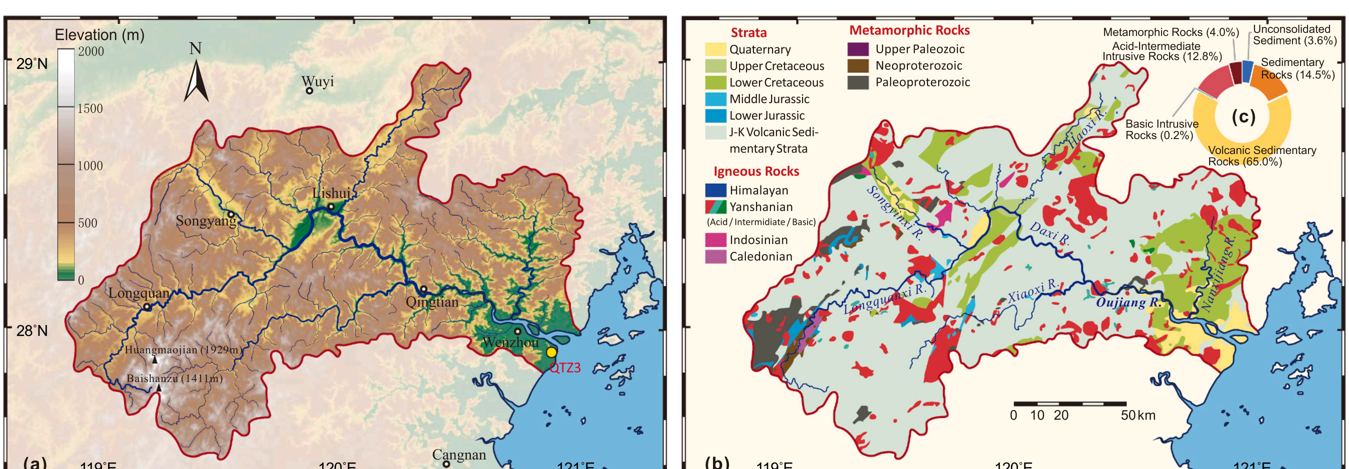

Fig. 2. Topographic map (a) and geologic map (b) of the Oujiang River basin. The Oujiang River watershed (red line) was delimited according to local water conservancy records. The location of the map is shown in Fig. 1. Compositions of each kind of lithology (area %) in the basin (c) are calculated based on area statistics. The basement of the Oujiang River basin is mainly Jurassic-Cretaceous volcanic-sedimentary strata (65%), followed by sedimentary rocks (15%) and igneous rocks (13%).

seasonal variations. As a result, these rivers are considered important sources for the ECMS sediment.

Rivers on the Taiwan Island (e.g., Zhuoshui, Gaoping, Lanyang, Tsengwen Rivers) contribute to the ECMS by transporting sediments into the Taiwan Strait. Previous studies have estimated that about 85% of the Taiwan rivers-derived fine-grained sediments left the Taiwan Strait, which either outflux southward to the northern SCS or transport northward to the Okinawa Trough (Kao et al., 2008; Liu et al., 2008a; Zheng et al., 2015). Taiwan is a part of the collision orogen bounded by subduction zones, which is therefore located in a tectonic-active region (Garzanti et al., 2023; Zhang et al., 2022b). The bedrock is dominated by Cenozoic sedimentary and metasedimentary rocks (Huang et al., 2012). There are 151 rivers on the island, of which the largest one, the Zhuoshui River, is only about 190 km in length (Kao et al., 2008; Li et al., 2023). The Taiwan rivers mostly originate from the Central Range area with elevations approaching 4000 m (Wang et al., 2016). The active tectonic background and high gradient of the river channel lead to fast erosion and rapid transport, resulting in extremely high sediment load of the Taiwan rivers (Kao et al., 2008). For example, the sediment load of the Gaoping River, another representative river in Taiwan, has high variation from 30.37 Mt/yr (2001–2020 average, Sun et al., 2024b) to 70.8 Mt/yr (1999–2004 average, Wang et al., 2022a). The sediment load is one order of magnitude higher than that of the Minjiang River (~6.9 Mt/yr), the largest one among the Zhejiang-Fujian rivers (Wang et al., 2024).

3.3. *The Oujiang River: an example of the strongly tide-dominated Zhejiang-Fujian rivers*

The Oujiang River is one of the most typical mountainous river systems on mainland China, yet its downstream and estuary areas are significantly affected by external sediment from the ECS, which is primarily transported landward via tidal processes (Guang et al., 2025; Xue et al., 2018a; Wu, 2019). Its estuary is under a macrotidal environment with a tidal range exceeds 4 m on average (7 m in maximum) at the river mouth and a tidal reach extending 83 km upstream to Qingtian County (Fig. 2) (Zhejiang Water Resources Department, 2020). Therefore, it is an ideal research target for investigating how the Yangtze-derived sediment transported by the coastal current interact with sediment from mountainous rivers.

The Oujiang River is the second-longest river in Zhejiang Province with a drainage area of 18165 km^2 and a mainstream length of 384 km (Ding et al., 2019; Wu et al., 2019; Xue et al., 2018a). The watershed of the Oujiang River mainly sits 500–1500 m above sea level and is high in the southwest and low in the east (Shang et al., 2018). The Asian monsoonal climate characterizes the catchment, resulting in seasonally variable rainfall reaching 1746 mm per year that concentrates in the summer, and a mean temperature of about 19 °C (Bi et al., 2015). As a

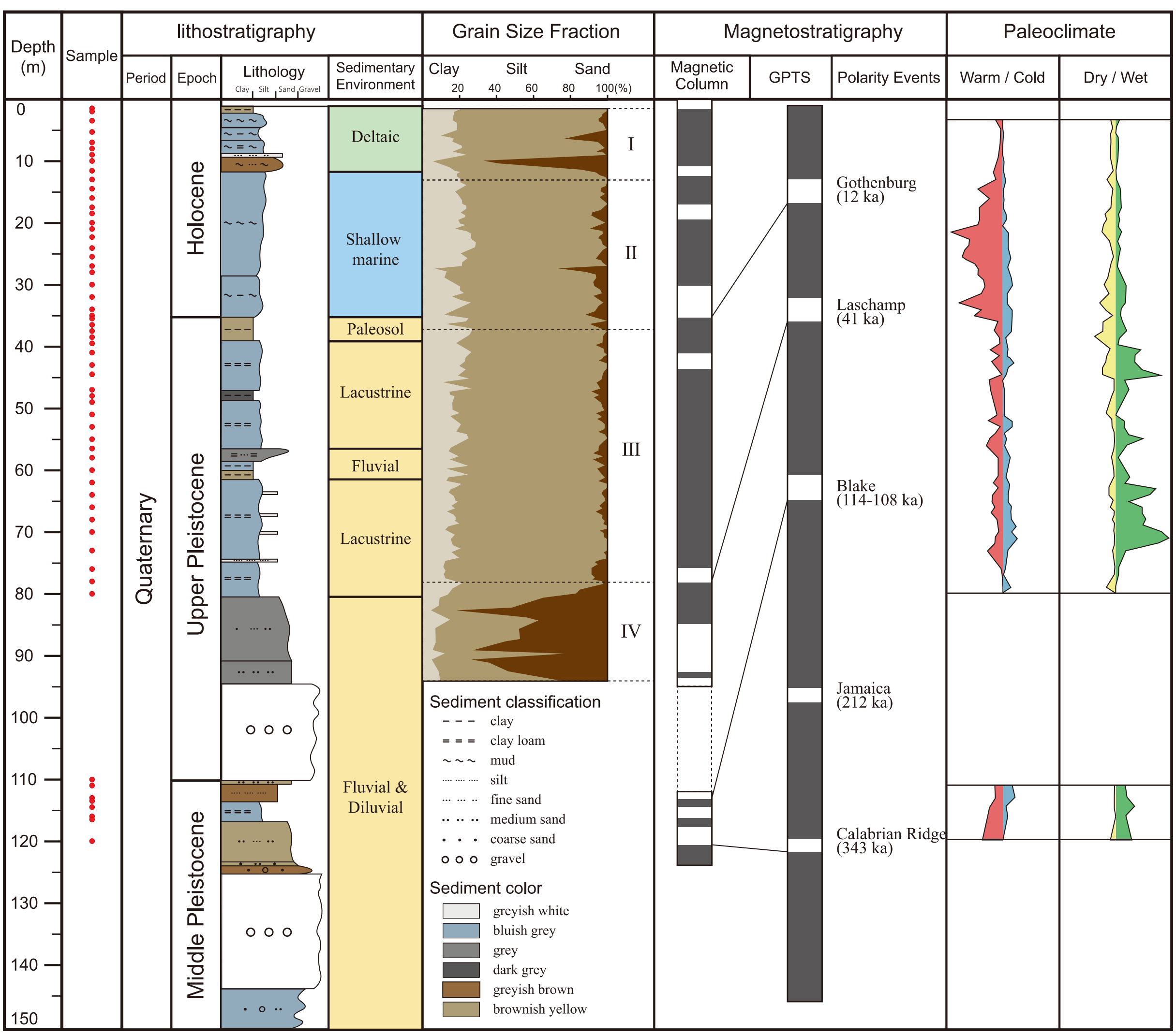

Fig. 3. Sampling position, down-core changes of lithostratigraphy, grain size fraction, paleoclimate proxy, and magneto-stratigraphy in core QTZ3. Modified after Wu (2019).

result, the Oujiang River has an asymmetrical water discharge at 18.692 km^3 per year, in which 2/3 is concentrated from May to September, and a sediment load at 266.5 kt per year (Zhejiang Water Resources Department, 2020). Typhoons, monsoon variation, and human activities increase interannual variation of the runoff and sediment load of the Oujiang River (Bi et al., 2015; Wei et al., 2025).

The Oujiang River basin is located in the eastern Cathaysia Block and is predominantly covered by late Mesozoic volcanic-intrusive complexes, with volcanic-sedimentary rocks and granitic rocks occupying 65.0% and 12.8% of the drainage area, respectively (Fig. 2). The Mesozoic volcanic eruption products in the area are mainly felsic pyroclastic rocks and rhyolitic lava flows (Yan et al., 2016; Liu et al., 2019). Mafic rocks like basalt, gabbro are relatively rare in the river basin (Jia et al., 2020). Only a few Mesozoic and Cenozoic mafic intrusions are exposed, taking up less than 0.2% of the basin. Metamorphic rocks are distributed in the western part of the upstream regions, occupying 4% of the river basin. In the middle and eastern part of the basin, about 14.5% and 3.6% are Mesozoic sedimentary strata and unconsolidated Quaternary sediments, respectively. In response to this lithological composition, the detrital zircon U-Pb ages from modern Oujiang River sediments shows a prominent peak at 130–150 Ma and a minor peak at 1850 Ma, indicating the contribution of Yanshanian igneous rocks and the ancient Paleoproterozoic bedrocks, respectively (Xu et al., 2007; Zhang et al., 2017). The heavy minerals in sediments from the Oujiang River are mainly composed of hornblende, magnetite, epidote and micas (Ma et al., 2018; Song et al., 2018). Clay minerals in the river sediment are predominated by illite, followed by kaolinite and chlorite, with scarce smectite content (Guang et al., 2025; Xue et al., 2018a).

Previous investigations indicate that the coastal plain and the shallow sea around the Wenzhou district have ~150 m thick unconsolidated Quaternary sediment above the granitic bedrock (Wu et al., 2017; Zhang, 1991; Yang et al., 2022). The Lower Pleistocene strata are generally lacking in sedimentary records therein. The littoral deposit during the Middle Pleistocene was buried 100–120 m below the surface. The strata since the Upper Pleistocene have been well preserved and have recorded the sedimentary environment evolution due to climate-related sea level change with 50–100 m of thickness (Fan et al., 2019; Wu et al., 2019; Zhang, 1991; Yuan et al., 2023). The Holocene strata have several transgression-regression sequences that are affected by the eustatic changes. A layer of stiff clay was found at ~30 m below the sea level, which is supported by ^{14}C chronology as a paleosol formed during the Pleistocene-Holocene boundary (Fan et al., 2019; Shang et al., 2018; Zhang et al., 2012).

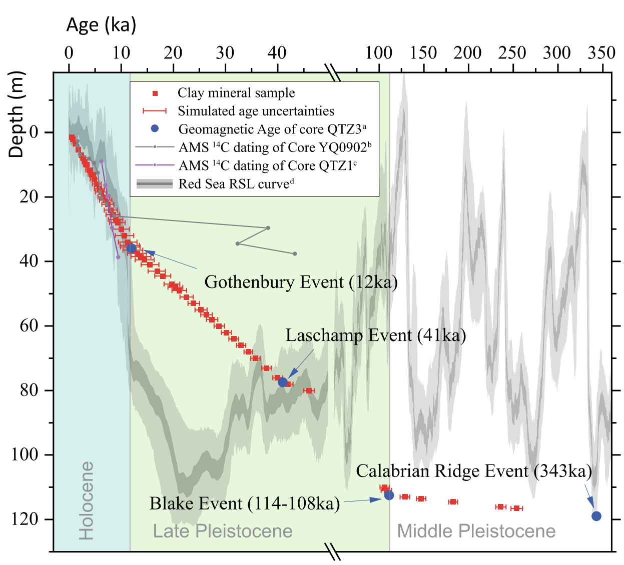

Fig. 4. Age model for the sediment core QTZ3 based on the magnetostratigraphic correlation, compared with AMS ^{14}C dating samples (YQ0902 and QTZ1) from adjacent areas at the Oujiang River delta and relative sea level (RSL) change of the Red Sea in the last 500 ka. The interpolated age uncertainty ranges are simulated by a Monte Carlo sensitivity analysis. [a] data from Wu (2019). [b] data from Shang et al. (2018). [c] data from Li et al. (2024). [d] data from Grant et al. (2014). Note that the dating sample depth is the location in cores, and is not normalized to real elevation.

4. Materials and methods

4.1. Core sediment samples and clay mineral analysis

4.1.1. Drilling core sediment samples from the Oujiang Delta

The sediment core QTZ3 (27°52′41.3″ N, 120°50′27.4″ E) was drilled in 2017 on the coastal plain at the southern side of the Oujiang Delta in Wenzhou, Zhejiang Province (Figs. 1 & 2). Detailed descriptions of lithology, color, and texture were recorded in a previous study (Wu, 2019). The paleoenvironmental reconstruction based on grain size, geomagnetic, palynologic, and microfossil analysis was previously described by Wu (2019) and is summarized in Fig. 3. Most of the core is composed of bluish-grey mud, interspersed with a few layers containing coarse sediments. Thick tuffaceous gravel layers at the bottom of the core were inferred to be mountainous flood deposits. Magnetostratigraphic analysis was conducted previously that can correlate with the geomagnetic polarity time scale (GPTS): the specific reversals at 32–36 m, 77.5 m, 112.5 m, and 119 m correspond to the Gothenburg event (12 ka), the Laschamp event (41 ka), the Blake event (114–108 ka), and the Calabrian Ridge event (343 ka), respectively (Figs. 3 & 4). The gravel layers in the lower part were absent for geomagnetic analysis in the previous study (Wu, 2019). According to AMS ^{14}C dating of two adjacent sediment cores on the coastal plain, QTZ1 (28°0′11.2″ N, 120°56′58.6″ E) (Li et al., 2024b) and YQ0902 (27°55′27″ N, 120°50′35″ E) (Shang et al., 2018), the uppermost ~40 m of the coastal plain preserved sediments from the Holocene. Therefore, we propose that the sediment above 80 m in core QTZ3 has a relatively reliable age model since 40 ka. Due to the errors of the specific geomagnetic events ages adopted, a Monte Carlo sensitivity analysis on the age model was conducted to evaluate the age uncertainty. A randomly perturbed age within a given standard deviation from the GPTS (Ogg, 2020) was estimated for each control points and the age–depth curve was established via repeated linear interpolation for 1000 times (Fig. 4). This allows us to assess whether the observed clay mineral trends during critical climatic transitions are robust against age uncertainties.

4.1.2. Clay mineralogy analysis

A total of 59 sediment samples were collected at 0.5–1.5 m intervals in the core QTZ3 for clay mineral analysis. The treatment procedure for X-ray diffraction (XRD) analysis is the same as reported in a previous study (Mei et al., 2021). Clay fractions (< 2 μm) in each sediment sample were separated based on the Stokes' setting principle. Thereafter, organic matters and carbonates were removed by 10% hydrogen peroxide and 1 mol/L acetic acid, respectively, under a 60°C water bath condition. After cleaning and concentrating with deionized water, clay samples were transferred to quartz slides and dried at room temperature for natural air-dried sheets (N). After an XRD test on the N sheet, the same slide underwent saturated ethylene glycol vapour treatment for 48h at room temperature for the EG sheet. A Rigaku Ultima-IV X-ray diffractometer was used for the XRD scanning at Xiamen University. Each slide was continuously scanned under 40 kV and 30 mA, with scanning degree range from 3° to 35°, step width of 0.02°, and scanning speeds at 4°/min conditions.

The MDI Jade 6 software was used for clay minerals quantitative analysis. According to the calculating method by Biscaye (1965), relative percentages of smectite, illite, kaolinite, and chlorite were determined using ratios of (001) peak series of their basal reflections according to the XRD diffractogram of EG sheets, and were weighted by empirically estimated factors (Mei et al., 2021). Furthermore, the full width at half maximum of the illite peak at 10 Å and the ratio of peak area at 5 Å/10 Å were calculated to obtain the Kübler index (KI) and the chemical index (CI) of illite, respectively (Esquevin, 1969; Kübler and Jaboyedoff, 2000). The KI reflects the sharpness of the diffraction peak shape on the XRD spectrum, which is indicative of the degree of illite's crystallization (Kübler and Jaboyedoff, 2000; Wang et al., 2015a). The CI of illite is defined by the ratio of the illite (002) peak at 5 Å and the illite (001) peak at 10 Å, representing the long-range order in the vertical direction of the illite structure.

4.2. Compilation of previously reported clay mineral data from the eastern China margin

4.2.1. Data filtration and standardized calibration

Previously published clay mineral composition data of sediments from the ECMS and the surrounding regions were compiled for further comparative analysis. The database encompasses samples from surface sediments, suspended sediments, and sediment cores. The riverbed sediments were also taken into compilation as analogues of river-borne sediment sources within the eastern China margin. For modern sediments, the location of each sample was labeled and used as the classification basis, documenting the sampling river, sea region, and the longitude and latitude of sampling sites. For core sediments, the sampling position (depth in the core) was verified and correlated with the age of the sample. Cores with too short (<1 ka) or too long (>1 Ma) time spans are not included in this study because the time resolution of samples is expected to be controlled within 5 ka. Interpolated ages were calculated based on the chronology model by AMS ^{14}C or OSL dating data. To keep the consistency in the data for comparison with our results, data were required to calculate the clay mineral proxies using the same method as in this study. Data that were not calculated from the peak area in XRD diffractogram of EG sheets were excluded from our database.

The clay mineral datasets include six parameters: the relative content of smectite, illite, kaolinite, and chlorite, alongside the values of CI and KI. The compositions of the four clay minerals were recalculated for those cases where the Biscaye's empirical weighing factors were not used. Since the raw XRD spectra were not provided in most published studies, the originally reported relative percentages of each clay mineral were used to recalculate the final clay mineral content (CM_{cal}):

$$CM_{cal} = \frac{f_{mineral} \times P_{mineral}}{\sum (f_{mineral} \times P_{mineral})} \times 100\%$$

where the f represents the Biscaye (1965) empirical factors ($f_{smectite} = 1$, $f_{illite} = 4$, $f_{kaolinite} = 2$, and $f_{chlorite} = 2$), P indicates uncalibrated percentage of each four clay minerals ($P_{smectite} + P_{illite} + P_{kaolinite} + P_{chlorite} = 100\%$). Previous studies generally report an analytical uncertainty of 5–10% (e.g., Dou et al., 2014; Li et al., 2014b; Liu et al., 2019a) for the relative content of each clay mineral. The numerical error after calibration still remains within ~10%. The CI and KI values of compiled data were strictly required to be defined as the 5 Å/10 Å peak area ratio and the full width at half maximum at 10 Å, respectively. Otherwise, it was regarded as irrelevant indicator data and would be systematically excluded from the database.

In cases where numerical data were unavailable in the published documents, we extracted the sample coordinates and clay minerals manually by correlating datapoints with the axes on the published diagrams using the GetData software. Due to the limited resolution of these figures, the summation of extracted clay mineral contents may not be exactly 100%. Cross-validation between the originally published data and manually-obtained values from the same documents demonstrates that this extraction method introduces a negligible error of <1% for core samples and 2%–5% for surface sediments. These data are only used for plotting in spatial or temporal distribution trends and are highlighted in the appendix materials. Although these treatments would introduce larger errors than the original data, the variation trend can still be preserved and enhances the richness of the database.

4.2.2. Descriptions of the clay mineral database and data sources

Data of 458 modern river sediment samples and 1480 marginal sea sediment samples are compiled to demonstrate the modern framework of clay mineral distributions; additional 621 samples were obtained from the published spatial distribution isograms without raw data. A total of 19 cores with clay mineral composition data are collected from 15 literatures, among which the CI and KI values are reported in 10 cores from 6 literatures (Table 1, Appendix Table S4). Data from 7 cores (MZ01 (Liu et al., 2010b), F15 (Chen et al., 2017b), YSC-1, YSC-4 (Li et al., 2014b), ZX-1 (Wang et al., 2006), ECS-1601 (Cong et al., 2021), R24 (Jia et al., 2012) are obtained manually from figures since no available data are provided in the source literature (Fig. 1, Table 4).

The dataset of river sediment samples comprises riverbed and suspended sediment from the catchment of the Yangtze River, Yellow River, Huaihe River, and medium-to-small-scale rivers at Zhejiang, Fujian,

Table 1
Brief information for compiled core data in this study.

Sample name	Region	Longitude (°E)	Latitude (°N)	Elevation (m)	Length (m)	Reference
QTZ3	Oujiang River, ECS	120°50′27.4″	27°52′41.3″	–	150	this study
MZ01	ECS mud	120°50′56.4″	26°32′49.2″	−64.7	2.96	Liu et al., 2010b
MZ02	ECS mud	121°53′24″	28°10′7.8″	−32.4	35.3	Liu et al., 2014
MZ03	ECS mud	120°30′00″	26°00′00″	−65	25.5	Shan et al., 2023
C5	ECS mud	122°17′59.4″	28°44′16.8″	−40	5.3	Zhang et al., 2022c
C7	ECS mud	121°42′11.4″	27°45′46.8″	−40	5.15	Zhang et al., 2022c
C9	ECS mud	120°54′00″	26°58′44.4″	−40	7.35	Zhang et al., 2022c
C10	ECS mud	119°52′12.6″	25°49′58.8″	−25	5.3	Zhang et al., 2022c
ECS1302	ECS mud	122°22′17.36″	29°01′28.29″	−38.2	60.9	Liu et al., 2023a
ECS1601	ECS mud	120°39′36″	26°50′24″	−38.5	90	Cong et al., 2021
R24	ECS tidal sand	124°11′00″	28°39′00″	−81	10.1	Jia et al., 2012
CSHC-15	Okinawa Trough	127°20′19.8″	28°49′54″	−940	60	Shi et al., 2024
U1429	Okinawa Trough	128°59′51.00″	31°37′2.40″	−732	200	Zhao et al., 2017
YSC-1	Central YS mud	123°40′00″	35°32′00″	−76.2	4.37	Li et al., 2014b
YSC-4	Central YS mud	122°50′00″	35°58′00″	−69.8	4.61	Li et al., 2014b
CSDP-1	Western South Yellow Sea	122°22′00″	34°18′00″	−52.5	300	Zhang et al., 2019
ZX-1	Yangtze Delta	121°11′02″	31°08′01″	2.67	20	Wang et al., 2006
CJK11	Yangtze Estuary, ECS	122°27′00″	31°19′48″	−21	72.2	Xu et al., 2024
JRD-N	Zhuoshui River, Taiwan	120°18′09″	23°54′10.2″	1.79	98	Zhang et al., 2022b
F15	Taiwan Strait	119°02′06″	24°45′46.44″	−47.1	2.5	Chen et al., 2017a
MD18-3569	Northern SCS	119°49′14.4″	22°9′18″	−1320	40.08	Bertaz et al., 2024

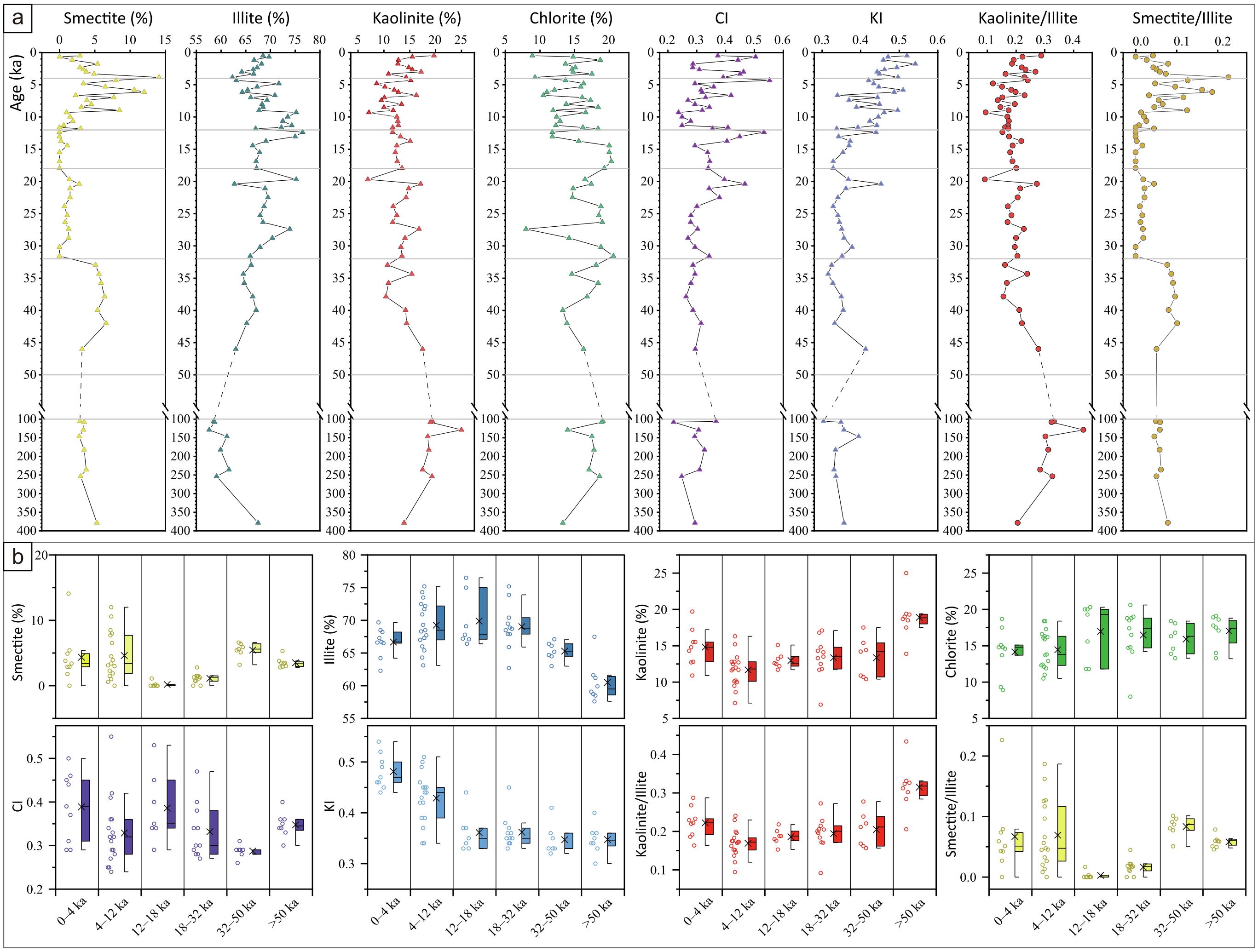

Fig. 5. a) Down core distribution and b) box plots of clay mineral contents (%), illite chemical index (CI), illite crystallinity (KI), kaolinite/illite, and smectite/illite for analyzed samples in core QTZ3. The X mark in the box plot indicates the average value in the corresponding time intervals.

Table 2
Average of clay mineral compositions of the core QTZ3 in each sedimentary stage

Depth (m)	Time period (ka)	Sedimentary environment	Smectite (%)	Illite (%)	Kaolinite (%)	Chlorite (%)	Illite CI	Illite KI	Sample number
0–12	Late Holocene (0–4)	transitional	3.2	67.2	14.9	14.8	0.39	0.48	8
12–36	Early and Middle Holocene (4–12)	marine	5.1	68.9	11.8	14.2	0.33	0.43	18
36–45	Deglaciation (12–18)	terrestrial	0.2	69.9	13.0	17.0	0.39	0.36	7
45–65	LGM (18–32)	terrestrial	1.1	69.0	13.4	16.5	0.33	0.36	11
65–80	Interstadial (32–50)	terrestrial	5.5	65.3	13.3	15.9	0.29	0.35	7
110–120	Middle Pleistocene (> 50)	terrestrial	3.5	60.5	18.9	17.0	0.30	0.35	8

Taiwan, and Bohai-rimming regions (Table 3, Appendix Table S2). Seafloor surface samples are classified into 5 categories (i.e., BS, YS, ECS, SCS and the Taiwan Strait) based on their distribution and geographical regions of the seas (Table 3, Appendix Table S3). The locations of compiled surface samples and core samples are mainly concentrated in the muddy depocenters of the ECMS (Tables 1 & 3). Among them, the core MZ03 lacks a reasonable age correlation and is not used for temporal analysis in this study (Shan et al., 2023). Typical cores from the Okinawa Trough (CSHC-15, U1429) and the northern SCS (MD18-3569) are involved in this study as a response of terminal sediment outputs to the environmental change within the ECMS (Fig. 1) (Bertaz et al., 2024; Shi et al., 2024; Zhao et al., 2017).

5. Clay mineralogy of river-borne sediments in the ECMS and the surrounding regions

5.1. Clay mineral variation in the core sediments from the Oujiang Delta

The down-core clay mineral compositions of the core QTZ3 are shown in Fig. 5, and detailed data are shown in Appendix Table S1. Illite shows high proportions in the core (58%–76%). Kaolinite and chlorite are comparatively low with proportions ranging 7%–25% and 8%–21%, respectively. Smectite is scarce in most samples (0–14%) and 10 of 59 samples failed to detect smectite in clay minerals. The KI value ranges between 0.30–0.54, exhibiting an increasing trend from the bottom to

Table 3
Average of clay mineral compositions of modern sediments.

Sample region	Smectite %	Illite %	Kaolinite %	Chlorite %	Illite CI	Illite KI	Sample number	Reference
Yangtze River	3.0	69.4	13.8	13.8	0.49	0.52	140	An et al., 2020; He et al., 2013; Wang et al., 2021; Zhao et al., 2018c
Yellow River	19.0	60.7	6.8	13.4	0.33	0.32	46	An et al., 2020; Pang et al., 2018; Zhang et al., 2019
North China Rivers	21.1	54.8	13.4	11.0	–	0.46	26	Dou et al., 2014
Huaihe River	13.1	56.4	17.1	13.3	–	–	21	An et al., 2020; Zhang et al., 2011
Zhejiang Rivers	9.1	57.6	13.8	19.5	–	–	31	Liu et al., 2016b; Xue et al., 2018a; Yang, 1995
Fujian Rivers	0.5	30.8	49.1	19.6	0.62	0.39	117	Mei et al., 2021; Liu et al., 2016b
Taiwan Rivers	0.8	72.9	1.8	24.5	0.35	0.16	73	Liu et al., 2008a; Liu et al., 2010c; Liu et al., 2016b; Wang et al., 2016
Bohai Sea (BS)	15.7	58.1	13.5	12.7	–	0.40	131	Dou et al., 2014; Ma et al., 2010
Yellow Sea (YS)	2.8	66.8	12.4	18.0	–	0.21	187	Ma et al., 2010; Cho et al., 2012; Koo et al., 2018; Rho, 2015
East China Sea (ECS)	7.1	63.9	12.1	17.0	–	0.51	214	Liu et al., 2006; Liu et al., 2016b; Zhao et al., 2018c; Ma et al., 2010; Youn et al., 2007; Xue et al., 2018a; Xu et al., 2009; Zhou et al., 2003
Taiwan Strait	5.0	69.1	8.5	17.4	–	–	696	Li et al., 2021; Liu et al., 2016b; Xu et al., 2009; Ma et al., 2010
NE South China Sea	1.8	71.0	3.8	23.4	0.35	0.17	186	Liu et al., 2008b; Liu et al., 2010c; Liu et al., 2016b; Wang et al., 2016; Xu et al., 2009; Ma et al., 2010
NW South China Sea	18.7	47.3	19.7	14.2	–	–	62	Liu et al., 2016b

Note: Extracted clay mineral data from published diagrams are not involved in the table.

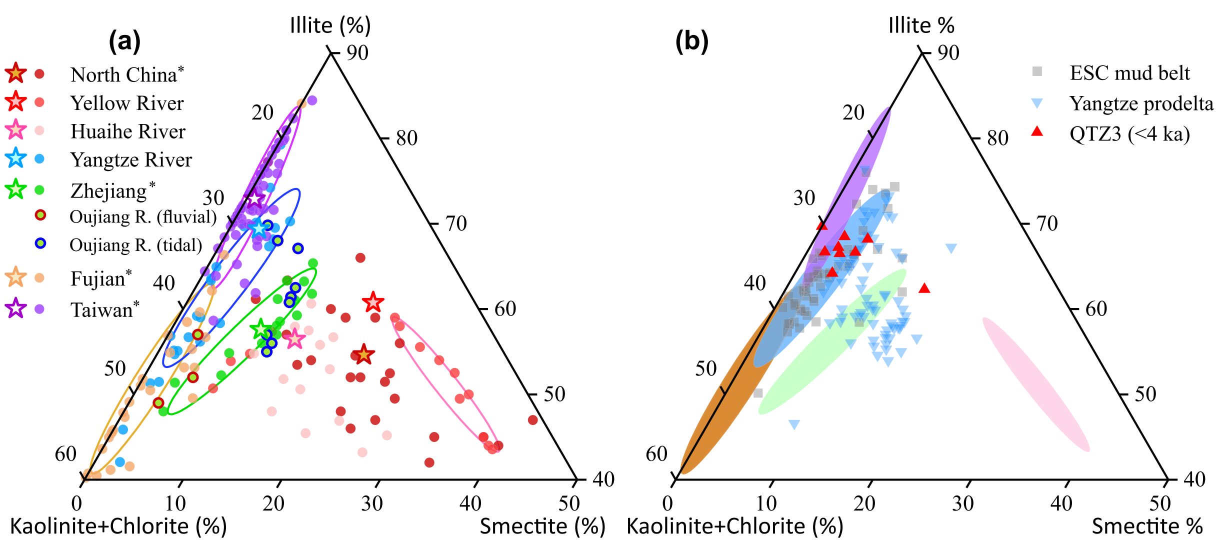

Fig. 6. Ternary plots of clay mineral assemblages: a) modern sediment samples from the major rivers around the ECMS. Pentacles represent the average assemblage of the whole drainage (* multiple rivers in the region). Points from the middle and lower reaches of the Yangtze, Yellow, and Huaihe Rivers are selected for mapping. Note the range of axes, and some data fall outside the figure. b) core QTZ3 (the uppermost 10 m) and sediment from the subaqueous Yangtze Estuary and ECS mud belt.

the top in the core. The CI value ranges between 0.22–0.55 and has higher variation in the uppermost 40 m (~15 ka).

The clay mineral compositions change significantly among different time periods (Table 2, Fig. 5). The Monte Carlo simulation on age uncertainty shows a significant deviation for samples ranging from 20 to 40 m (Fig. 4). Lithostratigraphy correlation and the dating data of adjacent cores indicated the strata above 36 m was basically formed since the Holocene. Significant transition periods of clay mineral assemblages are distinguished by utilizing the linear interpolated ages (Table 2). Smectite proportion shows the minimum average in the last glacial period (0.2%), and shows high values and high variation during the Holocene (4.5%) with the maximum of 14% at about 4 ka. Illite proportion increases to 69.9% during the Late Pleistocene from 60.5% in the Middle Pleistocene, and decreases to 68.4% in the Holocene. The proportion of kaolinite reaches the highest average in the Middle Pleistocene (18.9%), decreases during the Late Pleistocene (13%), and increases to ~20% in modern time. Chlorite has the highest proportion in the Middle Pleistocene (17.0%), the lowest proportion in the Holocene (14.4%), and relatively high proportion during deglaciation (17.0%).

5.2. Clay mineral composition and distribution of sediment from the ECMS area

5.2.1. The modern framework of clay mineral distributions

The clay mineral compositions of the present river and shelf sediments are shown in Table 3, and Figs. 6 and 7. Detailed information is given in Appendix Tables S2 and S3. The clay mineral assemblages of the Yangtze River basin are dominated by illite (69.4%), with less abundant chlorite (13.8%) and kaolinite (13.8%), and scarce smectite (3.0%). The CI and KI of illite in the Yangtze River basin are 0.49 and 0.52, respectively. Compared with the Yangtze River sediments, the clay mineral assemblage of the Yellow River basin features higher smectite content (19.0%), lower illite (60.7%) and kaolinite contents (6.8%), and similar chlorite content (13.4%). The CI and KI of illite in the Yellow River basin are 0.33 and 0.32, respectively. The clay mineral

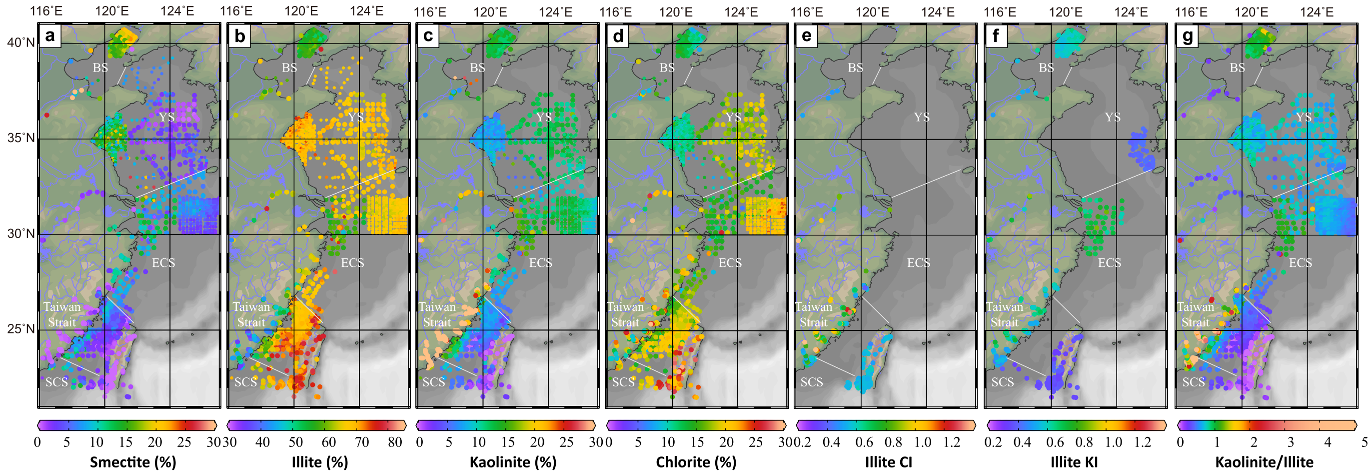

Fig. 7. Spatial distribution of clay minerals (smectite, illite, kaolinite, and chlorite) in ECMS. Detailed data are shown in Appendix Table S2 and S3, samples with manually obtained data (latitude, longitude, and clay mineral compositions) are shown in smaller dots.

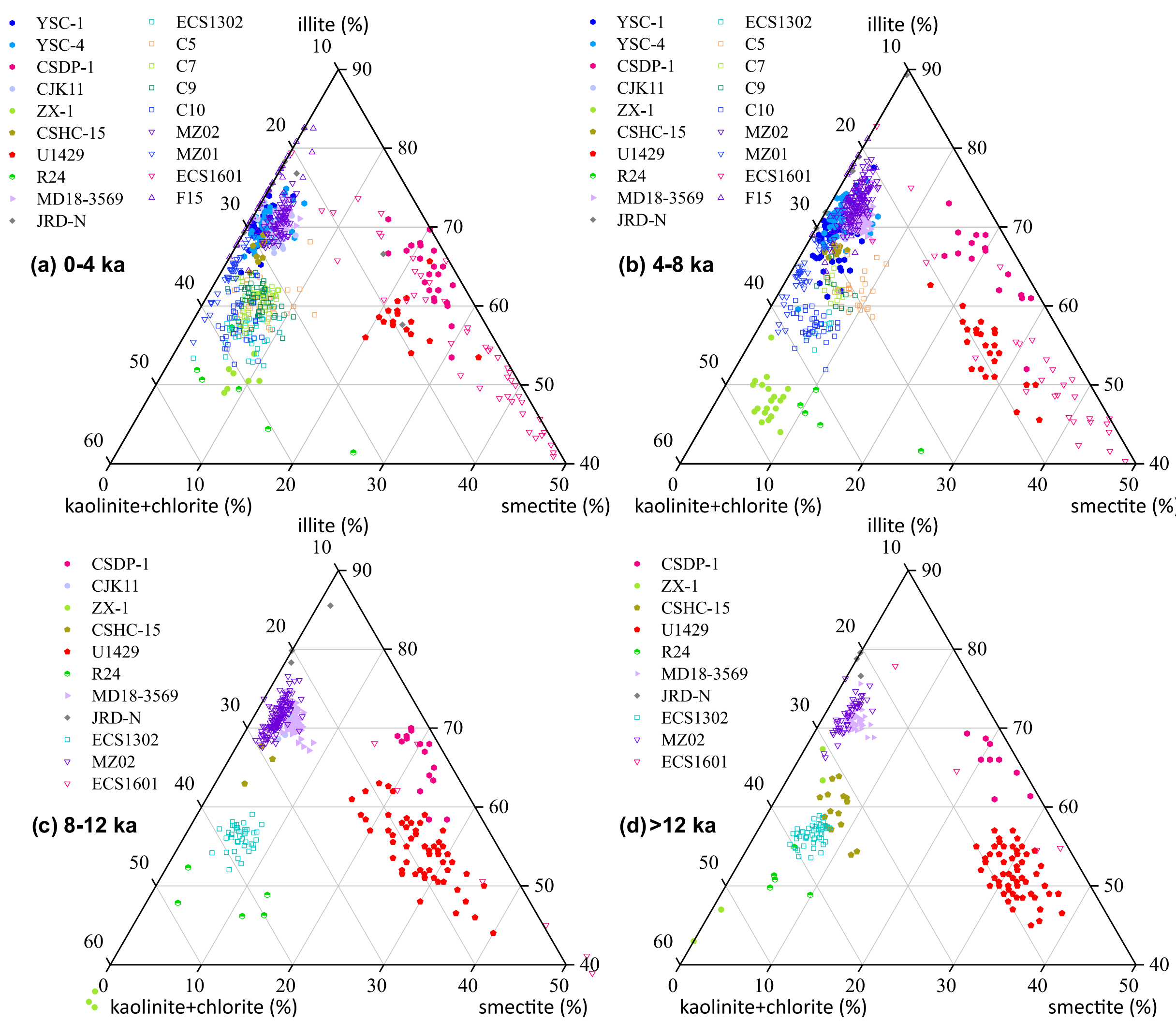

Fig. 8. Clay minerals assemblages in cores from the ECMS in the following periods: 0-4 ka; 4-8 ka; 8-12 ka; >12 ka. The locations of sediment cores are shown in Fig. 1.

assemblages of the Huaihe River basin show fewer illite content (56.4%) and more kaolinite content (17.1%) than those from the Yangtze and Yellow River, and approximate smectite (13.1%) and chlorite contents (13.3%). Clay mineral assemblages in Taiwan rivers are dominantly illite (72.9%) and chlorite (24.5%), with very scarce smectite (0.8%) and kaolinite (1.8%). For river sediment on the continent side, illite is

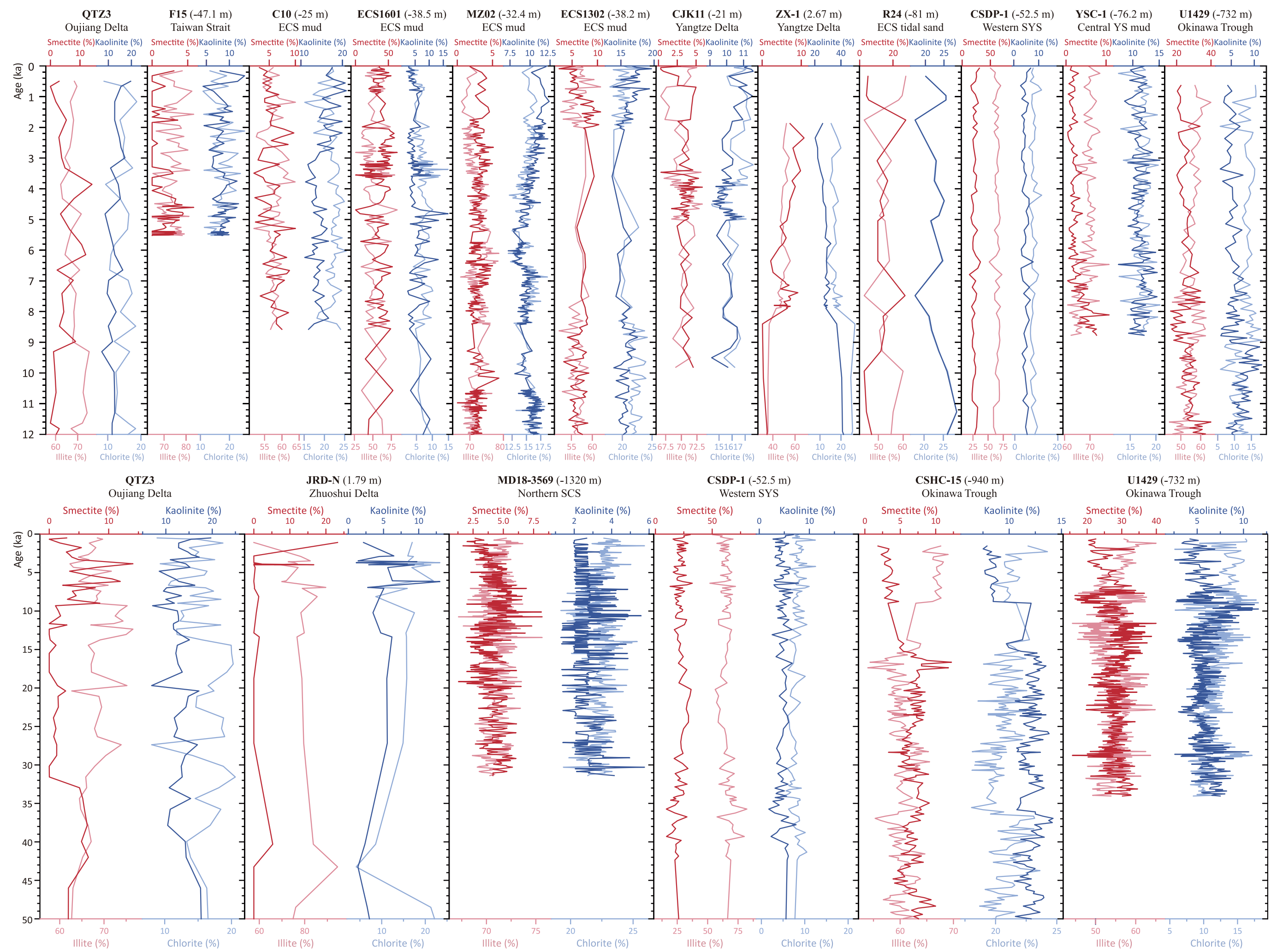

Fig. 9. Downcore changes of clay mineral contents (smectite, illite, kaolinite, and chlorite) in sediment cores since the Holocene (<12 ka) and last glaciation (< 50 ka). Sampling elevations and sampling regions are marked beside each sediment core.

also dominant in rivers from North China (54.8%), and Zhejiang (57.6%), but shows a low proportion in Fujian rivers (30.8%). Inversely, Fujian rivers feature the highest kaolinite content (49.1%), while kaolinite is relatively low in North China (13.4%) and Zhejiang (13.8%). Smectite content is high in North China (21.1%) and decreased to 9.1% in Zhejiang rivers and 0.5% in Fujian rivers. Furthermore, the CI and KI in sediments from Fujian and Taiwan rivers vary significantly. Fujian rivers exhibit high CI values (0.62) and moderate KI values (0.39), while Taiwan rivers exhibit low CI values (0.35) and the lowest KI values (0.16). Note that the quantity of samples from each river basin and region may cause analytical bias in the averaged contents.

Clay minerals in surface sediments from the ECMS show regional disparity distribution (Fig. 7, Table 3). Generally, illite (32%–85%) is still dominant in the clay mineral assemblages of sea surface sediments of ECMS and appears highest content on the seafloor close to Taiwan Island (71.0%), including eastern Taiwan Strait and northeastern SCS. Smectite (0–33%) is relatively low in the sea, showing high contents at the Liaodong Bay in northern BS, the Jiangsu Coast in eastern YS, and the Beibu Gulf in SCS. Smectite contents of sediment from the inner shelf of ECS are relatively higher than those from the central YS and Taiwan Strait. Kaolinite (0–41%) appears higher in the north while lower in the south, with the lowest values around the Taiwan Island and the highest values near the Pearl River Estuary on northern SCS shelf. Chlorite (6%–33%) in clay minerals show similar distribution pattern as illite, with high values around the Taiwan Island and in areas close to the Korean Peninsula. The CI values of illite were rarely reported for surface sediments in the previous studies, only 146 samples have reported the CI values at 0.28–0.44, which are mainly distributed close to the Taiwan Island in the northeastern SCS (Fig. 7e). The KI values of illite were analyzed for 387 samples in northern BS, northeastern SCS, eastern SYS, and the Yangtze River estuary (Fig. 7f). The distribution of KI values in the surface sediments is similar to those in river sediments. For example, the high KI values in ECS samples (0.51) and BS samples (0.40) are approximate to those from the Yangtze River and the North China rivers, respectively. Samples in northeastern SCS exhibit very low KI values (0.17), which are similar to the Taiwan rivers.

5.2.2. *Records of clay minerals since the last glaciation*

Clay mineral compositions of the core sediments are shown in Figs. 8 and 9. Original data and detailed statistics are given in Appendix Table S4 and S5, respectively. Illite in most of the samples appears highest content, which is consistent with the modern distribution patterns in the ECMS (Figs. 6 & 8). Smectite contents are generally low in most cores, but appears commonly high values in cores U1429 in the northern Okinawa Trough (Zhao et al., 2017), CSDP-1 in the YS (Zhang et al., 2019), and ECS1601 in the ECS (Cong et al., 2021). Kaolinite content in the core ZX-1 at the Yangtze Delta Plain (Wang et al., 2006) and the core R24 on the ECS shelf (Jia et al., 2012) is obviously higher than samples from the ECS mud belt (Fig. 9). Chlorite contents exceed 30% in the core MZ01 (Liu et al., 2010b) and are lower than 10% in the

Table 4
Variation trends of clay mineral compositions of compiled core sediments.

Core name	Time period (ka)	Sample number	Smectite	Illite	Kaolinite	Chlorite	Illite CI	Illite KI
QTZ3	0–4	9	↑↑	↓↓	–	–	–	–
	4–8	8	–	–	–	–	–	–
	8–12	9	–	–	–	–	–	–
	12–18	7	–	↓↓	–	↑↑	↓	↓
	18–24	5	–	–	–	–	–	–
	24–32	6	–	–	–	–	–	–
	32–50	7	–	–	↑	–	–	–
	50–130	3	–	–	↑	↓	–	–
	0–4	75	–	↑↑	↓↓	↓	–	–
	4–8	134	–	↓	–	↑	–	–
MZ02	8–12.68	178	–	↓↓	–	↑	–	–
	0–4	28	–	–	↓	–	–	–
	4–8	20	–	–	–	–	–	↑
	8–12	15	–	↓	–	↑	↑	–
	12–18	8	↑↑	↓↓	–	–	–	–
	18–24	7	–	–	–	–	–	–
	24–32	12	–	–	–	–	–	–
CSDP-1	32–58	30	↓	–	–	↑	–	–
	0–4	11	↓	–	–	–	–	–
	4–8	5	–	–	–	–	–	–
JRD-N	32–58	6	–	–	↑	–	–	–
	0–4	33	↑	–	↓	–	no data	no data
	4–8	32	–	–	–	–	no data	no data
CJK11	8–9.81	5	–	–	–	–	no data	no data
	0–4	40	↑↑	–	↓↓	–	↑	–
C5	4–7.32	28	–	–	↓	–	–	–
C7	0–4.84	61	↑	↑	↓↓	↑	–	–
	0–4	49	↑	–	↓↓	↑	–	–
C9	4–5.09	10	–	–	↓↓	–	↓	–
	0–4	30	–	↑	↓↓	↑↑	–	↓
C10	4–8.58	37	↑	–	–	↓	–	↑
	0–4	8	–	–	–	↓↓	–	–
	4–8	9	–	–	–	–	–	–
	8–12	3	–	–	–	–	–	–
	12–18	15	↑↑	↓↓	↑↑	–	–	↑
	18–24	39	–	–	–	–	–	–
	24–32	40	–	↑	–	↓	↓	–
	32–58	89	–	–	–	–	–	–
	58–75	52	–	–	–	–	–	–
CSHC-15	75–130	64	–	–	–	–	–	–
	0–4	38	↑↑	–	↓↓	↓	no data	no data
	4–8	7	–	–	–	–	no data	no data
	8–12	41	↓	–	–	–	no data	no data
ECS-1302	12–14.77	46	↓↓	–	↓	↑↑	no data	no data
	0–4	47	↑	↓	–	–	–	–
	4–8	74	↑	–	–	↓	–	–
	8–12	72	–	–	–	–	–	–
	12–18	82	–	–	–	–	–	–
	18–24	43	–	–	–	–	–	–
MD18-3569	24–31.38	63	–	–	–	–	–	–

↑↑: Significantly increase ($p < 0.05$ and regression slope > 0.5); ↓↓: Significantly decrease ($p < 0.05$ and regression slope < -0.5); ↑: Slightly increase; ↓: Slightly decrease; –: Balanced or no significant change. For detailed data and statistic results, please see Appendix Tables S4 and S5.

core ECS1601 (Cong et al., 2021), both cores are located in the center of the ECS mud belt (Fig. 9). The fluctuation of clay mineral composition in most cores is less than 3% between each time interval, except for cores ZX-1, R24, CSHC-15, U1429, CSDP-1, JRD-1 and MZ03 (Appendix Table S5). Obvious clay mineral changes mainly appeared during the deglaciation (18–12 ka) to the early Holocene (12–8 ka) in these cores, indicating possible changes in the clay mineral provenance from the low sea-level and high sea-level periods (Fig. 9, Table 4). Some of the cores also exhibit clay mineral changes during the late Holocene (4–0 ka).

The difference among sediment cores is higher than the temporal variation in clay minerals in a single core, even though the cores are close to each other in position (Figs. 8 & 9). For example, the core ECS1601 (120°39′36″ E, 26°50′24″ N) at the central part of the mud belt shows extremely high percentages of smectite (Cong et al., 2021), while the core C9 (120°54′00″ E, 26°58′44.4″ N) and MZ01 (120°50′56.4″ E, 26°32′49.2″ N) contain smectite less than 10% and 5%, respectively (Liu et al., 2010b; Zhang et al., 2022c). Sediment cores that are analyzed in the same study or taken by the same research team appear to have similar clay mineral composition, although their position may be quite distant from each other. The cores C5, C7, C9, and C10 (119°52′12.6″–122°17′59.4″ E, 25°49′58.8″–28°44′16.8″ N) (Zhang et al., 2022c) exhibit similar compositions of clay minerals. The reported clay mineral data were given an analytical error of ~5% by replicate analysis each in the original articles. However, it is also suggested that the smearing method during XRD analysis and quantification programs (TOPAS, MDI Jade, etc.) have inherent errors for about 2%–10% (Warr, 2022; Xu et al., 2016; Xu et al., 2023b). Thus, the obtained results by using different programs may cause such inconsistency in clay mineral compositions within the mud belt. Besides, the local input from coastal rivers or rocks can also introduce influences that remain hard to estimate. The cores YSC-1 and YSC-4 located on the central YS mud show similar compositions of clay minerals to those on the ECS mud or the Yangtze River sediments, which is characterized by high contents of illite. The core CSDP-1 on the southwestern part of the YS has approximate smectite-high composition to the Yellow River sediments (Fig. 9).

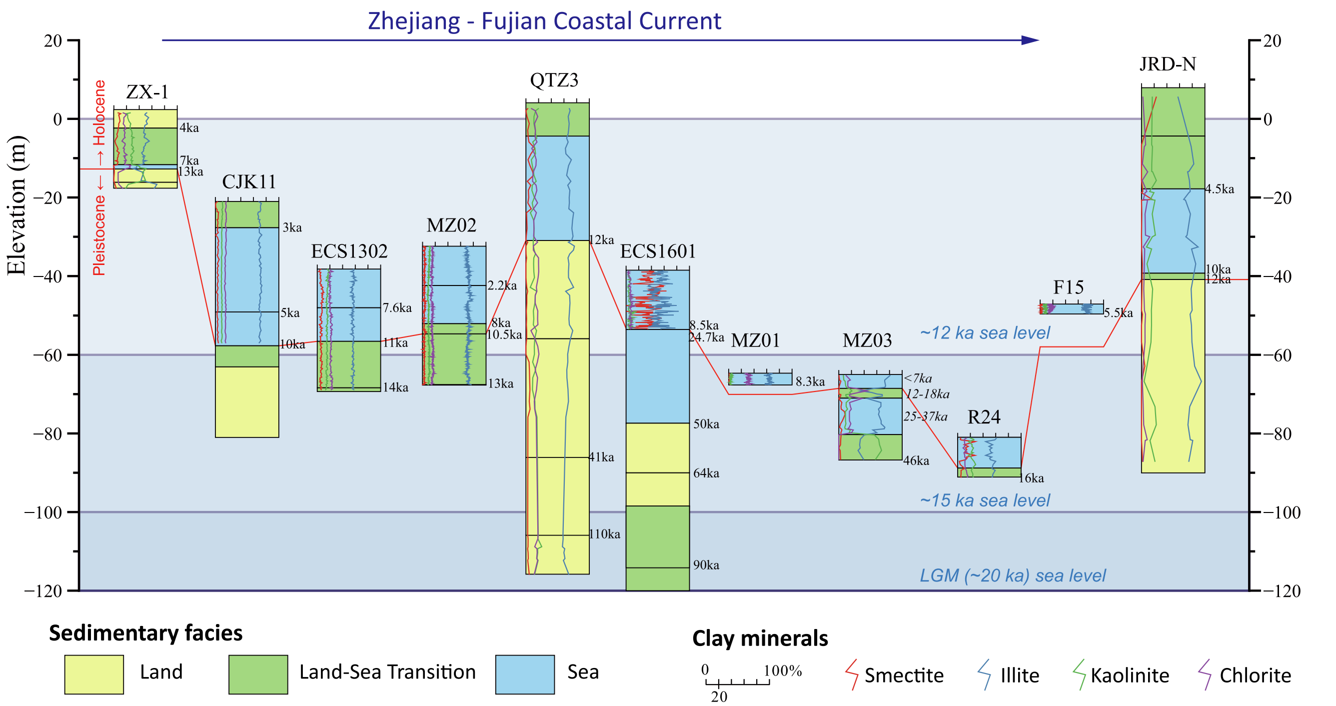

Fig. 10. The clay mineral variation and sedimentary facies for the late Quaternary sequences in cores around the ECS mud belt. The elevation of each core's top corresponds to the sampling altitude. Clay mineral compositions in cores are shown in a line graph overlapping the columns. Ages of dating samples are marked on the right side of the column. Red line correlates the isochrone of the Holocene-Pleistocene boundary in each core. Blue lines indicate the rough sea level elevation at LGM, 15 ka, 12 ka and today, according to the sea level rise curve from Li et al. (2014a). The locations of cores are shown in Fig. 1. Division of sedimentary facies for cores are from Chen et al. (2017a); Liu et al. (2014); Wang et al. (2006); Xu et al. (2022); Xu et al. (2013); Yang et al. (2017); Jia et al. (2012).

6. Discussion

6.1. Sedimentary environment and climate evolution in the eastern China margin since the last glaciation

The East Asian monsoon mainly controlls the climate conditions in the eastern China margin, primarily including temperature and precipitation aspects. Paleoclimate reconstructions in the last decades have revealed that the mean annual temperature (MAT) was ~5 °C lower during the LGM and ~1.5 °C higher in the Holocene thermal optimum during 5–7 ka BP, while the mean annual precipitation (MAP) was decreased for 54%–62% but higher varied in seasons during the LGM (Lu et al., 2024). Due to the global ice volume changes, the sea level was about 60–100 m below present in MIS 3 (Marine Isotope Stage 3) and about 120 m below present in the LGM period (Fig. 4) (Grant et al., 2014; Rohling et al., 2014; Siddall et al., 2008). During MIS 4 and MIS 2 with low sea levels, fine-grained sediments were transported to the continental slope and deposited mainly in the Okinawa Trough (Shi et al., 2024). The incised paleochannel systems were filled with fluvial and subsequently estuarine sediments, truncated by transgressive as sea level rose (Liu et al., 2023a; Liu et al., 2010a; Yang et al., 2022). Few fine-grained sediment was preserved on the exposed shelf area as a terrestrial environment until the sea level rose rapidly during the last deglaciation (Li et al., 2014a; Wang et al., 2015b). During the sea-level rising period from ~14–10 ka, the river channel and flats were submerged and became estuarine (Jin et al., 2023; Liu et al., 2023a; Yang et al., 2017) and shallow marine (Liu et al., 2021a; Shan et al., 2023; Shang et al., 2018) environments (Fig. 10). The sediment sources for the continental shelf have become more diverse due to the ocean circulation system (Li et al., 2014a; Liu et al., 2018b). The mud deposits in the modern ECMS were mainly developed after the strongest transgression in the Holocene (Fig. 10) (Dong et al., 2020). It is suggested that there was a shift of sediment provenance in the Okinawa Trough from primarily supplied by the large rivers (i.e., the Yellow River and Yangtze River) in the glacial period to increasing contribution of Taiwan, Kyushu, and reworking of sediments on the ECS shelf during the Holocene (Li et al., 2019; Shi et al., 2024).

Since the middle Holocene, as the sea-level approached its present position, river sediment accumulation led to progradation of modern deltas and coastal plains along the eastern China coast, such as the Yangtze River (Hori et al., 2001; Zhao et al., 2018a), the Qiantangjiang River (Zhang et al., 2014), and the Mulanxi River (Li et al., 2025). The coastal plain of the Oujiang Delta at present was formed since ~6 ka when the transgression drowned the Oujiang River channel (Zhejiang Water Resources Department, 2020; Wu et al., 2019). A paleosol layer was found in the strata beneath ~30 m at the Wenzhou coastal plain (Fan et al., 2019; Shang et al., 2018). The paleosol was widely distributed in the strata of the Yangtze Delta and northern Zhejiang Plain when the lowlands of the southeastern China were exposed and suffered weathering and oxidation during the Holocene-Pleistocene boundary (Wang et al., 2006; Zhang, 1991). The sedimentary succession in the core QTZ3 above the paleosol layer was composed of shallow shelf and deltaic deposits (Fig. 3), reflecting the submerging of the Oujiang River estuary from ~12 ka and the buildup of the Oujiang Delta in ~4–5 ka, which is comparable with other cores drilled in the adjacent area (Fan et al., 2019; Shang et al., 2018; Yang et al., 2022; Yuan et al., 2023). The succession below the paleosol layer was interpreted as terrestrial deposits, including diluvial, fluvial and lacustrine sediments. Two lacustrine layers with different characteristics in lithology appear in 39.0–56.7 m and 61.5–80.5 m, indicating that the two paleo-lakes had diverse attributes in the Oujiang River basin during their depositional processes (Fig. 3). Given that no visible unconformity were found in the sediment core, we infer the upper and lower segment of lacustrine deposits correspond to the LGM and MIS 3, respectively, which is consistent with the paleoenvironmental characteristics in previous studies (Fan et al., 2019; Wu, 2019; Wu et al., 2019).

6.2. Provenance of the fine-grained sediments in the eastern China margin since the last glaciation

6.2.1. Clay-mineral-based provenance interpretations for the Oujiang Delta

We recognize that the river drainage and weathering conditions varied with climate change (Hu et al., 2014; Wang et al., 2011; Wei et al., 2025; Zhao et al., 2017). The variability of sediment composition is higher in small mountainous rivers compared to large rivers (Jian et al., 2020b; Zhang et al., 2011; Zhang et al., 2022b). Therefore, it is essential to identify how the clay minerals in the sediment have evolved within the river basin.

Weathering and erosion of rocks in the river basin contribute to most sediments in the Oujiang Delta. Clay mineral compositions of the present riverbed sediments exhibit differences between the fluvial reach and the tidal reach of the Oujiang River (Fig. 12). Kaolinite content is much higher in the fluvial reach (24%–31%) than that in the tidal reach (9%–12%). Smectite has increased from 3%–5% in the upper reach to 10%–11% in the tidal reach (Fig. 12a). Illite and chlorite have also increased by 5.7% and 3.6% on average, respectively. It is noteworthy that tidal reach samples reported by Yang (1995) are suspended sediment, while other samples of the Oujiang River are riverbed deposits (Fig. 12a) (Guang et al., 2025; Liu et al., 2016b; Xue et al., 2018a). Other mountainous rivers in the Zhejiang-Fujian area show similar clay mineral composition and spatial distribution to the Oujiang River (Liu et al., 2016b; Mei et al., 2021; Wang et al., 2024). Kaolinite is common in sediment with intense chemical weathering from acid-intermediate igneous rocks. Conversely, smectite is known as a product of weathering from mafic rocks (Chamley, 1989; Fagel, 2024; Liu et al., 2009). The widely distributed volcanic sedimentary rocks and granitic rocks in the Zhejiang-Fujian area are suitable for kaolinite production (Wang et al., 2024). The Mesozoic and Paleoproterozoic sedimentary strata can also provide recycled grains to river sediments (Zhu et al., 2025; Li et al., 2018b; Deng et al., 2018). Clay minerals in the Cretaceous strata contain a high percentage of illite (~80%) with low CI (0.2–0.3) and moderate KI (0.5–0.6) values (Liu et al., 2012c), which possibly produced inherited illite within the river basin (Fig. 2).

Marine sediments transported by tidal currents are another important material source of the delta sediment, which originates primarily from large rivers in the ECMS case (Cai et al., 2020; Liu et al., 2006, 2018c). Clay mineral compositions of river sediments vary along the river from the upper to lower stream, mixing up under the tidal influence at the terminal estuary (Guyot et al., 2007; He et al., 2013). Generally, sediments in the estuarine environments of most rivers in eastern China exhibit higher smectite and lower kaolinite contents than those in the mainstream (Wang et al., 2024; Zhao et al., 2018c). A study on the surface ECS mud sediment has shown that clay mineral composition has no significant change after leaving the Yangtze Estuary (Gao et al., 2004), which is also supported by our data collection results (Figs. 6 & 7, Table S2). Combined with the modern distribution of sediment clay minerals across the Oujiang River, we suggest that the increased smectite content (~5%–10%) in estuary samples is possibly related to the influx of muddy sediments from the ECS.

For the core QTZ3, smectite contents in sediments are generally decreasing during the Late Pleistocene, while the KI values of illite maintained fluctuating at a low level. An obvious reduction of smectite contents was found at 32 ka (~65 m in core) (Figs. 5 & 12). The smectite reduction is consistent with the sedimentary facies shifting from a lacustrine deposit in MIS 3 to a fluvial deposit (Fig. 3). Since the

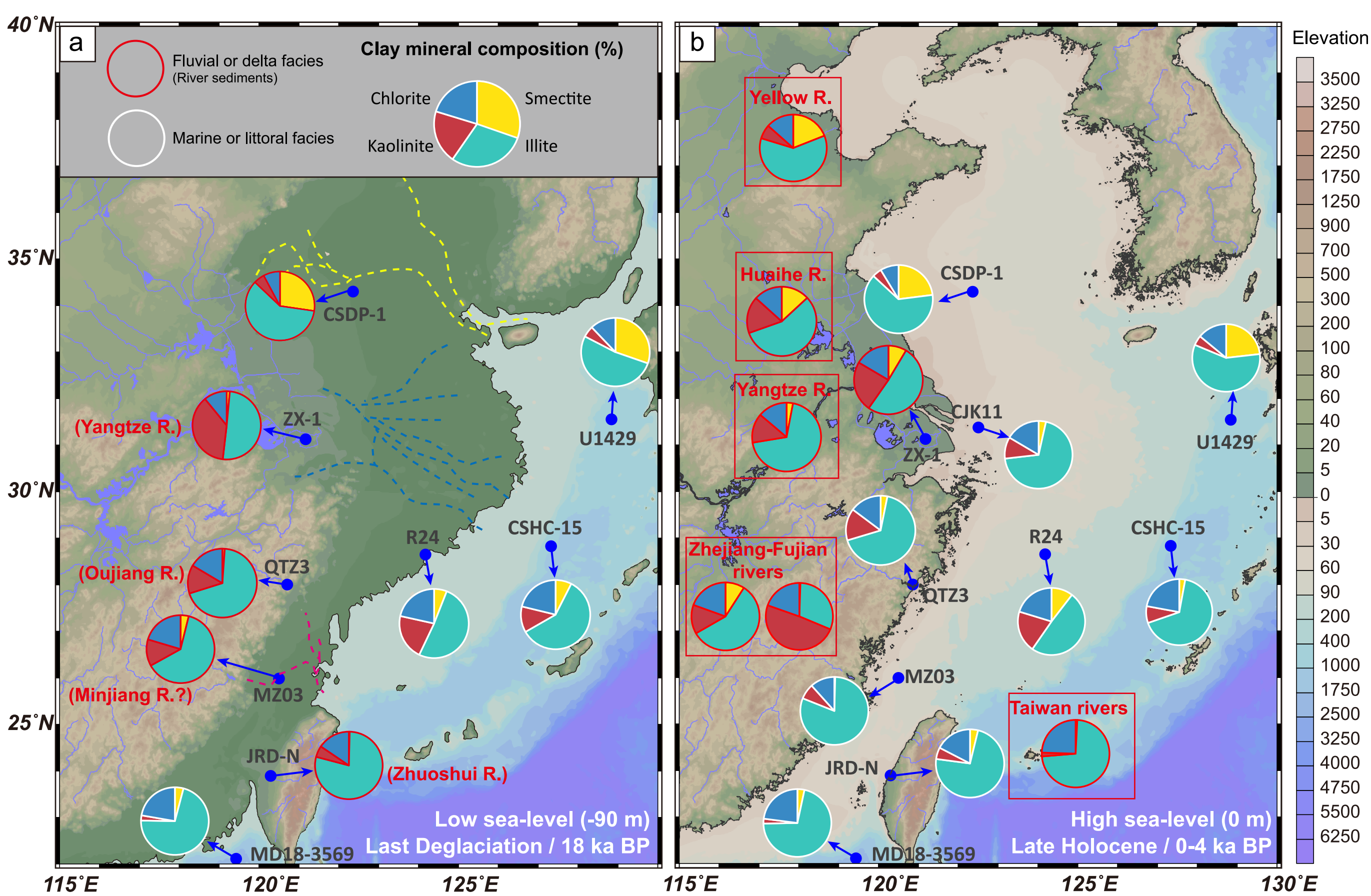

Fig. 11. Spatial distribution of clay minerals during a) low sea-level period (last deglaciation) and b) high sea-level period (late Holocene). The outline colors of pie charts indicate the sedimentary facies, including river-dominated (fluvial and delta, red) and ocean-influenced (marine and littoral, white). Clay mineral compositions of modern river sediments are shown in boxes. The paleo-river channels during low sea-level are modified from Li et al. (2019) and Xu et al. (2022).

sediments within 50–12 ka represents a terrestrial environment under the Oujiang River control, we infer that the relatively high smectite content in this segment was not from the ocean at that time. The smectite content reduction might be related to changes in the upstream water system of the Oujiang River basin. On the other hand, the damp and cool climate in the interstadial period (MIS 3) might be suitable for smectite preservation within the Oujiang River basin (Galán and Ferrell, 2013; Steudel et al., 2009). The smectite proportion and its variation in clay minerals significantly increased within the Holocene period (0–36 m). At the same period, the KI values also increased by ~0.12 (Table 2, Fig. 5), indicating the provenance change and strengthened marine influence (e.g., tidal effect, coastal current intensity, sea level changes). Clay minerals assemblages of sediment from the deltaic deposits within 4 ka exhibit reduction in smectite and increase in illite, kaolinite, and CI values than these during the early Holocene period (Fig. 5). The clay mineral composition of the QTZ3 sediment within 4 ka is similar to that from the Yangtze River prodelta, ECS mud belt and part of tidal reach samples of Oujiang River (Figs. 6 & 12). Consequently, we conclude that the Holocene sediments from the uppermost 36 m of the core are both contributed by eroded materials within the Oujiang River basin, and muddy deposits from the southern ECS.

6.2.2. *Clay-mineral-based provenance interpretations for the ECMS*

In the ECMS region, illite is the most abundant among the four major clay minerals in river and marine sediments (Fig. 7). The clay mineral proxies of modern river sediment are quite varied in each river basin and exhibit uncorrelated changes with climate zones. The distribution pattern reflects the combined effect of source area bedrock lithology and climate (Table 3, Fig. 13). For example, clastic rocks have primarily produced the illite-rich sediments in Taiwan rivers and the Yellow River basins where chemical weathering is limited, leading to low values and small variation of CI and kaolinite/illite values (Pang et al., 2018). Clastic rocks in the Zhejiang-Fujian area also produce considerable illite-rich sediments with low CI values in mountainous river sediments (Figs. 6 & 7) (Fu et al., 2025; Wang et al., 2024). The spatial distribution of smectite in estuary and shelf sediments possibly indicates the effect of the sea rather than chemical weathering in the river basin, as discussed above concerning the Oujiang Delta. Moreover, the variation of smectite also exists among the present surface sediments within the YS (Fig. 6). Except for the experimental errors across research, this variation may indicate distinct formations of the central YS and ancient Yellow River Delta (Hanebuth et al., 2015; Qiao et al., 2017).

Some of the sediment cores from the ECMS have recorded the fluvial deposits during the low sea-level period in the last glaciation, which are regarded as river signals (Fig. 11a). Compared to modern river sediments (Table 3), clay mineral compositions from sediment cores exhibit higher smectite contents in the paleo-Yellow River (CSDP-1), higher kaolinite contents in the paleo-Yangtze River (ZX-1), and higher illite contents in the paleo-Oujiang River (QTZ3), the paleo-Minjiang River (MZ03), and the paleo-Zhuoshui River (JRD-N) (Fig. 11). The variation in river clay mineral signals can be related to evolution in the drainage system, weathering characteristics, and changes in sediment

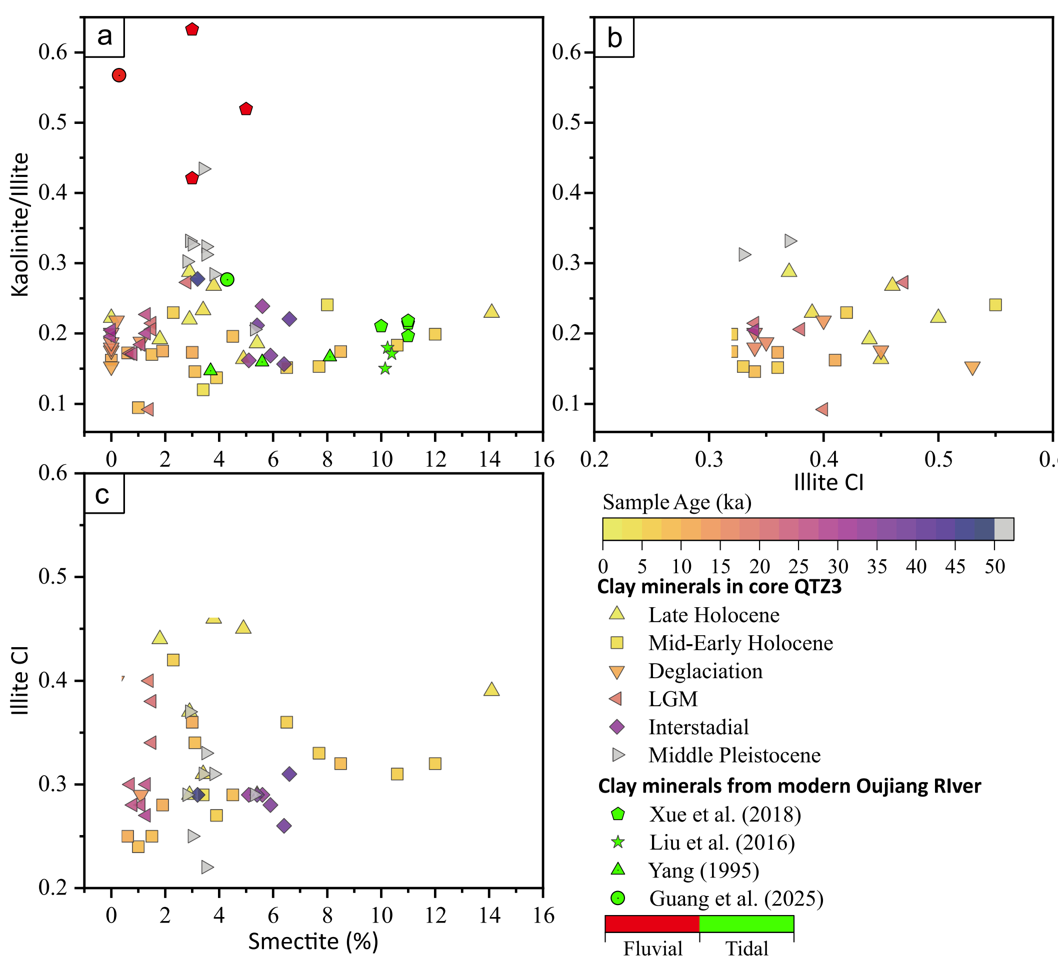

Fig. 12. Pairwise correlation between kaolinite/illite ratio, illite CI, and smectite composition in core QTZ3 and in river sediments from modern Oujiang River. Different colors are used to distinguish the age of the sample, and shapes of point marks the samples from each time period. Sediment samples from the fluvial and tidal reach are mapped in red and green, respectively. Due to the lack of illite CI data in the previous studies, the reference points are not displayed in (a) and (b). Modern sediment data are from Xue et al. (2018a) and Liu et al. (2016b).

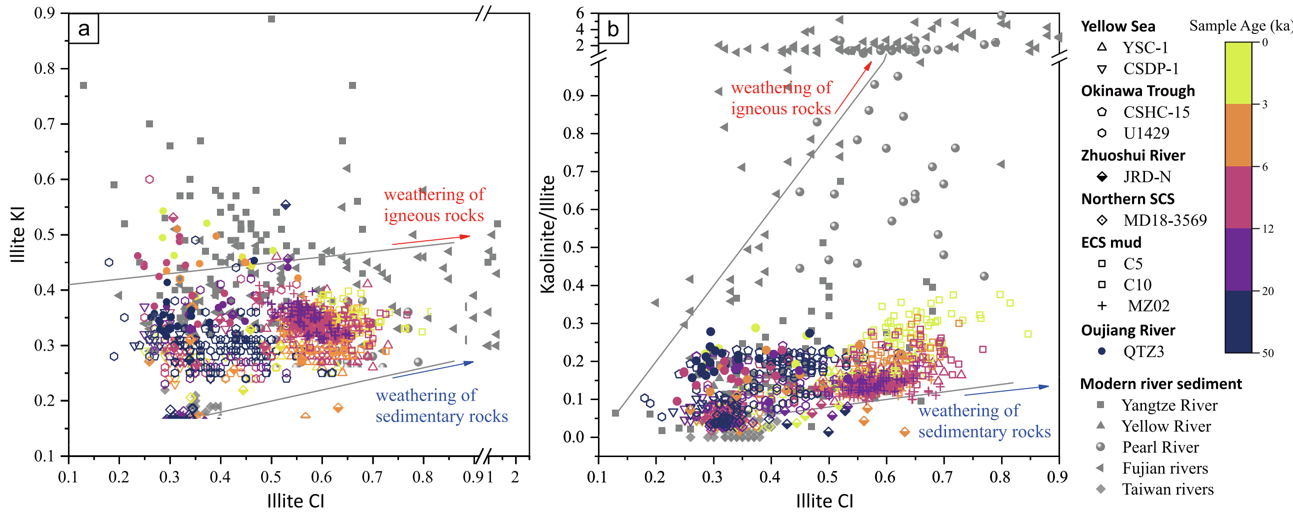

Fig. 13. Diagram showing illite chemical index (CI) values versus (a) illite crystallinity (KI) values and (b) kaolinite/illite of sediment samples from core QTZ3 (colored circle), collected cores (colored contours), and modern river sediment (shaded symbols). The colors of data points in core samples are mapped to the age since the last 50 ka. The data shown in the figure is from core YSC-1 (Li et al., 2014b), CSDP-1 (Zhang et al., 2019), CSHC-15 (Shi et al., 2024), U1429 (Zhao et al., 2017), JRD-N (Zhang et al., 2022b), MZ02 (Liu et al., 2014), and C5 to C10 (Zhang et al., 2022c); river sediment from Fujian rivers (Mei et al., 2021), Taiwan rivers (Liu et al., 2008b; Wang et al., 2016), Yellow River (Zhang et al., 2019), Yangtze River (He et al., 2013; Wang et al., 2021), and Pearl River (Liu et al., 2007).

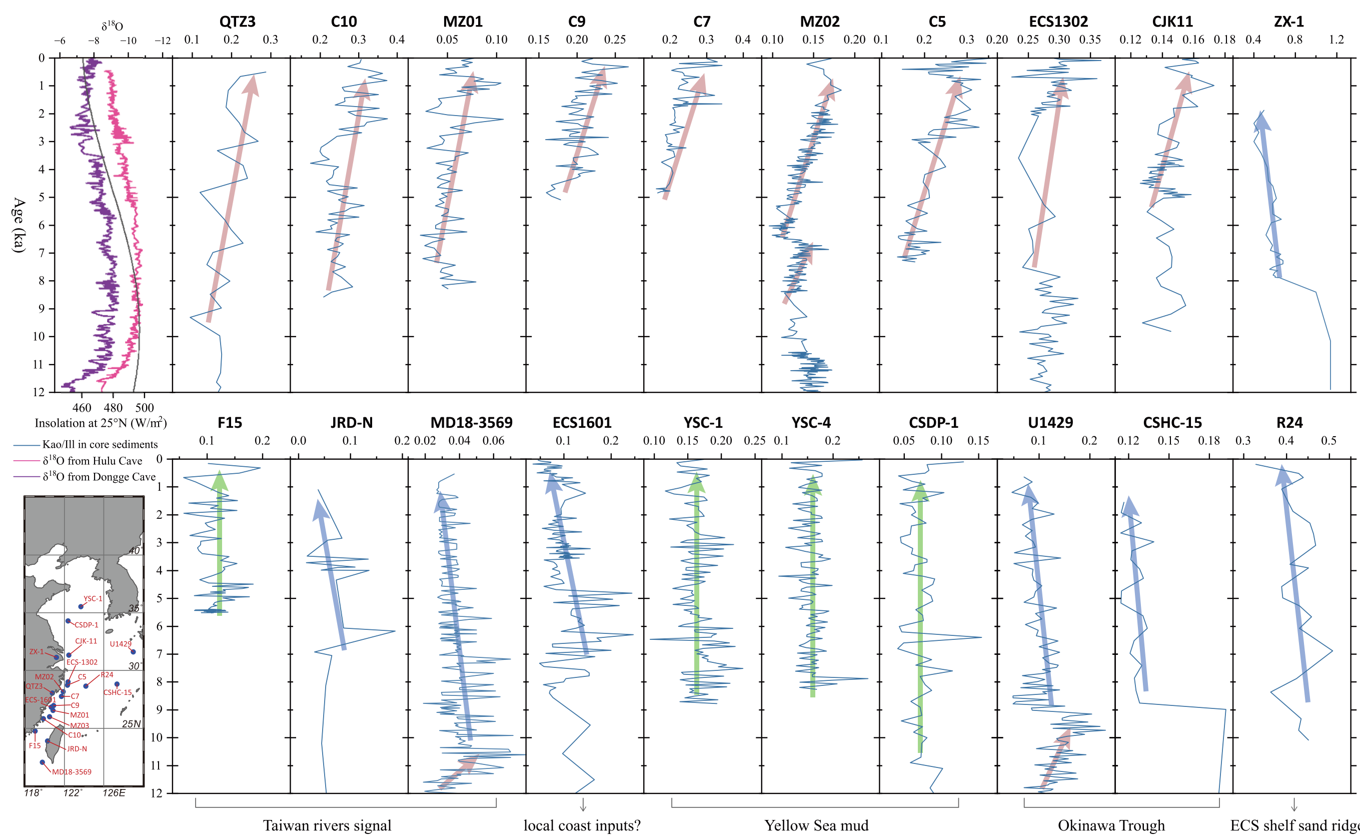

Fig. 14. Variation of kaolinite/illite ratio in cores with comparison to oxygen isotope value from the Hulu Cave (Wang et al., 2001), the Dongge Cave (Dykoski et al., 2005), and average summer insolation for 25°N (Laskar et al., 2004) since 12 ka BP. The core QTZ3, cores at the Yangtze Delta (CJK11) and the inner ECS shelf (C10, C9, C7, C5, MZ01, MZ02 and ECS1302) exhibit an increasing trend. There is no similar pattern or even opposite trend for clay minerals in cores from the Taiwan Strait (JRD-N and F15), the northern SCS (MD18-3569), the Okinawa Trough (U1429 and CSHC-15), and the YS (YSC-1 and CSDP-1).

provenance. The contrast between illite-rich Taiwan strata and kaolinite-rich continental sediment has led to the clay mineral mixing and fluctuation at the river mouth (e.g., JRD-N) and in the Taiwan Strait (e.g., F15 and MZ03) during the Holocene (Fig. 14) (Shan et al., 2023; Zhang et al., 2022b). The sand ridges on the outer shelf of the ECS are thought to be recycled sediment at the paleo-Yangtze Delta (Li et al., 2014a; Yang et al., 2014). Sediment in the core R24 during the last deglaciation at the ECS tidal ridge shows similarity to the modern Yangtze Delta sediment in the core ZX-1 (Berné et al., 2002; Liu et al., 2007) (Fig. 11). The deep-sea Okinawa Trough is also implicated as

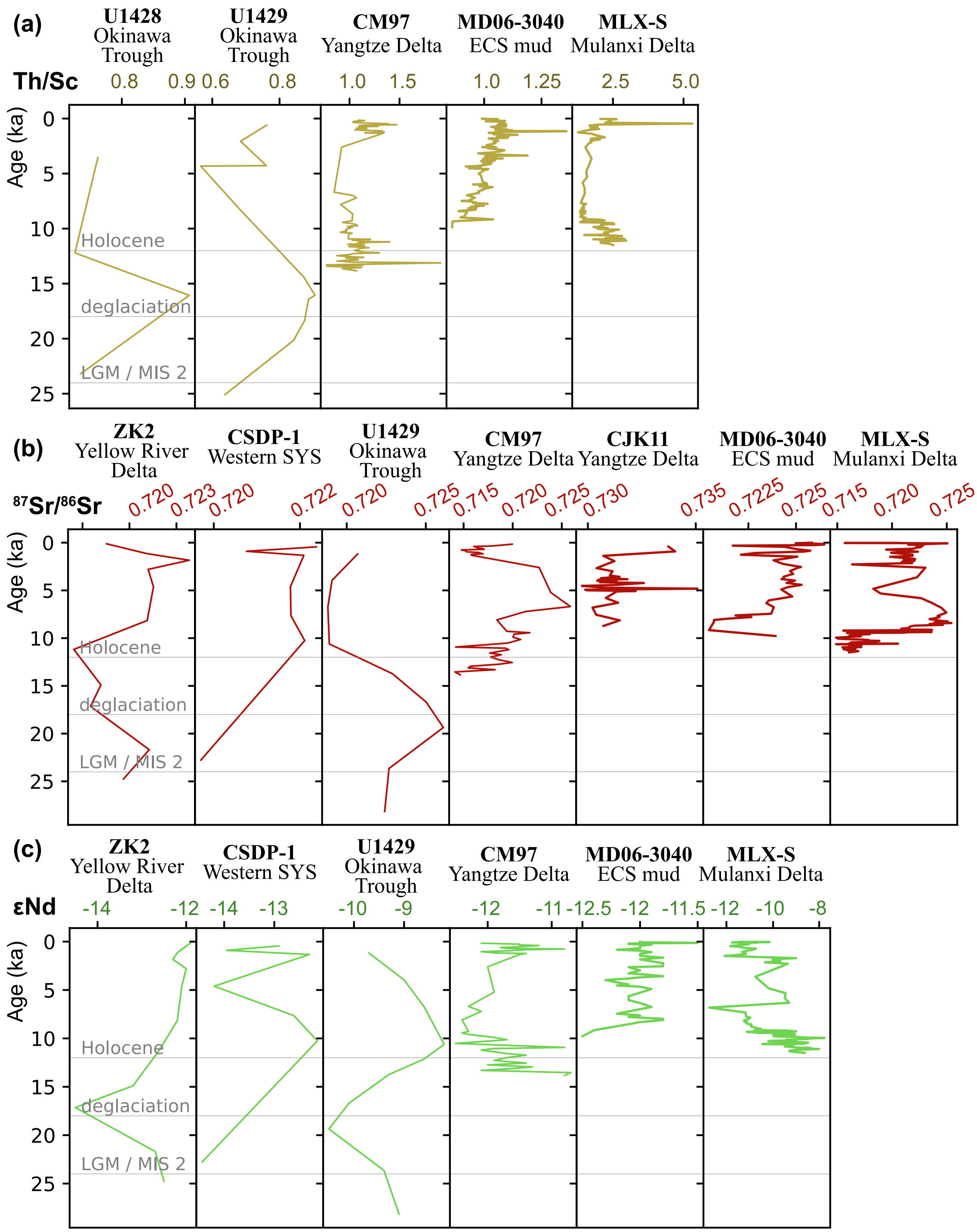

Fig. 15. Downcore changes of sediment provenance indicators: (a) Th/Sc ratio, (b) $^{87}Sr/^{86}Sr$, and (c) εNd in sediment cores since the last glacial maximum (< 30 ka). The temporal variations of sediment provenance responses in different regions show varying trends. The data shown in the figure is from core ZK2 (Hu et al., 2012), CSDP-1 (Huang et al., 2019), U1428 (Anderson et al., 2018), U1429 (Zhao et al., 2018b; Zhao et al., 2017), CM97 (Bi et al., 2017), CJK-11 (Xu et al., 2024), MD06-3040 (Bi et al., 2017), MLX-S (Li et al., 2025).

sediment signals from the inner shelf changed (Figs. 9 & 10) (Shi et al., 2024; Zhao et al., 2017). The cores CSHC-15 and U1429 in the Okinawa Trough remain marine settings as the sea level fluctuations. The clay mineral compositions of these two cores showed decreases in smectite and kaolinite, as well as an increase in illite and chlorite after the LGM (Figs. 9 & 11), which indicates a remote response of sea-level-induced provenance change on the continental shelves. The core MD18-3569 at northern SCS shows small changes in clay mineral composition in the glacial–interglacial cycle (Fig. 11), representing a stable sink of sediment from southwest Taiwan Island (Bertaz et al., 2024).

The kaolinite/illite in sediment cores show opposite trends in different regions during the middle-late Holocene (Fig. 14). Specifically, cores that are affected by the Yangtze River sediment appear increasing trends of kaolinite/illite values, including the Yangtze Delta, the ECS mud belt, and the Oujiang Delta. Inversely, kaolinite/illite values do not obviously change or even show opposite trends in the Yellow Sea (YSC-1, YSC-4 and CSDP-1), the ECS sand ridge (R24), the Okinawa Trough (U1429 and CSHC-15), the northeastern SCS (MD18-3569), the Taiwan

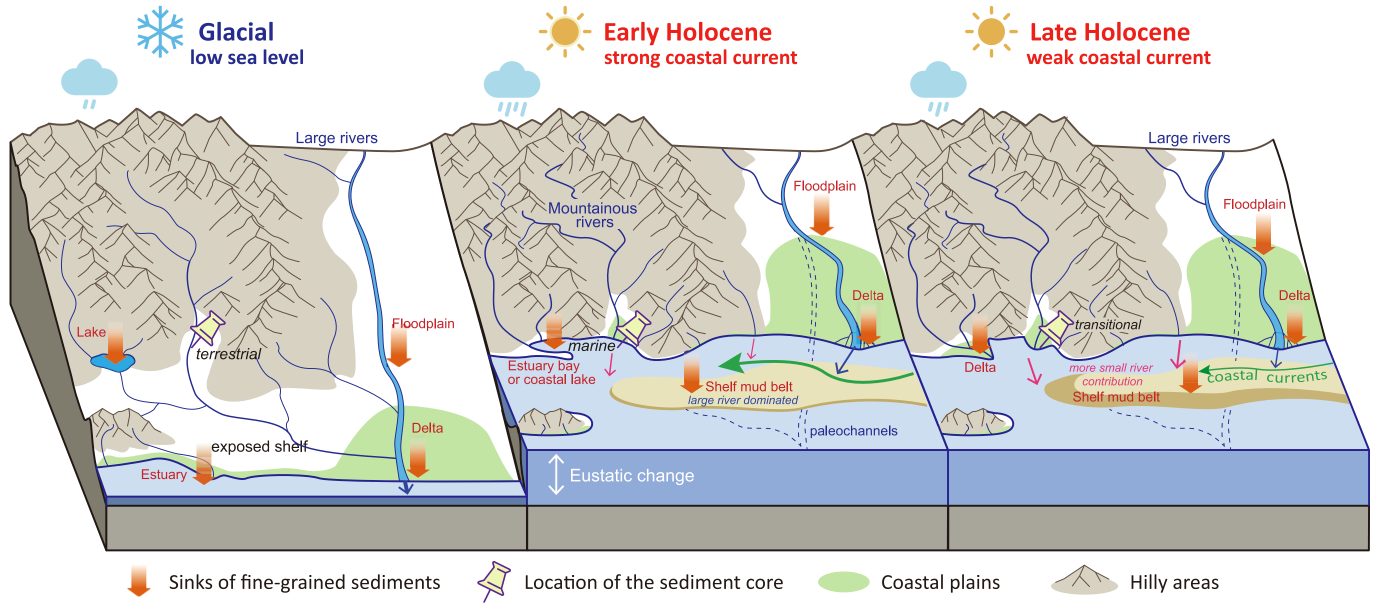

Fig. 16. Schematic fine-grained sedimentary process within land-sea transition zone during the glacial–interglacial cycle, showing variations from low sea-level and high sea-level periods. Sedimentary facies of the investigated core (the thumbtack icon) changed during the sea level rise and delta development. Previous fine-grained sediment depocenters migrate as the terrestrial and marine processes interact. Coastal currents intensity impacts the river sediment signals that preserved in the shelf mud belts.

rivers estuary (JRD-N), or the Taiwan Strait (F15). Given that modern sediments exhibit higher kaolinite/illite values in Zhejiang-Fujian rivers than those from the Taiwan rivers or the Yangtze River (Fig. 13b), we infer that these opposite trends in cores indicate enhanced Zhejiang-Fujian rivers' contribution to the ECS during the middle-late Holocene. Previous studies have utilized the smectite as an indicator of the Yellow River-derived contribution to the ECS (Liu et al., 2024). However, we realize that the local input from mafic rocks in the Zhejiang-Fujian area may influence the smectite contents in clay minerals (Liu et al., 2016b; Qi and Jian, 2026). Furthermore, the smectite-rich sediment derived from the Yellow River can hardly bypass a majority of core samples during the ECS mud belt formation and only deposit in specific locations such as the core ECS1601 (Fig. 14).

6.2.3. A multi-proxy perspective on the fine-grained sediment provenance of the ECMS

Other sedimentary proxies such as Sr-Nd isotope (e.g., Cai et al., 2020; Gao et al., 2025; Guo et al., 2021; Rao et al., 2017) and elemental geochemistry (e.g., Bi et al., 2015, 2017; Su et al., 2017; Wei et al., 2012) have been utilized as indicators of fine-grained sediment provenance in the ECMS. Previous investigations on shelf sediments from the YS (Hu et al., 2018; Koo and Cho, 2020; Um et al., 2015) and ECS (Dou et al., 2016; Wu et al., 2023; Xu et al., 2023a) reveal that the two large rivers–the Yellow River and the Yangtze River–collectively dominate the sediment budget, whereas small rivers (e.g., the Mulanxi River) only affect the nearshore area at their estuaries (Fig. 15). However, the geochemical characteristics of the Yangtze Delta, Yellow River Delta and the muddy depocenters exhibits similarities, while sediments from mountainous rivers show greater differences (Gao et al., 2025; Li et al., 2025; Xu et al., 2019). The dispersion of reference values causes ambiguous quantification on the relative contributions of the two large rivers. By using modern river sediments as the end-member, some studies implied that the Yellow River has contributed 20%–60% of the sediment in the Yangtze Delta during the Holocene (Xu et al., 2024; Zhang et al., 2023). For the sedimentary sink in the Okinawa Trough, it is suggested that sediment contribution from Taiwan and Kyushu have increased during the transgression (Fig. 15), while the sediment outputs by the Yangtze River and the Yellow River were trapped in the ECS and YS (Li et al., 2019; Shi et al., 2024).

Quantifying the sediment contribution from recycled sedimentary strata remains difficult, as most conventional geochemical provenance indicators (e.g., εNd, Th/Sc) are primarily based on the characteristics of the magmatic rocks or the original magmatic parent-rocks of the sedimentary strata in the source area. Due to the extensive distribution of Mesozoic granitic rocks within the basin, fluvial sediments from the small-scale Zhejiang-Fujian rivers (e.g., Mulanxi River, Jiulongjiang River) show more positive εNd values and broader ranges of $^{87}Sr/^{86}Sr$ values than sediments from the Yangtze River and the Yellow River (Gao et al., 2025; Li et al., 2025). The core MD06-3040 from the ECS mud belt (Fig. 1) shows increasing Th/Sc, εNd values and $^{87}Sr/^{86}Sr$ ratios during the middle-late Holocene (Fig. 15). A previous study suggested that MD06-3040 sediment originated from the Yangtze River, and changes in geochemical proxies were interpreted the contribution from the upper and lower catchment of the Yangtze River (Bi et al., 2017). However, when compared with the CM97 from the Yangtze Delta and the core MLX-S from the Mulanxi Delta (Figs. 1 & 15), we believe that variation of these geochemical indicators of the ECS mud sediment supports an increasing contribution from the Zhejiang-Fujian rivers, which is consistent with the clay-mineral-based interpretations. We realize that differentiated hydrodynamic sorting during transport and deposition processes may introduce additional deviations in both geochemical and clay mineral data (Schieber et al., 2023; Schieber and Yawar, 2025; Warr et al., 2024). The grain-size effect of the investigated sediments disturbs the geochemical compositions by concentrating different minerals (Dou et al., 2022; Frings, 2019; Fu et al., 2025; Gao et al., 2025; Wang et al., 2015b). While clay minerals can indicate the erosion of sedimentary rocks, their limitation to a narrow grain size range causes a poor indicative effect in sandy sediments (Garzanti, 2017; Warr, 2022). A regional compilation of various proxies can enhance the robustness of provenance interpretation. For example, the smectite in clay minerals may originate from mafic rocks weathering, which can be combined with the Th/Sc ratio or other heavy metal element (e.g., Cr and Ni) proxies (Bayon et al., 2023; Murray and Jagoutz, 2024) to comprehensively indicate the contribution of felsic and mafic components to the ECMS sediments.

6.3. Decoupled clay-mineral-based weathering intensity and local climate in land-sea transition zones

Clay mineralogical proxies are widely utilized for evaluating weathering intensity in sediment source-to-sink systems (Chen et al., 2014; Nayak et al., 2022; Wang et al., 2024; Warr et al., 2024; Zhang et al., 2019). A low KI value indicates good crystallization, which may be either resulting from the illitization during diagenesis or weak alteration during chemical weathering. The low and high CI values are used to indicate Fe-Mg-rich and Al-rich illite, respectively, which further imply the lower and higher intensity of chemical weathering (Steinke et al., 2008; Wang et al., 2024; Yu et al., 2020). Ratios of clay minerals (kaolinite/illite, smectite/illite, (kaolinite+smectite)/(illite+chlorite), etc.) are also important proxies reflecting the enrichment of specific minerals. For instance, kaolinite and smectite are considered weathering products of a deeper stage than illite, thus a high kaolinite/illite (or smectite/illite) ratio indicates strong chemical weathering degrees (Fagel, 2024; Kumari and Mohan, 2021; Mei et al., 2021; Wang et al., 2024). However, the weathering intensity evaluation based on clay mineral data was disturbed as sediment sources, transport and deposit conditions change with climate.

Clay minerals in the sediment core QTZ3 during the Late Pleistocene period (including Interstadial, LGM, and Deglaciation) were primarily from the Oujiang River drainage. In comparison to modern fluvial reach sediments, sediments from these periods were characterized by higher illite and lower kaolinite contents (Figs. 5 & 11). The relatively low kaolinite/illite values in this period may correspond to the cold climate conditions during the last glaciation. Inversely, the CI and KI values of illite show opposite variation to the kaolinite/illite values. The CI values have increased in the LGM period while the KI values remained stable (Fig. 5, Table 2), which seems inconsistent with the theoretical lower weathering intensity. Furthermore, clay-mineral-based weathering reconstruction diverges from previous palynologically inferred paleoclimate trends of the core QTZ3 (Fig. 3). The previous reconstruction on coastal plain vegetation succession using pollen from herbs, ferns, and *Quercus* species that have limited transmission ability, reflected predominantly local conditions around the Oujiang Delta (Wu, 2019). Inversely, clay minerals are smaller in grain size and can record basin-wide environmental signals across the river drainage (Fagel, 2024; Fu et al., 2023; Wang et al., 2023). The difference in spatial representativity leads to a decoupling between clay-mineral-based weathering intensity and local paleoclimate conditions. During the Holocene period (~12 ka), the variability of CI, KI, and kaolinite/illite values increased as marine sources were involved (Fig. 5). Clay minerals in the core QTZ3 for this period do not reliably reflect the weathering intensity and climatic conditions within the Oujiang River basin.

In the ECMS region, the fine-grained sediment fluxes are predominantly from large river systems, which integrate weathering signals from extensive catchment with heterogeneous material source and climate (He et al., 2013; Zhang et al., 2022b; An et al., 2020). The weathering signals from numerous rivers may be mixed by the tide and current effects along the marginal sea. As a result, the spatial distribution of clay minerals in the ECMS shows inconsistency with regional climate patterns (Figs. 7, 9 & 13). This complexity implies that the interpretation of clay-mineral-based weathering indicators in marginal sea settings requires a broader spatial perspective, and accounting for non-weathering factors such as sediment source, transport agents, and depositional environments.

Based on the clay mineral database of surface and core sediments, we find that among the commonly used weathering indicators of clay minerals, the KI value is restrictedly changed by weathering and it is more sensitive to the lithological composition of parent rocks (Fig. 13a), whereas the slope of the correlation between CI and kaolinite/illite values can reflect the weathering effects on different parent rock types (Fig. 13b) (Fu, 2025). From a regional perspective, the distribution of KI, CI, and kaolinite/illite values in modern and past sediments indicate that clay minerals within the ECMS sediments are mainly derived from sedimentary rocks. This implies that recycled clay minerals and their further weathering may mislead or overprint the weathering signals. Consequently, variations in clay mineral assemblage and single-mineral indices (CI and KI) are related to both weathering and non-weathering effects on fine-grained sediments from the entire sediment source-to-sink system. These findings highlight that the paleoclimate reconstruction by clay mineral proxies is conditional upon a clear understanding of provenance lithology and sedimentary recycling history.

6.4. Controls on clay mineral formation and transport dynamics in the land-sea transition zone: a review

As described in the sections above, the clay mineral assemblages exhibit great variation in cores from different areas and in time intervals with diverse climatic conditions. Climate is a crucial factor that affects clay mineral composition on the Earth's surface (Fagel, 2024). However, sediment formation and clay mineral composition therein are of course not only determined by climate (Li et al., 2014a; Wang et al., 2022b). There are also other factors that control clay minerals in sediment, such as the source, transport process, and preservation environment (Bi et al., 2015; Li et al., 2021; Liu et al., 2012b; Liu et al., 2016b). We realize that these processes and factors are also highly influenced by climate change. Thus, the impacts of climate change on sediment composition can be indirect and indistinct because of the complicated mixing processes, especially in the land-sea transition zone.

6.4.1. Parent rock types: the clay mineral sources

The source of sediment is the fundamental factor that controls clay mineral composition (Galán and Ferrell, 2013). Original minerals in parent rocks supply either inherited clay minerals or materials for secondary clay mineral formation (Chamley, 1989; Fagel, 2024; Galán, 2006). Various lithologies exhibit different preferences and easiness to produce clay minerals under different weathering degrees (e.g., Deepthy and Balakrishnan, 2005; Nesbitt and Young, 1989; Tan et al., 2017). This lithological controls is evident in large rivers (e.g., the Yangtze, Yellow, Mississippi, and Amazon Rivers), where tributaries originating from different lithological areas induce sediments with diverse clay mineral assemblages to the mainstream, and subsequently to the estuary and the marginal seas (Zhao et al., 2018c; Pang et al., 2018; Zhang et al., 2019; Sionneau et al., 2008; Guyot et al., 2007; Huang et al., 2019). Similarly, this lithological control also plays an important role in distinct clay mineral compositions between river sediments from small-scale Fujian rivers (e.g., Tongshanxi, Mulanxi, Jiaoxi Rivers) (Mei et al., 2021; Wang et al., 2024) and Taiwan rivers (e.g., Zhuoshui, Gaoping, Daan, Lanyang Rivers) (Liu et al., 2008b; Nayak et al., 2022; Xu et al., 2009) under similar climatic settings. The Mesozoic volcanic-sedimentary or sedimentary strata and granitic igneous rocks are widely distributed within Fujian rivers basins, and the Cenozoic clastic and slightly metamorphosed sedimentary strata on the Taiwan Island would be considered as primary control (Nayak et al., 2022; Wang et al., 2024). Our results suggest that a large proportion of clay minerals in marine sediment originated from clastic rocks in the ECMS case (Fig. 13), the newly-formed clay minerals from modern weathering on igneous rocks, such as granitic rocks in Zhejiang-Fujian province, seem to contribute a small proportion (Fu et al., 2023; Garzanti et al., 2021; Warr, 2022).

6.4.2. Climatic conditions on the land surface: effects from weathering, vegetation, and hydrology

The climate change directly impacts the sediment composition through weathering, including chemical, physical, and biological aspects. These processes are highly related to local temperature, precipitation, and extreme weather events. A significant factor is the hydrolysis process that causes alteration in minerals during chemical weathering, leading to higher CI and KI values in illite (Chamley, 1989; Wang et al., 2016). With further weathering, silica concentration decreases, chlorite and mica group minerals may degrade to swelling vermiculite and smectite, and smectite further turns into kaolinite, gibbsite, and allophane (Chamley, 1989; Fagel, 2007; Galán and Ferrell, 2013). Our result shows that under the climatic conditions of present and last glacial period, the weathering conditions around eastern China were conducive to the preservation of illite and kaolinite (Figs. 6, 7 & 11). Another effect on clay mineral production comes from biological weathering. In river basins around eastern China, diverse climatic zones—from subtropical to temperate monsoonal regimes and localized mountain settings—shape distinct biota that may modulate weathering and clay mineral assemblages (Hazen et al., 2013; Tazaki, 2013; Warr, 2022), but the understanding of microorganisms and vegetation processes in clay mineral formation is still limited (Cuadros, 2017; Perelomov, 2023; Schieber and Yawar, 2025).

Climate conditions also affect the distribution of vegetation and drainage systems, which in turn influence transport dynamics in sediment source-to-sink systems. Vegetation reconstruction in the eastern China margin indicates significant changes in plant type and density since the last glaciation (e.g., Dai et al., 2015; Guiot et al., 2008; Jiang et al., 2003; Wu, 2019). Except for its role in clay mineral formation, the vegetation distribution also contributes to fine-grained sediment yields in rivers (Hoffmann et al., 2010; Mei et al., 2021; Ouyang et al., 2010; Zhang et al., 2006). Rainfall can increase the water discharge and extend the river channel headward, subsequently influencing the ability of fluvial erosion and transport (Rădoane et al., 2019; Roy et al., 2021). Such headward erosion in sloping areas can cause drainage capture gradually or suddenly, which induces sediments with diverse clay mineral composition from the extended catchment (Fan et al., 2021; He et al., 2024; Zhang et al., 2022b). Consequently, these climate-driven dynamics on land collectively shape the clay mineral signals delivered to the ECMS.

6.4.3. Anthropogenic modifications in river systems: source erosion and river transport

Influences of human activities are mainly manifested in source erosion and fluvial transport capabilities, thereby resulting in the mixing proportions of clay mineral assemblages in the land-sea transition zones. In the eastern China, particularly in the Yangtze Delta and the Hangzhou Bay, anthropogenic modifications began since Neolithic Period in the early Holocene (~10 ka) (Li et al., 2024b; Zhang et al., 2022a). There was no obvious influence from human activities until the past 2 ka when the agricultural productivity and population developed (Hoffmann et al., 2010; Kemp et al., 2020). Agricultural activities have modified the land cover, resulted in soil erosion that introduces more fine-grained sediment flux to the river basin (Jenny et al., 2019; Zhang et al., 2022a). Over the past 100 years, a series of engineering projects have been established around river systems and coastal areas (e.g., reservoirs, dams, large bridges) (Bianchi et al., 2024; Wang et al., 2011). For example, recent sediment from the Zhejiang-Fujian coastal area exhibits a fining trend and decreasing contribution from the Yangtze River after the Three Gorges Dam impoundment (Wang et al., 2008; Xu et al., 2016). Collectively, human-induced changes in sediment contributions must be considered when interpreting clay mineral records from modern and ancient rivers.

6.4.4. Sea-level and ocean dynamic impacts on river catchment, estuarine, and marginal sea environment: provenance, transport pathway and preservation controls

The strong tidal effect modified the neritic seafloor as the sea level rose. Since the last deglaciation, tidal-related landforms have formed in areas such as the outer ECS shelf, the Yangtze Estuary, southeastern YS, and the Shandong Peninsula (Berné et al., 2002; Uehara and Saito, 2003; Xue et al., 2018b). Thus previously deposited sediments on the exposed shelf can be reworked and retransported (Fagel, 2024; Rao et al., 2017; Jia et al., 2012). Furthermore, the tidal effect spreads the impact from sea-level change onto the land through river estuaries and lower

Table 5
Comparisons between typical continental shelf regions discussed in this study.

Region	Climate	Average depth (m)	Continental shelf width (km)	River-borne sediment flux (Mt/a)	Oceanic currents	Typical mud depocenter	Clay mineral assemblages	References
Bay of Bengal	Tropic, monsoon	2586	~160	>1000	Monsoon Current and East India Coastal Current	The Bengal Fan	Illite, chlorite and kaolinite	Borromeo et al., 2019; Goodbred Jr and Kuehl, 2000
Gulf of Mexico	Tropic-subtropic, humid	1512	10-320	~488	Gulf Stream	The Texas Mud Blanket	Illite-dominated	Bernardes et al., 2012; Weight et al., 2011
Arctic Ocean	Polar, cold	1296	100-1000	~315	Beaufort Gyre and Transpolar Drift	Mainly distributed in deep shelf area	Predominantly illite and chlorite	Eidam et al., 2025
ECMS	Subtropic-temperate, monsoon	370	~550	>1000	Kuroshio Current and monsoon-driven coastal currents	The ECS mud belt	Illite-dominated or smectite-dominated	Gao and Collins, 2014; Liu et al., 2016a; Qiao et al., 2017; Zhao et al., 2018a

reaches. Mountainous rivers in southeastern China have tens to over one hundred kilometers of tidal reaches on their coastal plains (Fujian Province Local Chronicles Compilation Committee, 2001; Zhejiang Water Resources Department, 2020; Chen et al., 2024; Tu et al., 2014). As a result, fluvial sediment samples do not entirely represent signals of the river itself in the lower reach where tidal effect exists (Liu et al., 2018a; Wang et al., 2024; Xue et al., 2018a). Furthermore, tidal-induced changes in fluid dynamics and characteristics (velocity, salinity, etc.) lead to various sedimentary behaviors for clay minerals such as flocculation and settling (Khojasteh et al., 2020; Schieber et al., 2023; Schieber and Yawar, 2025).

The formation of coastal circulation systems around the ECMS since 8 ka has been a combined effects of sea level fluctuation and monsoon climate (Li et al., 2009; Xu et al., 2023a). The East Asian summer monsoon reached a maximum intensity in the early Holocene, enhancing precipitation in subtropical East Asia (Chen et al., 2017c), as recorded by the stalagmite $\delta^{18}O$ values (Fig. 14) (Chen et al., 2015; Liu et al., 2020). Since then, the hydrodynamic framework in the marginal seas has interacted with river plumes at estuarine areas and has impacted the fine-grained sediment transport (Bernardes et al., 2012; Liu et al., 2021b). Coastal current intensity changes during the high sea-level period not only altered sediment contributions from rivers, but also affect the fine-grained sediment depocenters migration (Hanebuth et al., 2015; Zhang et al., 2020). Evidence from sedimentary rates of the ECS mud shows that the depocenter moves northward to the Yangtze Estuary (Liu et al., 2024; Zhang et al., 2022c), while the sediment production in the Yangtze River basin has intensified in the late Holocene (Dong et al., 2020). The central YS mud formed under circulation-vortex dynamic action, where the sediment contribution from the Yangtze River and Korean rivers plays more influential roles (Hu et al., 2018; Li et al., 2014b; Qiao et al., 2017; Zhang et al., 2020). Our provenance interpretations (mainly revealed by kaolinite/illite values, Fig. 14) suggest an increased sediment contribution from the Zhejiang-Fujian rivers since the middle Holocene, which coincide with decreased sedimentation rates in the muddy depocenter, supporting a weakening of coastal current at that time (Liu et al., 2024; Zhang et al., 2022c) (Fig. 16). The attenuated coastal current also accords with the well-accepted weakening trend of the East Asian winter monsoon (Lu et al., 2024; Sagawa et al., 2014; Zhang et al., 2022c).

6.5. Other continental margin fine-grained sedimentary systems worldwide: comparison with the ECMS

Global eustatic changes during the last glacial period have significantly controlled the sedimentation processes on shallow shelves, such as the Bay of Bengal (Liu et al., 2019b; Sun et al., 2024a), the Gulf of Mexico (Anaya-Gregorio et al., 2018; Davis, 2017), the Arctic continental shelf (Eidam et al., 2025), as well as the ECMS case (Gao and Collins, 2014; Hanebuth et al., 2015). Their dominant transport pathways, depositional settings, and the primary controls on sediment accumulation show obvious differences and similarities (Table 5). For example, the Bay of Bengal features large river systems (the Ganges-Brahmaputra River) and small-to-medium-scale river basins on the Indian Peninsula but has a relatively narrow shelf (Borromeo et al., 2019; Goodbred Jr and Kuehl, 2000; Sun et al., 2024a). Terrestrial sediments from South Asia primarily flow directly into deep seas, thereby developing into submarine fans (Khan et al., 2019; Prajith et al., 2022; Ye et al., 2022). On the western Atlantic coast of North America, relict sediments from the continental shelves were reworked and transported to the shoreline during the Holocene sea level rise, leading to widely distributed barrier islands and lagoons (Bernardes et al., 2012; Gao and Collins, 2014). The Texas Mud Blanket, located in the northern Gulf of Mexico, represents a typical mud depocenter that formed by distal current transport of relict sediments (Weight et al., 2011). Arctic continental shelves exhibit similar transport pathways of fine-grained sediment by waves and currents as lower-latitude shelves, but are uniquely impacted by ice-driven processes such as ice-rafting, sea-ice keels, and permafrost degradation (Eidam et al., 2025).

The ECMS have witnessed the coupling of intense East Asian monsoon climate, enormous sediment fluxes from both large rivers and small mountainous rivers, wide and shallow shelf submarine morphology, complex oceanic circulation system, and a long history of human activity (Frings, 2019; Hantoro, 2018; Yang et al., 2014; Yoshimura et al., 2021). It offers an ideal window for deciphering the combined effect of sea-level change, monsoon variability, and river dynamics on sedimentary systems in mid-low-latitude marginal seas. Although the hydrodynamic condition and fine-grained sediment delivery pattern vary among regions (Table 5), the global impact of sea-level rise during the Holocene transgression has left obvious change on these sedimentary systems (Liu et al., 2019b; Reed and William, 2010; Shi et al., 2021). How the fine-grained sediment depocenters worldwide have developed and evolved under different tectonic, climatic, and oceanographic settings, and how the interplay between global sea-level forcing and climate-driven terrestrial sediment outputs have shaped the continental margin sedimentary systems since the last glacial period, remain important questions that deserve further comparative studies.

6.6. Implications

6.6.1. Implications for future study of detrital clay mineralogy

We have realized that the clay mineral analytical methods, procedures, and raw data interpretations for surface and core sediments vary across previous studies. When comparing clay mineral data from different sources, it is necessary to ensure consistency in analytical methods. For example, pre-treatments utilizing 0.5 mol/L (Liu et al., 2014; Xu et al., 2024) to 1 mol/L HCl (Shan et al., 2023) or 6% (Chen et al., 2017a) to 25% acetic acid (Shi et al., 2024; Zhang et al., 2019) are applied to remove carbonates in different studies. Some recent studies have argued that high acid concentrations (e.g., >1mol/L HCl) can cause excessive removal of carbonate components and lead to dissolution of certain kinds of clay minerals (Hu et al., 2022; Lai et al., 2025). Systematic methodological validations, specifically concerning optimal concentration, reaction time, and calibration of XRD data from different treatments, are needed for standardized analysis and comparison in the field of detrital clay mineralogy. The compiled clay mineral dataset in this study can provide verifiable references from various research approaches for future studies.

Our findings indicate that clastic rocks provide the majority of clay minerals to the fine-grained sedimentary systems in the ECMS (Fig. 13). Thus, the response of clay mineral proxies to climate change not only includes the newly-formed weathering products, but also the recycled clay minerals that inherit the weathering effect from the previous sedimentary cycles. Considering the lithological influence on clay mineral production, we suggest that the relationship between multiple clay-mineral based weathering indicators, rather than absolute values of a single parameter, can provide a more robust weathering intensity evaluation accounting for parent rock composition. In studies where the source bedrock types are not clear, a high proportion of illite with a low KI value in sediment samples likely indicates recycled illite from sedimentary strata (Fig. 13). The characteristics of inherited clay minerals from sedimentary strata, and their differences to newly-formed clay minerals under modern climate and geologic settings deserve more attention in future works.

6.6.2. Implications for sediment source-to-sink system studies in the mid-low latitude Asian continental margin

The regional perspective and big data compilation employed in this contribution are worthy of promotion in sediment source-to-sink system studies for the mid-low latitude continental margins. In modern situations, accelerated sea-level rise (Lin et al., 2025), frequent extreme weather events (Chen et al., 2025; Wei et al., 2025), and increasingly prominent anthropogenic impacts (Hoffmann et al., 2010; Li et al., 2024b) introduce challenges in this field. Anthropogenic impacts, such as river channel modification, sluices and dams construction, land reclamation, and soil erosion, further complicate the quantitative assessment of sediment flux from modern and historical perspectives (Bianchi et al., 2024; Greenberg and Ganti, 2024; Hoffmann et al., 2010; Qiao et al., 2017). Thus, it is essential to identify appropriate analogues that represent past fluvial inputs for specific time intervals. Integrating multiple sedimentary proxies in marine sedimentology research requires a clearer understanding of terrestrial sediment output signals and their controlling mechanisms. This contribution provides a regional compilation of clay mineral proxies that can be applied in future multi-proxy investigations. Furthermore, organic matter and pollutants that are transported to marginal seas by rivers interact with clay minerals particles (Bianchi et al., 2024; Blattmann et al., 2019; Yuan et al., 2013). Investigating these interactions under varying environmental conditions—temperature, salinity, fluid velocity, and sediment concentration—are suggested to be included in future researches. It contributes to a deeper understanding of the Earth's carbon cycle and related environmental changes in land-sea transition zones, both in the past and future.

6.6.3. Implications for deep-time sediment source-to-sink system studies and paleoclimate reconstruction

Our findings on the complex climatic records over the last glaciation further indicate that deep-time sedimentary studies should be more cautious of the variability in sedimentary proxies that respond to signals from the source areas. It remains challenging to utilize clay mineral proxies in tracing sediment provenance and evaluating paleoclimate in deep-time studies with source areas poorly constrained. A comprehensive perspective from the sediment source-to-sink system is crucial to clastic-sediment-based paleoclimate reconstruction that includes climate, provenance, transport agents, and depositional environments (Bi et al., 2015; Liu et al., 2023b). We further argue that weathering intensity evaluation based on clay minerals is often decoupled from local climate conditions in sedimentary basins (Chen et al., 2014; Fagel, 2024; Fu et al., 2022; Wang et al., 2023). To avoid ambiguous interpretations in paleoclimate reconstruction, distinguishing influences of non-weathering factors on each sedimentary proxy is therefore important. Multi-proxy analysis across spatially distributed sediment cores is recommended to better reveal sediment sources and transport pathways through time, thereby strengthening paleoenvironmental interpretations.

7. Conclusions and prospects

We have combined our newly obtained clay mineral data from the sediment core QTZ3 in the Oujiang Delta with previously published data (458 modern river sediment samples, 2101 marginal sea surface sediment samples, and 2871 samples from 19 sediment cores). Our results indicate that the clay minerals in the ECMS sediments are primarily derived from sedimentary rocks that produce inherited and further weathered minerals, rather than newly-formed weathered products. The temporal and spatial distributions of clay mineral proxies (smectite/illite, kaolinite/illite, chemical index, crystallinity index, etc.) exhibit various sensitivities to changes in climate, parent rock lithology, and sedimentary environment. Terrestrial sediment signals are inconstant during the glacial cycles due to the combined effect of climatic changes. The sediment core data compilation indicates the attenuated Yangtze River signals in the ECS mud belt during the middle-late Holocene, supporting the idea that coastal currents have weakened during the high sea-level period (Fig. 16).

Our findings emphasize that the clay-mineral-based paleo-weathering and paleoclimatic reconstruction involves climatic conditions across sediment sources, transport agents, and depositional environments. This contribution is an important step towards a better understanding of sedimentary processes in one of the most unique and typical marginal seas around the world and is applicable to global continental margin systems. Further multi-proxy comparative studies on these fine-grained sedimentary systems are thus valuable to answer how they have developed and evolved under different backgrounds. Our findings also have significant implications for understanding detrital clay mineralogical proxies, modern sediment source-to-sink system investigations, and deep-time paleoclimate reconstruction.

Declaration of competing interest

The authors declare that they have no known competing financial interests or personal relationships that could have appeared to influence the work reported in this paper.

Acknowledgements

This research was supported by the National Natural Science Foundation of China (Nos. 42476051, 41806052) and the Natural Science Foundation of Xiamen, China (No. 3502Z20227006). We sincerely thank those who involved in the obtainment and analysis of sediment cores and the authors who provided us with the original data of their researches. We also thank previous and current graduate students Hanghai Liang, Dongming Hong, Shuo Zhang, Xiaotian Shen, Shuhuai Ye, and Siyuan Fang from Xiamen University for their contributions to laboratory work and fruitful discussions. We greatly appreciate the constructive reviews of two anonymous reviewers for improving the final manuscript.

Appendix A. Supplementary data

Supplementary data to this article can be found online at https://doi.org/10.1016/j.earscirev.2026.105687.

Data availability

I have shared the data in supplementary materials at the Attach File step

References

An, Y., Liu, J., Zhang, J., Chen, B., Chen, L., Zhang, X., Sheng, C., 2020. Comparative researches on the provenance indicators of Huaihe River, Yangtze River and Yellow River sediment. Quat. Sci. 40, 837–850 (in Chinese). 10.11928/j.issn.1001-7410.2020.03.20.

Anaya-Gregorio, A., Armstrong-Altrin, J.S., Machain-Castillo, M.L., Montiel-García, P.C., Ramos-Vázquez, M.A., 2018. Textural and geochemical characteristics of late Pleistocene to Holocene fine-grained deep-sea sediment cores (GM6 and GM7), recovered from southwestern Gulf of Mexico. J. Palaeogeogr. 7, 3. https://doi.org/10.1186/s42501-018-0005-3.

Anderson, C.H., Murray, R.W., Dunlea, A.G., Giosan, L., Kinsley, C.W., McGee, D., Tada, R., 2018. Climatically driven changes in the supply of terrigenous sediment to the East China Sea. Geochem. Geophys. Geosyst. 19, 2463–2477. https://doi.org/10.1029/2017GC007339.

Barbier, E.B., 2015. Climate change impacts on rural poverty in low-elevation coastal zones. Estuar. Coast. Shelf Sci. 165, A1–A13. https://doi.org/10.1016/j.ecss.2015.05.035.

Barbier, E.B., Hacker, S.D., Kennedy, C., Koch, E.W., Stier, A.C., Silliman, B.R., 2011. The value of estuarine and coastal ecosystem services. Ecol. Monogr. 81, 169–193. https://doi.org/10.1890/10-1510.1.

Barceló, M., Vargas, C.A., Gelcich, S., 2023. Land–sea interactions and ecosystem services: research gaps and future challenges. Sustainability 15, 8068. https://doi.org/10.3390/su15108068.

Bayon, G., Patriat, M., Godderis, Y., Trinquier, A., De Deckker, P., Kulhanek, D.K., Holbourn, A., Rosenthal, Y., 2023. Accelerated mafic weathering in Southeast Asia linked to late Neogene cooling. Sci. Adv. 9, eadf3141. https://doi.org/10.1126/sciadv.adf3141.

Bernardes, M.C., Knoppers, B.A., Rezende, C.E., Souza, W.F.L., Ovalle, A.R.C., 2012. Land-sea interface features of four estuaries on the South America Atlantic coast. Braz. J. Biol. 72, 761–774. https://doi.org/10.1590/S1519-69842012000400011.

Berné, S., Vagner, P., Guichard, F., Lericolais, G., Liu, Z., Trentesaux, A., Yin, P., Yi, H.I., 2002. Pleistocene forced regressions and tidal sand ridges in the East China Sea. Mar. Geol. 188, 293–315. https://doi.org/10.1016/S0025-3227(02)00446-2.

Bertaz, J., Liu, Z., Colin, C., Dapoigny, A., Lin, A.T.-S., Li, Y., Jian, Z., 2024. Climatic and environmental impacts on the sedimentation of the SW Taiwan margin since the last deglaciation: geochemical and mineralogical investigations. Paleoceanogr. Paleoclimatol. 39, e2023PA004745. https://doi.org/10.1029/2023PA004745.

Bi, L., Yang, S., Li, C., Guo, Y., Wang, Q., Liu, J.T., Yin, P., 2015. Geochemistry of river-borne clays entering the East China Sea indicates two contrasting types of weathering and sediment transport processes. Geochem. Geophys. Geosyst. 16, 3034–3052. https://doi.org/10.1002/2015GC005867.

Bi, L., Yang, S., Zhao, Y., Wang, Z., Dou, Y., Li, C., Zheng, H., 2017. Provenance study of the Holocene sediments in the Changjiang (Yangtze River) estuary and inner shelf of the East China sea. In: Quaternary International, Environmental and Climatic Changes Inferred from Sedimentary Records on Asian Shelf Margins: Part II, 441, pp. 147–161. https://doi.org/10.1016/j.quaint.2016.12.004.

Bianchi, T.S., Mayer, L.M., Amaral, J.H.F., Arndt, S., Galy, V., Kemp, D.B., Kuehl, S.A., Murray, N.J., Regnier, P., 2024. Anthropogenic impacts on mud and organic carbon cycling. Nat. Geosci. 17, 287–297. https://doi.org/10.1038/s41561-024-01405-5.

Biscaye, P.E., 1965. Mineralogy and sedimentation of recent deep-sea clay in the Atlantic Ocean and adjacent seas and oceans. GSA Bull. 76, 803–832.

Blattmann, T.M., Liu, Z., Zhang, Y., Zhao, Y., Haghipour, N., Montluçon, D.B., Plötze, M., Eglinton, T.I., 2019. Mineralogical control on the fate of continentally derived organic matter in the ocean. Science 366, 742–745. https://doi.org/10.1126/science.aax5345.

Borromeo, L., Andò, S., France-Lanord, C., Coletti, G., Hahn, A., Garzanti, E., 2019. Provenance of Bengal shelf sediments: 1. Mineralogy and geochemistry of silt. Minerals 9, 640. https://doi.org/10.3390/min9100640.

Cai, G., Li, S., Zhao, L., Zhong, L., Chen, H., 2020. Clay minerals, Sr-Nd isotopes and provenance of sediments in the northwestern South China Sea. J. Asian Earth Sci. 202, 104531. https://doi.org/10.1016/j.jseaes.2020.104531.

Cao, L., Shao, L., van Hinsbergen, D.J.J., Jiang, T., Xu, D., Cui, Y., 2023. Provenance and evolution of East Asian large rivers recorded in the East and South China Seas: a review. GSA Bull. 135, 2723–2752. https://doi.org/10.1130/B36559.1.

Chamley, H., 1989. Clay minerals. In: Chamley, H. (Ed.), Clay Sedimentology. Springer, Berlin, Heidelberg, pp. 3–20. https://doi.org/10.1007/978-3-642-85916-8_1.

Chandana, K.R., Banerji, U.S., Bhushan, R., 2018. Review on Indian Summer Monsoon (ISM) reconstruction since LGM from Northern Indian Ocean. Earth Sci. India XI 71–84.

Chen, Y., Syvitski, J.P.M., Gao, S., Overeem, I., Kettner, A.J., 2012. Socio-economic impacts on flooding: a 4000-year history of the Yellow River, China. AMBIO 41, 682–698. https://doi.org/10.1007/s13280-012-0290-5.

Chen, J., Wang, Z., Wei, T., Zhao, B., Chen, Z., 2014. Clay minerals in the Pliocene–Quaternary sediments of the southern Yangtze coast, China: sediment sources and palaeoclimate implications. J. Palaeogeogr. 3, 297–308. https://doi.org/10.3724/SP.J.1261.2014.00057.

Chen, F., Xu, Q., Chen, J., Birks, H.J.B., Liu, J., Zhang, S., Jin, L., An, C., Telford, R.J., Cao, X., Wang, Z., Zhang, X., Selvaraj, K., Lu, H., Li, Y., Zheng, Z., Wang, H., Zhou, A., Dong, G., Zhang, J., Huang, X., Bloemendal, J., Rao, Z., 2015. East Asian summer monsoon precipitation variability since the last deglaciation. Sci. Rep. 5, 11186. https://doi.org/10.1038/srep11186.

Chen, J., Ma, J., Xu, K., Liu, Y., Cao, W., Wei, T., Zhao, B., Chen, Z., 2017a. Provenance discrimination of the clay sediment in the western Taiwan Strait and its implication for coastal current variability during the late-Holocene. The Holocene 27, 110–121. https://doi.org/10.1177/0959683616652706.

Chen, L., Liu, J., Xing, L., Krauss, K.W., Wang, J., Xu, G., Li, L., 2017b. Historical changes in organic matter input to the muddy sediments along the Zhejiang-Fujian Coast, China over the past 160 years. Org. Geochem. 111, 13–25. https://doi.org/10.1016/j.orggeochem.2017.06.003.

Chen, Q., Liu, Z., Kissel, C., 2017c. Clay mineralogical and geochemical proxies of the East Asian summer monsoon evolution in the South China Sea during Late Quaternary. Sci. Rep. 7, 42083. https://doi.org/10.1038/srep42083.

Chen, Y.-H., Su, C.-C., Yu, P.-S., Hsu, T.-W., Hsu, S.-T., Juan, H.-C., Chang, Y.-P., Ma, Y.-F., Chiu, S.-D., 2025. Sedimentary signatures of super Typhoon Haiyan: insight from core record in South China Sea. J. Mar. Sci. Eng. 13, 10. https://doi.org/10.3390/jmse13010010.

Chen, Y., Zhu, G., Lin, X., Wu, F., 2024. The changes of nitrogen and phosphorus contents and their occurrence forms in surface water as affected by flood tide and ebb tide in the tidal reach of the Minjiang River. Acta Sci. Circumst. 516–525 (in Chinese). 10.13671/j.hjkxxb.2023.0237.

Cho, H.-G., Kim, S.-O., Yi, H.-I., 2012. Clay mineral distribution and characteristics in the Southeastern Yellow Sea Mud Deposits. J. Mineral. Soc. Korea 25, 163–173. https://doi.org/10.9727/jmsk.2012.25.3.163.

Cong, J., Hu, G., Jonell, T.N., Zhang, Y., Li, Y., Bi, S., 2021. Source-to-sink and evolutionary processes of the East China Sea inner-shelf mud belt and its response to environmental changes since the Holocene: new evidence from the distal mud belt. The Holocene 31, 1071–1088. https://doi.org/10.1177/09596836211003202.

Cuadros, J., 2017. Clay minerals interaction with microorganisms: a review. Clay Miner. 52, 235–261. https://doi.org/10.1180/claymin.2017.052.2.05.

Dai, L., Weng, C., Mao, L., 2015. Patterns of vegetation and climate change in the northern South China Sea during the last glaciation inferred from marine palynological records. Palaeogeogr. Palaeoclimatol. Palaeoecol. 440, 249–258. https://doi.org/10.1016/j.palaeo.2015.08.041.

Davis, R.A., 2017. Sediments of the Gulf of Mexico. In: Ward, C.H. (Ed.), Habitats and Biota of the Gulf of Mexico: Before the Deepwater Horizon Oil Spill: Volume 1: Water Quality, Sediments, Sediment Contaminants, Oil and Gas Seeps, Coastal Habitats, Offshore Plankton and Benthos, and Shellfish. Springer, New York, NY, pp. 165–215. https://doi.org/10.1007/978-1-4939-3447-8_3.

Deepthy, R., Balakrishnan, S., 2005. Climatic control on clay mineral formation: evidence from weathering profiles developed on either side of the Western Ghats. J. Earth Syst. Sci. 114, 545–556. https://doi.org/10.1007/BF02702030.

Deng, K., Yang, S., Huang, X., Xu, J., 2018. The comparison of detrital zircon geochronology between mountainous rivers in Eastern China and its implications for marine sediment provenance. Mar. Geol. Quat. Geol. 38, 178–186 (in Chinese). 10.16562/j.cnki.0256-1492.2018.01.018.

Denton, G.H., Anderson, R.F., Toggweiler, J.R., Edwards, R.L., Schaefer, J.M., Putnam, A.E., 2010. The Last glacial termination. Science 328, 1652–1656. https://doi.org/10.1126/science.1184119.

Dianto, A., Subehi, L., Ridwansyah, I., Hantoro, W.S., 2019. Clay minerals in the sediments as useful paleoclimate proxy: lake sentarum case study, West Kalimantan, Indonesia. IOP Conf. Ser. Earth Environ. Sci. 311 (1), 012036. https://doi.org/10.1088/1755-1315/311/1/012036.

Ding, D., Zhang, X., Yu, J., Wang, X., 2019. Progress in sedimentary sources and palaeoclimate evolution in Zhejiang-Fujian Mud Area in Holocene. J. Jilin Univ. (Earth Sci. Ed.) 49, 178–195 (in Chinese). 10.13278/j.cnki.jjuese.20180114.

Dong, J., Li, A., Liu, X., Wan, S., Xu, F., Shi, X., 2020. Holocene climate modulates mud supply, transport, and sedimentation on the East China Sea shelf. J. Geophys. Res.: Earth Surf. 125, e2020JF005731. https://doi.org/10.1029/2020JF005731.

Dou, Y., Li, J., Zhao, J., Wei, H., Yang, S., Bai, F., Zhang, D., Ding, X., Wang, L., 2014. Clay mineral distributions in surface sediments of the Liaodong Bay, Bohai Sea and surrounding river sediments: sources and transport patterns. Cont. Shelf Res. 73, 72–82. https://doi.org/10.1016/j.csr.2013.11.023.

Dou, Y., Yang, S., Shi, X., Clift, P.D., Liu, S., Liu, J., Li, C., Bi, L., Zhao, Y., 2016. Provenance weathering and erosion records in southern Okinawa Trough sediments since 28 ka: geochemical and Sr–Nd–Pb isotopic evidences. Chem. Geol. 425, 93–109. https://doi.org/10.1016/j.chemgeo.2016.01.029.

Dou, R., Zou, J., Shi, X., Zhu, A., Dong, Z., Zou, X., Gorbarenko, S., 2022. Provenance discrimination of siliciclastic sediments in the Western Sea of Japan over the Past 30 kyr: evidence from major, trace elements, and Pb Isotopes. Lithosphere 2022, 6405238. https://doi.org/10.2113/2022/6405238.

Dykoski, C.A., Edwards, R.L., Cheng, H., Yuan, D., Cai, Y., Zhang, M., Lin, Y., Qing, J., An, Z., Revenaugh, J., 2005. A high-resolution, absolute-dated Holocene and deglacial Asian monsoon record from Dongge Cave, China. Earth Planet. Sci. Lett. 233, 71–86. https://doi.org/10.1016/j.epsl.2005.01.036.

Eidam, E.F., Stark, N., Nienhuis, J.H., Keogh, M., Obelcz, J., 2025. Arctic continental-shelf sediment dynamics. Annu. Rev. Mar. Sci. 17, 435–460. https://doi.org/10.1146/annurev-marine-040423-023827.

Esquevin, J., 1969. Influence de la composition chimique des illites sur leur cristallinité. Bull. Centre Rech. Pau-SNPA 3, 147.

Fagel, N., 2007. Chapter four clay minerals, deep circulation and climate. In: Hillaire-Marcel, C., De Vernal, A. (Eds.), Developments in Marine Geology, Proxies in Late Cenozoic Paleoceanography. Elsevier, pp. 139–184. https://doi.org/10.1016/S1572-5480(07)01009-3.

Fagel, N., 2024. Climatic significance of clay minerals in Cenozoic marine and lacustrine sediments. Clay Miner. 59, 228–257. https://doi.org/10.1180/clm.2024.17.

Fan, D., Shang, S., Burr, G., 2019. Sea level implications from Late Quaternary/Holocene paleosols from the Oujiang Delta, China. Radiocarbon 61, 83–99. https://doi.org/10.1017/RDC.2018.77.

Fan, N., Kong, P., Robl, J.C., Zhou, H., Wang, X., Jin, Z., Liu, X., 2021. Timing of river capture in major Yangtze River tributaries: insights from sediment provenance and morphometric indices. Geomorphology 392, 107915. https://doi.org/10.1016/j.geomorph.2021.107915.

Frings, P.J., 2019. Palaeoweathering: How do weathering rates vary with climate? Elements 15, 259–265. https://doi.org/10.2138/gselements.15.4.259.

Fu, H., 2025. Chemical Weathering Intensity Evaluation in River Sediment Source-to-sink Systems: Assessment and Verification of Weathering Indices, (PHD thesis). Xiamen University (in Chinese).

Fu, H., Jian, X., Liang, H., Zhang, W., Shen, X., Wang, L., 2022. Tectonic and climatic forcing of chemical weathering intensity in the northeastern Tibetan Plateau since the middle Miocene. CATENA 208, 105785. https://doi.org/10.1016/j.catena.2021.105785.

Fu, H., Jian, X., Pan, H., 2023. Bias in sediment chemical weathering intensity evaluation: a numerical simulation study. Earth Sci. Rev. 246, 104574. https://doi.org/10.1016/j.earscirev.2023.104574.

Fu, H., Jian, X., Zhang, Z., Pan, H., 2025. Source-rock, grain-size, weathering, and recycling controls on the feldspar/quartz ratio in silt-sized sediments. Palaeogeogr. Palaeoclimatol. Palaeoecol. 660, 112700. https://doi.org/10.1016/j.palaeo.2024.112700.

Fujian Province Local Chronicles Compilation Committee, 2001. Annals of Fujian Province. Local Chronicles Publishing House, Beijing.

Galán, E., 2006. Chapter 14 genesis of clay minerals. In: Bergaya, F., Theng, B.K.G., Lagaly, G. (Eds.), Developments in Clay Science, Handbook of Clay Science. Elsevier, pp. 1129–1162. https://doi.org/10.1016/S1572-4352(05)01042-1.

Galán, E., Ferrell, R.E., 2013. Genesis of clay minerals. In: Developments in Clay Science. Elsevier, pp. 83–126. https://doi.org/10.1016/B978-0-08-098258-8.00003-1.

Gao, S., 2013. Holocene shelf-coastal sedimentary systems associated with the Changjiang River: an overview. Acta Oceanol. Sin. 32, 4–12. https://doi.org/10.1007/s13131-013-0390-5.

Gao, S., Collins, M.B., 2014. Holocene sedimentary systems on continental shelves. Mar. Geol. 352, 268–294. https://doi.org/10.1016/j.margeo.2014.03.021, 50th Anniversary Special Issue.

Gao, S., Zhou, X., Jia, J., 2004. Clay mineral suites of the coastal mud belt associated with the changjiang river. Revista de la Asociación Argentina de Sedimentología 11, 1–8.

Gao, X., Li, C., Duan, Z., Guo, Y., Yang, S., 2025. Sr-Nd isotopic characteristics and their significance in provenance tracing of detrital sediment in major rivers and marginal seas of eastern China. Sci. China Earth Sci. 68, 523–537. https://doi.org/10.1007/s11430-024-1464-5.

Garzanti, E., 2017. The maturity myth in sedimentology and provenance analysis. J. Sediment. Res. 87, 353–365. https://doi.org/10.2110/jsr.2017.17.

Garzanti, E., He, J., Barbarano, M., Resentini, A., Li, C., Yang, L., Yang, S., Wang, H., 2021. Provenance versus weathering control on sediment composition in tropical monsoonal climate (South China) - 2. Sand petrology and heavy minerals. Chem. Geol. 564, 119997. https://doi.org/10.1016/j.chemgeo.2020.119997.

Garzanti, E., Nayak, K., Padoan, M., Vezzoli, G., Resentini, A., Castelltort, S., Lin, A.T.-S., Babonneau, N., Ratzov, G., Hsu, S.-K., Huang, K.-F., 2023. Fast-eroding Taiwan and transfer of orogenic sediment to forearc basins and trenches in the Philippine and South China seas. Earth Sci. Rev. 244, 104523. https://doi.org/10.1016/j.earscirev.2023.104523.

Gingele, F.X., De Deckker, P., Hillenbrand, C.-D., 2001. Clay mineral distribution in surface sediments between Indonesia and NW Australia—source and transport by ocean currents. Mar. Geol. 179 (3–4), 135–146.

Goodbred Jr., S.L., Kuehl, S.A., 2000. Enormous Ganges-Brahmaputra sediment discharge during strengthened early Holocene monsoon. Geology 28, 1083–1086. https://doi.org/10.1130/0091-7613(2000)28%3C1083:EGSDDS%3E2.0.CO;2.

Grant, K.M., Rohling, E.J., Ramsey, C.B., Cheng, H., Edwards, R.L., Florindo, F., Heslop, D., Marra, F., Roberts, A.P., Tamisiea, M.E., Williams, F., 2014. Sea-level variability over five glacial cycles. Nat. Commun. 5, 5076. https://doi.org/10.1038/ncomms6076.

Greenberg, E., Ganti, V., 2024. The pace of global river meandering influenced by fluvial sediment supply. Earth Planet. Sci. Lett. 634, 118674. https://doi.org/10.1016/j.epsl.2024.118674.

Grotzinger, J., Jordan, T., 2014. Understanding Earth, 7th ed. Macmillan Education, New York.

Guang, X., Yin, P., Cao, K., Gao, F., Tian, Y., Huang, X., Chen, B., Li, M., Liu, J., 2025. Impact of the Yangtze River on sediment source-to-sink processes in estuarine bays: a study of the Oujiang River Estuary, SE China. Front. Mar. Sci. 12. https://doi.org/10.3389/fmars.2025.1561138.

Guiot, J., Hai Bin, Wu, Jiang, Wen Ying, Luo, Yun Li, 2008. East Asian Monsoon and paleoclimatic data analysis: a vegetation point of view. Clim. Past 4, 137–145. https://doi.org/10.5194/cp-4-137-2008.

Guo, Y., Li, C., Wang, C., Xu, J., Jin, C., Yang, S., 2021. Sediment routing and anthropogenic impact in the huanghe river catchment, china: an investigation using Nd isotopes of river sediments. Water Resour. Res. 57, e2020WR028444. https://doi.org/10.1029/2020WR028444.

Guyot, J.L., Jouanneau, J.M., Soares, L., Boaventura, G.R., Maillet, N., Lagane, C., 2007. Clay mineral composition of river sediments in the Amazon Basin. CATENA Soil Water Erosion Rural Areas 71, 340–356. https://doi.org/10.1016/j.catena.2007.02.002.

Hanebuth, T.J.J., Lantzsch, H., Nizou, J., 2015. Mud depocenters on continental shelves—appearance, initiation times, and growth dynamics. Geo-Mar. Lett. 35, 487–503. https://doi.org/10.1007/s00367-015-0422-6.

Hantoro, W.S., 2018. Sunda epicontinental shelf and Quaternary glacial-interglacial sea level variation and their implications to the regional and global environmental change. IOP Conf. Ser.: Earth Environ. Sci 118, 012053. https://doi.org/10.1088/1755-1315/118/1/012053.

Hazen, R.M., Sverjensky, D.A., Azzolini, D., Bish, D.L., Elmore, S.C., Hinnov, L., Milliken, R.E., 2013. Clay mineral evolution. Am. Mineral. 98, 2007–2029. https://doi.org/10.2138/am.2013.4425.

He, M., Zheng, H., Huang, X., Jia, J., Li, L., 2013. Yangtze River sediments from source to sink traced with clay mineralogy. J. Asian Earth Sci. New Glob. Perspect. Paleontol. Stratigr. Paleoceanogr. Paleoclimatol. Tecton. East Asia West. Pacific 69, 60–69. https://doi.org/10.1016/j.jseaes.2012.10.001.

He, C., Braun, J., Tang, H., Yuan, X., Acevedo-Trejos, E., Ott, R.F., Stucky de Quay, G., 2024. Drainage divide migration and implications for climate and biodiversity. Nat. Rev. Earth Environ. 5, 177–192. https://doi.org/10.1038/s43017-023-00511-z.

Hoffmann, T., Thorndycraft, V.R., Brown, A.G., Coulthard, T.J., Damnati, B., Kale, V.S., Middelkoop, H., Notebaert, B., Walling, D.E., 2010. Human impact on fluvial regimes and sediment flux during the Holocene: review and future research agenda. Glob. Planet. Chang. 72, 87–98. https://doi.org/10.1016/j.gloplacha.2010.04.008.

Hori, K., Saito, Y., Zhao, Q., Cheng, X., Wang, P., Sato, Y., Li, C., 2001. Sedimentary facies of the tide-dominated paleo-Changjiang (Yangtze) estuary during the last transgression. Mar. Geol. 177, 331–351. https://doi.org/10.1016/S0025-3227(01)00165-7.

Hu, B., Li, G., Li, J., Bi, J., Zhao, J., Bu, R., 2012. Provenance and climate change inferred from Sr–Nd–Pb isotopes of late Quaternary sediments in the Huanghe (Yellow River) Delta, China. Quat. Res. 78, 561–571. https://doi.org/10.1016/j.yqres.2012.07.005.

Hu, B., Yang, Z., Qiao, S., Zhao, M., Fan, D., Wang, H., Bi, N., Li, J., 2014. Holocene shifts in riverine fine-grained sediment supply to the East China Sea Distal Mud in response to climate change. The Holocene 24, 1253–1268. https://doi.org/10.1177/0959683614540963.

Hu, B., Li, J., Zhao, J., Yan, H., Zou, L., Bai, F., Xu, F., Yin, X., Wei, G., 2018. Sr–Nd isotopic geochemistry of Holocene sediments from the South Yellow Sea: implications for provenance and monsoon variability. Chem. Geol. 479, 102–112. https://doi.org/10.1016/j.chemgeo.2017.12.033.

Hu, B., Zhang, C., Zhang, X., 2022. The effects of hydrochloric acid pretreatment on different types of clay minerals. Minerals 12. https://doi.org/10.3390/min12091167.

Huang, C.-Y., Yen, Y., Zhao, Q., Lin, C.-T., 2012. Cenozoic stratigraphy of Taiwan: window into rifting, stratigraphy and paleoceanography of South China Sea. Chin. Sci. Bull. 57, 3130–3149. https://doi.org/10.1007/s11434-012-5349-y.

Huang, J., Wan, S., Zhang, J., Liu, J., Mei, X., Hu, B., Dong, J., Zhang, X., Li, A., Li, T., 2019. Mineralogical and isotopic evidence for the sediment provenance of the western South Yellow Sea since MIS 3 and implications for paleoenvironmental evolution. Mar. Geol. 414, 103–117. https://doi.org/10.1016/j.margeo.2019.05.011.

Jenny, J.-P., Koirala, S., Gregory-Eaves, I., Francus, P., Niemann, C., Ahrens, B., Brovkin, V., Baud, A., Ojala, A.E.K., Normandeau, A., Zolitschka, B., Carvalhais, N., 2019. Human and climate global-scale imprint on sediment transfer during the Holocene. Proc. Natl. Acad. Sci. U.S.A. 116, 22972–22976. https://doi.org/10.1073/pnas.1908179116.

Jia, L., Mao, J., Zheng, W., 2020. Geochronology, geochemistry, and Sr–Nd–Hf–O isotopes of the Zhongqiuyang rhyolitic tuff in eastern Guangdong, SE China: constraints on petrogenesis and tectonic setting. Geol. J. 55, 5082–5100. https://doi.org/10.1002/gj.3702.

Jia, J., Zhang, X., Zhou, R., Meadows, M., Sengupta, D., Zhu, L., 2021. Sources of sediment in tidal flats off Zhejiang coast, southeast China. J. Oceanol. Limnol. 39, 1245–1255. https://doi.org/10.1007/s00343-020-0179-2.

Jia, P., Zhuang, Z., Ye, Y., Cao, Z., Cai, Q., 2012. Sedimentary strata after last glacial maximum on central and South East China Sea shelf and environmental evolution. Mar. Geol. Front. 28, 20–26 (in Chinese). 10.16028/j.1009-2722.2012.08.007.

Jian, Z., Wang, P., Saito, Y., Wang, J., Pflaumann, U., Oba, T., Cheng, X., 2000. Holocene variability of the Kuroshio Current in the Okinawa Trough, northwestern Pacific Ocean. Earth Planet. Sci. Lett. 184, 305–319. https://doi.org/10.1016/S0012-821X(00)00321-6.

Jian, X., Yang, S., Hong, D., Liang, H., Zhang, S., Fu, H., Zhang, W., 2020a. Seasonal geochemical heterogeneity of sediments from a subtropical mountainous river in SE China. Mar. Geol. 422, 106120. https://doi.org/10.1016/j.margeo.2020.106120.

Jian, X., Zhang, W., Yang, S., Kao, S., 2020b. Climate-dependent sediment composition and transport of mountainous rivers in tectonically stable, Subtropical East Asia. Geophys. Res. Lett. 47, e2019GL086150. https://doi.org/10.1029/2019GL086150.

Jiang, D., Wang, H., Drange, H., Lang, X., 2003. Last Glacial Maximum over China: sensitivities of climate to paleovegetation and Tibetan ice sheet. J. Geophys. Res.-Atmos. 108, 4102. https://doi.org/10.1029/2002JD002167.

Jin, L., Shan, X., Vaucher, R., Qiao, S., Wang, C., Liu, S., Wang, H., Fang, X., Bai, Y., Zhu, A., Yao, Z., Shi, X., 2023. Sea-level changes control coastal organic carbon burial in the southern East China Sea during the late MIS 3. Glob. Planet. Chang. 229, 104225. https://doi.org/10.1016/j.gloplacha.2023.104225.

Kao, S.-J., Jan, S., Hsu, S.-C., Lee, T.-Y., Dai, M., 2008. Sediment budget in the Taiwan Strait with high fluvial sediment inputs from mountainous rivers: new observations and synthesis. Terr. Atmos. Ocean. Sci. 19, 525. https://doi.org/10.3319/TAO.2008.19.5.525(Oc).

Kemp, D.B., Sadler, P.M., Vanacker, V., 2020. The human impact on North American erosion, sediment transfer, and storage in a geologic context. Nat. Commun. 11, 6012. https://doi.org/10.1038/s41467-020-19744-3.

Khan, M.H.R., Liu, J., Liu, S., Seddique, A.A., Cao, L., Rahman, A., 2019. Clay mineral compositions in surface sediments of the Ganges-Brahmaputra-Meghna river system of Bengal Basin, Bangladesh. Mar. Geol. 412, 27–36. https://doi.org/10.1016/j.margeo.2019.03.007.

Khojasteh, D., Hottinger, S., Felder, S., De Cesare, G., Heimhuber, V., Hanslow, D.J., Glamore, W., 2020. Estuarine tidal response to sea level rise: the significance of entrance restriction. Estuar. Coast. Shelf Sci. 244, 106941. https://doi.org/10.1016/j.ecss.2020.106941.

Koo, H.J., Cho, H.G., 2020. Changes in detrital sediment supply to the central Yellow Sea since the last deglaciation. Ocean Sci. 16, 1247–1259. https://doi.org/10.5194/os-16-1247-2020.

Koo, H., Lee, Y., Kim, S., Cho, H., 2018. Clay mineral distribution and provenance in surface sediments of Central Yellow Sea Mud. Geosci. J. 22, 989–1000. https://doi.org/10.1007/s12303-018-0019-y.

Kübler, B., Jaboyedoff, M., 2000. Illite crystallinity. Comptes Rendus de l'Académie des Sciences - Series IIA Earth Plan. Sci. 331, 75–89. https://doi.org/10.1016/S1251-8050(00)01395-1.

Kumari, N., Mohan, C., 2021. Basics of clay minerals and their characteristic properties. In: Morari Do Nascimento, G. (Ed.), Clay and Clay Minerals. https://doi.org/10.5772/intechopen.97672. IntechOpen.

Lai, W., Li, C., Ma, S., Guo, Y., Yue, W., He, M., Wan, S., Yang, S., 2025. The impact of different chemical leaching methods on REE and Sr-Nd isotopes analysis of sediment detrital components. Mar. Geol. Quat. Geol. 45, 203–214 (in Chinese). 10.16562/j.cnki.0256-1492.2024020201.

Lambeck, K., 2004. Sea-level change through the last glacial cycle: geophysical, glaciological and palaeogeographic consequences. Comptes Rendus. Géosci. 336, 677–689. https://doi.org/10.1016/j.crte.2003.12.017.

Lambeck, K., Chappell, J., 2001. Sea level change through the last glacial cycle. Science 292, 679–686. https://doi.org/10.1126/science.1059549.

Lambeck, K., Rouby, H., Purcell, A., Sun, Y., Sambridge, M., 2014. Sea level and global ice volumes from the last glacial maximum to the Holocene. Proc. Natl. Acad. Sci. 111, 15296–15303. https://doi.org/10.1073/pnas.1411762111.

Larsen, L.H., Cannon, G.A., Choi, B.H., 1985. East China Sea tide currents. In: Continental Shelf Research, Sediment Dynamics of the Changjiang Estuary and the Adjacent East China Sea, 4, pp. 77–103. https://doi.org/10.1016/0278-4343(85)90023-8.

Laskar, J., Robutel, P., Joutel, F., Gastineau, M., Correia, A.C.M., Levrard, B., 2004. A long-term numerical solution for the insolation quantities of the Earth. A&A 428, 261–285. https://doi.org/10.1051/0004-6361:20041335.

Lewis, S.E., Sloss, C.R., Murray-Wallace, C.V., Woodroffe, C.D., Smithers, S.G., 2013. Post-glacial sea-level changes around the Australian margin: a review. In: Quaternary Science Reviews, Linking Southern Hemisphere Records and Past Circulation Patterns: The AUS-INTIMATE Project, 74, pp. 115–138. https://doi.org/10.1016/j.quascirev.2012.09.006.
Li, T., Nan, Q., Jiang, B., Sun, R., Zhang, D., Li, Q., 2009. Formation and evolution of the modern warm current system in the East China Sea and the Yellow Sea since the last deglaciation. Chin. J. Oceanol. Limnol. 27, 237–249. https://doi.org/10.1007/s00343-009-9149-4.
Li, G., Li, P., Liu, Y., Qiao, L., Ma, Y., Xu, J., Yang, Z., 2014a. Sedimentary system response to the global sea level change in the East China Seas since the last glacial maximum. Earth Sci. Rev. 139, 390–405. https://doi.org/10.1016/j.earscirev.2014.09.007.
Li, J., Hu, B., Wei, H., Zhao, J., Zou, L., Bai, F., Dou, Y., Wang, L., Fang, X., 2014b. Provenance variations in the Holocene deposits from the southern Yellow Sea: clay mineralogy evidence. In: Continental Shelf Research, Sediment Dynamics and Related Biogeochemical Effects in the Eastern China Shelf Seas, 90, pp. 41–51. https://doi.org/10.1016/j.csr.2014.05.001.
Li, E., Mu, X., Zhao, G., Gao, P., Sun, W., 2017. Effects of check dams on runoff and sediment load in a semi-arid river basin of the Yellow River. Stoch. Env. Res. Risk A. 31, 1791–1803. https://doi.org/10.1007/s00477-016-1333-4.
Li, D., Xu, Y., Li, Y., Wang, J., Yin, X., Ye, X., Wang, A., Wang, L., 2018a. Sedimentary records of human activity and natural environmental evolution in sensitive ecosystems: a case study of a coral nature reserve in Dongshan Bay and a mangrove forest nature reserve in Zhangjiang River estuary, Southeast China. Org. Geochem. 121, 22–35. https://doi.org/10.1016/j.orggeochem.2018.02.011.
Li, X., Zhang, C., Wang, Y., Liu, L., 2018b. Geochronostratigraphy and relationship of the Late Mesozoic Terrestrial lithostratigraphic units in South China. Acta Geol. Sin. 92, 1107–1130 (in Chinese).
Li, Q., Zhang, Q., Li, G., Liu, Q., Chen, M.-T., Xu, J., Li, J., 2019. A new perspective for the sediment provenance evolution of the middle Okinawa Trough since the last deglaciation based on integrated methods. Earth Planet. Sci. Lett. 528, 115839. https://doi.org/10.1016/j.epsl.2019.115839.
Li, Y., Clift, P.D., Murray, R.W., Exnicios, E., Ireland, T., Böning, P., 2020. Asian summer monsoon influence on chemical weathering and sediment provenance determined by clay mineral analysis from the Indus Submarine Canyon. Quat. Res. 93, 23–39. https://doi.org/10.1017/qua.2019.44.
Li, T., Cai, G., Wang, C., Liang, K., Ma, S., Luo, W., 2021. Quantifying clay mineral sources in marine sediments by using end-member mixing analysis. Geo-Mar. Lett. 41, 6. https://doi.org/10.1007/s00367-020-00674-4.
Li, Y., Huang, X., Lian, E., Li, C., Xu, J., Yin, P., Song, Z., Yang, S., 2023. Geochemical and provenance heterogeneity of small mountainous river systems in Southeast China. Glob. Planet. Chang. 230, 104271. https://doi.org/10.1016/j.gloplacha.2023.104271.
Li, J., Yang, S., Liu, J., Mei, X., Guo, X., Zhang, X., Liu, J., Gu, F., Zheng, Z., 2024. Pollen evidence of enhanced Yellow River provenance into the South Yellow Sea after the Middle Pleistocene Transition. Quat. Sci. Rev. 344, 108961. https://doi.org/10.1016/j.quascirev.2024.108961.
Li, Y., Gu, Y., Liu, H., Fu, Z., Tang, X., Feng, H., Xu, X., Guan, S., 2024b. Holocene transgression and Neolithic human adaptations in the Zhejiang coastal Plain, East China. CATENA 245, 108340. https://doi.org/10.1016/j.catena.2024.108340.
Li, Y., Shan, X., Huang, X., Wang, Z., Gao, J., Yin, P., Zhao, Q., Xu, J., Song, Z., Yang, S., 2025. Tracing the Changjiang-derived sediments along the southeast coast of China during the Holocene. Glob. Planet. Chang. 248, 104770. https://doi.org/10.1016/j.gloplacha.2025.104770.
Liang, X., Yang, S., Yin, P., Zhao, Y., 2015. Distribution of clay mineral assemblages in the rivers entering Yellow Sea and East China Sea and the muddy shelve deposits and control factors. Mar. Geol. Quat. Geol. 35, 1–15 (in Chinese). 10.16562/j.cnki.0256-1492.2015.06.001.
Lin, Y., Kopp, R.E., Xiong, H., Hibbert, F.D., Zheng, Z., Yu, F., Kumar, P., Dangendorf, S., Yi, H., Zhang, Y., 2025. Modern sea-level rise breaks 4,000-year stability in southeastern China. Nature 1–9. https://doi.org/10.1038/s41586-025-09600-z.
Liu, J., Li, A., Xu, K., Velozzi, D.M., Yang, Z., Milliman, J.D., DeMaster, D.J., 2006. Sedimentary features of the Yangtze River-derived along-shelf clinoform deposit in the East China Sea. Cont. Shelf Res. 26, 2141–2156. https://doi.org/10.1016/j.csr.2006.07.013. Special Issue in Honor of Richard W. Sternberg's Contributions to Marine Sedimentology.
Liu, Z., Berné, S., Saito, Y., Yu, H., Trentesaux, A., Uehara, K., Yin, P., Paul Liu, J., Li, C., Hu, G., Wang, X., 2007. Internal architecture and mobility of tidal sand ridges in the East China Sea. Cont. Shelf Res. 27, 1820–1834. https://doi.org/10.1016/j.csr.2007.03.002.
Liu, J.P., Liu, C.S., Xu, K.H., Milliman, J.D., Chiu, J.K., Kao, S.J., Lin, S.W., 2008a. Flux and fate of small mountainous rivers derived sediments into the Taiwan Strait. Mar. Geol. 256, 65–76. https://doi.org/10.1016/j.margeo.2008.09.007.
Liu, Z., Tuo, S., Colin, C., Liu, J.T., Huang, C.-Y., Selvaraj, K., Chen, C.-T.A., Zhao, Y., Siringan, F.P., Boulay, S., Chen, Z., 2008b. Detrital fine-grained sediment contribution from Taiwan to the northern South China Sea and its relation to regional ocean circulation. Mar. Geol. 255, 149–155. https://doi.org/10.1016/j.margeo.2008.08.003.
Liu, Z., Zhao, Y., Colin, C., Siringan, F.P., Wu, Q., 2009. Chemical weathering in Luzon, Philippines from clay mineralogy and major-element geochemistry of river sediments. Appl. Geochem. 24, 2195–2205. https://doi.org/10.1016/j.apgeochem.2009.09.025.
Liu, J., Saito, Y., Kong, X., Wang, H., Wen, C., Yang, Z., Nakashima, R., 2010a. Delta development and channel incision during marine isotope stages 3 and 2 in the western South Yellow Sea. Mar. Geol. 278, 54–76. https://doi.org/10.1016/j.margeo.2010.09.003.
Liu, S., Shi, X., Liu, Y., Qiao, S., Yang, G., Fang, X., Wu, Y., Li, C., Li, X., Zhu, A., Gao, J., 2010b. Records of the East Asian winter monsoon from the mud area on the inner shelf of the East China Sea since the mid-Holocene. Chin. Sci. Bull. 55, 2306–2314. https://doi.org/10.1007/s11434-010-3215-3.
Liu, Z., Colin, C., Li, X., Zhao, Y., Tuo, S., Chen, Z., Siringan, F.P., Liu, J.T., Huang, C.-Y., You, C.-F., Huang, K.-F., 2010c. Clay mineral distribution in surface sediments of the northeastern South China Sea and surrounding fluvial drainage basins: Source and transport. Marine Geology 277, 48–60. https://doi.org/10.1016/j.margeo.2010.08.010.
Liu, F., Chen, S., Peng, J., Chen, G., 2012a. Temporal variations of water discharge and sediment load of Huanghe River, China. Chin. Geogr. Sci. 22, 507–521. https://doi.org/10.1007/s11769-012-0560-y.
Liu, J., Yan, W., Chen, Z., Lu, J., 2012b. Sediment sources and their contribution along northern coast of the South China Sea: evidence from clay minerals of surface sediments. Cont. Shelf Res. 47, 156–164. https://doi.org/10.1016/j.csr.2012.07.013.
Liu, L., Li, X., Wang, Y., Zhou, Y., Cao, K., 2012c. The Early-Mid Cretaceous changes of clay mineral composition from Zhejiang and Fujian Provinces, SE China: indications to paleoclimate changes. Acta Sedimentol. Sin. 30, 120–127 (in Chinese).
Liu, S., Shi, X., Fang, X., Dou, Y., Liu, Y., Wang, X., 2014. Spatial and temporal distributions of clay minerals in mud deposits on the inner shelf of the East China Sea: implications for paleoenvironmental changes in the Holocene. Quat. Internat. Quatern. East Asia West. Pacific: Part 2 349, 270–279. https://doi.org/10.1016/j.quaint.2014.07.016.
Liu, J., Xiang, R., Kao, S.-J., Fu, S., Zhou, L., 2016a. Sedimentary responses to sea-level rise and Kuroshio Current intrusion since the Last Glacial Maximum: grain size and clay mineral evidence from the northern South China Sea slope. Palaeogeogr. Palaeoclimatol. Palaeoecol. 450, 111–121. https://doi.org/10.1016/j.palaeo.2016.03.002.
Liu, Z., Zhao, Y., Colin, C., Stattegger, K., Wiesner, M.G., Huh, C.-A., Zhang, Y., Li, X., Sompongchaiyakul, P., You, C.-F., Huang, C.-Y., Liu, J.T., Siringan, F.P., Le, K.P., Sathiamurthy, E., Hantoro, W.S., Liu, J., Tuo, S., Zhao, S., Zhou, S., He, Z., Wang, Y., Bunsomboonsakul, S., Li, Y., 2016b. Source-to-sink transport processes of fluvial sediments in the South China Sea. In: Earth-Science Reviews, Source-to-Sink Systems: Sediment & Solute Transfer on the Earth Surface, 153, pp. 238–273. https://doi.org/10.1016/j.earscirev.2015.08.005.
Liu, J., Steinke, S., Vogt, C., Mohtadi, M., De Pol-Holz, R., Hebbeln, D., 2017. Temporal and spatial patterns of sediment deposition in the northern South China Sea over the last 50,000 years. Palaeogeogr. Palaeoclimatol. Palaeoecol. 465, 212–224. https://doi.org/10.1016/j.palaeo.2016.10.033.
Liu, X., Li, A., Dong, J., Lu, J., Huang, J., Wan, S., 2018a. Provenance discrimination of sediments in the Zhejiang-Fujian mud belt, East China Sea: implications for the development of the mud depocenter. J. Asian Earth Sci. 151, 1–15. https://doi.org/10.1016/j.jseaes.2017.10.017.
Liu, J., Zhang, X., Mei, X., Zhao, Q., Guo, X., Zhao, W., Liu, J., Saito, Y., Wu, Z., Li, J., Zhu, X., Chu, H., 2018b. The sedimentary succession of the last ~ 3.50 Myr in the western South Yellow Sea: paleoenvironmental and tectonic implications. Mar. Geol. 399, 47–65. https://doi.org/10.1016/j.margeo.2017.11.005.
Liu, J., Cao, K., Yin, P., Gao, F., Chen, X., Zhang, Y., Yu, Y., 2018c. The sources and transport patterns of modern sediments in Hangzhou Bay: evidence from clay minerals. J. Ocean Univ. China 17, 1352–1360. https://doi.org/10.1007/s11802-018-3710-8.
Liu, Y., Li, X., Xu, L., Chen, M., Liu, F., Chen, X., 2019. Identification and genesis of the Late Jurassic volcanic rocks in Longquan area, southern Zhejiang Province. Geol. China 46, 1530–1546 (in Chinese).
Liu, J., Cao, L., Yan, W., Shi, X., 2019a. New archive of another significant potential sediment source in the South China Sea. Mar. Geol. 410, 16–21. https://doi.org/10.1016/j.margeo.2019.01.003.
Liu, J., He, W., Cao, L., Zhu, Z., Xiang, R., Li, T., Shi, X., Liu, S., 2019b. Staged fine-grained sediment supply from the Himalayas to the Bengal Fan in response to climate change over the past 50,000 years. Quat. Sci. Rev. 212, 164–177. https://doi.org/10.1016/j.quascirev.2019.04.008.
Liu, X., Liu, J., Chen, S., Chen, J., Zhang, X., Yan, J., Chen, F., 2020. New insights on Chinese cave δ18O records and their paleoclimatic significance. Earth Sci. Rev. 207, 103216. https://doi.org/10.1016/j.earscirev.2020.103216.
Liu, X., Zhang, M., Li, A., Fan, D., Dong, J., Jiao, C., Chang, X., Gu, Y., Zhang, K., Wang, H., 2021a. Depositional control on carbon and sulfur preservation onshore and offshore the Oujiang Estuary: implications for the C/S ratio as a salinity indicator. Cont. Shelf Res. 227, 104510. https://doi.org/10.1016/j.csr.2021.104510.
Liu, Z., Gan, J., Wu, H., Hu, J., Cai, Z., Deng, Y., 2021b. Advances on Coastal and Estuarine circulations around the Changjiang Estuary in the recent decades (2000–2020). Front. Mar. Sci. 8. https://doi.org/10.3389/fmars.2021.615929.
Liu, J., Qiu, J., Saito, Y., Zhang, X., Wang, H., Wang, F., Chen, L., Xu, G., Chen, B., Li, M., An, Y., 2023a. Late Pleistocene to Holocene facies architecture and sedimentary evolution of the Zhejiang coast, East China Sea. Mar. Geol. 459, 107027. https://doi.org/10.1016/j.margeo.2023.107027.
Liu, X., Fan, D., Xu, F., Liu, J.P., 2023b. Editorial: sedimentation on the continental margins: from modern processes to deep-time records. Front. Earth Sci. 10. https://doi.org/10.3389/feart.2022.1048801.
Liu, X., Xu, T., Liu, Y., Liu, S., Fang, X., Xiong, Z., Shi, X., 2024. Sedimentary evolution of the Holocene mud belt in the East China Sea: evidence from spatial and temporal variations in accumulation rates and clay mineral composition. Geo-Mar. Lett. 44, 24. https://doi.org/10.1007/s00367-024-00788-z.

Lu, J., Li, A., Zhang, J., Dong, J., 2023. Sedimentary record off the Yangtze River estuary and its response to typhoons and human activities over the past 70 years. Reg. Stud. Mar. Sci. 65, 103074. https://doi.org/10.1016/j.rsma.2023.103074.

Lu, H., Wu, H., Meadows, M., 2024. Asian monsoon variations over the past 21 ka: an introduction. Glob. Planet. Chang. 237, 104452. https://doi.org/10.1016/j.gloplacha.2024.104452.

Ma, C., Chen, J., Zhou, Y., Wang, Z., 2010. Clay minerals in the major Chinese coastal estuaries and their provenance implications. Front. Earth Sci. China 4, 449–456. https://doi.org/10.1007/s11707-010-0130-5.

Ma, X., Han, Z., Zhang, Y., Bi, S., Hu, G., Liu, J., Xu, C., 2018. Heavy minerals in shelf sediments off Fujian-Zhejiang Coast of the East China Sea: their provenance and geological application. J. Ocean Univ. China 17, 1369–1381. https://doi.org/10.1007/s11802-018-3754-9.

Mei, H., Jian, X., Zhang, W., Fu, H., Zhang, S., 2021. Behavioral differences between weathering and pedogenesis in a subtropical humid granitic terrain: implications for chemical weathering intensity evaluation. CATENA 203, 105368. https://doi.org/10.1016/j.catena.2021.105368.

Mi, B., Liu, S., Shi, X., Li, X., Pan, H.-J., Chen, M.-T., Wang, X., 2017. A high resolution record of rare earth element compositional changes from the mud deposit on the inner shelf of the East China Sea: implications for paleoenvironmental changes. Quatern. Intern. AMS C14 Appl. 447, 35–45. https://doi.org/10.1016/j.quaint.2016.09.056.

Milliman, J., Farnsworth, K., 2011. River Discharge to the Coastal Ocean – A Global Synthesis. https://doi.org/10.1017/CBO9780511781247.

Murray, J., Jagoutz, O., 2024. Palaeozoic cooling modulated by ophiolite weathering through organic carbon preservation. Nat. Geosci. 17, 88–93. https://doi.org/10.1038/s41561-023-01342-9.

Nayak, K., Garzanti, E., Lin, A.T.-S., Castelltort, S., 2022. Taiwan river muds from source to sink: provenance control, inherited weathering, and offshore dispersal pathways. Sediment. Geol. 438, 106199. https://doi.org/10.1016/j.sedgeo.2022.106199.

Nesbitt, H.W., Young, G.M., 1989. Formation and diagenesis of weathering profiles. J. Geol. 97, 129–147. https://doi.org/10.1086/629290.

Ogg, J.G., 2020. Chapter 5 - geomagnetic polarity time scale. In: Gradstein, F.M., Ogg, James G., Schmitz, M.D., Ogg, G.M. (Eds.), Geologic Time Scale, 2020. Elsevier, pp. 159–192. https://doi.org/10.1016/B978-0-12-824360-2.00005-X.

Ouyang, W., Hao, F., Skidmore, A.K., Toxopeus, A.G., 2010. Soil erosion and sediment yield and their relationships with vegetation cover in upper stream of the Yellow River. Sci. Total Environ. 409, 396–403. https://doi.org/10.1016/j.scitotenv.2010.10.020.

Pang, H., Pan, B., Garzanti, E., Gao, H., Zhao, X., Chen, D., 2018. Mineralogy and geochemistry of modern Yellow River sediments: implications for weathering and provenance. Chem. Geol. 488, 76–86. https://doi.org/10.1016/j.chemgeo.2018.04.010.

Perelomov, L.V., 2023. The role of interactions between bacteria and clay minerals in pedochemical processes. Geochem. Int. 61, 1026–1035. https://doi.org/10.1134/S0016702923100105.

Pittman, J., Armitage, D., 2016. Governance across the land-sea interface: a systematic review. Environ. Sci. Pol. 64, 9–17. https://doi.org/10.1016/j.envsci.2016.05.022.

Prajith, A., Tyagi, A., Kurian, P.J., 2022. Influences of summer monsoon variations on the terrigenous influx, bioproductivity and early diagenetic changes in the southwest Bay of Bengal during Late Quaternary. Mar. Geol. 449, 106825. https://doi.org/10.1016/j.margeo.2022.106825.

Qi, S., Jian, X., 2026. Evaluation of rock resources for carbon dioxide removal by enhanced weathering: a South China case. Appl. Geochem. 203, 106812. https://doi.org/10.1016/j.apgeochem.2026.106812.

Qiao, S., Shi, X., Wang, G., Zhou, L., Hu, B., Hu, L., Yang, G., Liu, Y., Yao, Z., Liu, S., 2017. Sediment accumulation and budget in the Bohai Sea, Yellow Sea and East China Sea. Mar. Geol. 390, 270–281. https://doi.org/10.1016/j.margeo.2017.06.004.

Qiu, J., Jiang, S., Wang, J., Feng, J., Chen, J., Dong, C., Jiang, Y., Zhang, D., 2024. Mechanism and genesis of Sanmen Bay as a sink of Holocene Yangtze River sediment, Zhejiang Province, China. Front. Earth Sci. 11. https://doi.org/10.3389/feart.2023.1329921.

Rădoane, M., Chiriloaei, F., Sava, T., Nechita, C., Rădoane, N., Gâza, O., 2019. Holocene fluvial history of Romanian Carpathian rivers. Quat. Int. 527, 113–129. https://doi.org/10.1016/j.quaint.2018.11.014.

Rao, W., Mao, C., Wang, Y., Huang, H., Ji, J., 2017. Using Nd-Sr isotopes and rare earth elements to study sediment provenance of the modern radial sand ridges in the southwestern Yellow Sea. Appl. Geochem. 81, 23–35. https://doi.org/10.1016/j.apgeochem.2017.03.011.

Reed, W., William, Robert, 2010. The Texas Mud Blanket: Understanding Fine-grained Sediment Flux in the NW Gulf of Mexico during the Previous Transgression (Master's thesis). Rice University.

Rho, K.-C., 2015. Distribution of clay minerals in surface sediments of Kunsan Basin, Yellow Sea and their Transport Pathway. SeaJOURNAL KOREAN Soc. Oceanogr. 20, 169–179. https://doi.org/10.7850/jkso.2015.20.4.169.

Rohling, E.J., Foster, G.L., Grant, K.M., Marino, G., Roberts, A.P., Tamisiea, M.E., Williams, F., 2014. Sea-level and deep-sea-temperature variability over the past 5.3 million years. Nature 508, 477–482. https://doi.org/10.1038/nature13230.

Roy, D.B., Tandon, S.K., Singh, V., 2021. Drainage evolution in a Holocene landscape that hosted a 'lost river' system in the Punjab-Haryana plains, NW India. In: Quat. Int., Dynamic Terranes: Surface Deformation, Seismicity, and Climate Change, 585, pp. 99–110. https://doi.org/10.1016/j.quaint.2021.01.029.

Sagawa, T., Kuwae, M., Tsuruoka, K., Nakamura, Y., Ikehara, M., Murayama, M., 2014. Solar forcing of centennial-scale East Asian winter monsoon variability in the mid- to late Holocene. Earth Planet. Sci. Lett. 395, 124–135. https://doi.org/10.1016/j.epsl.2014.03.043.

Schieber, J., Yawar, Z., 2025. Controls on flocculation and accumulation of mud from moving suspensions: experimental insights into the roles of mineralogy, salinity, suspended sediment concentration, flow velocity and microbes. Sedimentology. https://doi.org/10.1111/sed.70053.

Schieber, J., Li, Z., Yawar, Z., Cao, X., Ashley, T., Wilson, R., 2023. Kaolinite deposition from moving suspensions: the roles of flocculation, salinity, suspended sediment concentration and flow velocity/bed shear. Sedimentology 70, 121–144. https://doi.org/10.1111/sed.13034.

Seibert, S.L., Degenhardt, J., Ahrens, J., Reckhardt, A., Schwalfenberg, K., Waska, H., 2020. Investigating the land-sea transition zone. In: YOUMARES 9-The Oceans: Our Research, Our Future: Proceedings of the 2018 Conference for YOUng MArine RESearcher in Oldenburg, Germany. Springer International Publishing, pp. 225–242.

Shan, X., Dalrymple, R.W., Shi, X., Jin, L., Liu, S., Liu, C., Liu, S., Qiao, S., Zhou, Q., Fang, X., 2023. Changjiang coastal mud-belt deposits in Taiwan Strait: controls on its distribution and facies. Sedimentology 70, 1131–1163. https://doi.org/10.1111/sed.13076.

Shang, S., Fan, D., Yin, P., Burr, G., Zhang, M., Wang, Q., 2018. Late Quaternary environmental change in Oujiang delta along the northeastern Zhe-Min Uplift zone (Southeast China). Palaeogeogr. Palaeoclimatol. Palaeoecol. 492, 64–80. https://doi.org/10.1016/j.palaeo.2017.12.012.

Shi, X., Qiao, S., Yang, S., Li, J., Wan, S., Zou, J., Xiong, Z., Hu, L., Yao, Z., Dong, L., Wang, K., Liu, S., Liu, Y., 2021. Progress in sedimentology research of the Asian Continental Margin (2011-2020). Bull. Mineral. Petrol. Geochem. 40, 319–336 (in Chinese). 10.19658/j.issn.1007-2802.2021.40.023.

Shi, X., Dou, Y., Zhang, C., Yang, S., Zhang, Y., Cong, J., Qiao, S., Zou, J., Wu, Y., 2024. Sea level and East Asian winter monsoon-controlled periodic transition of sinks in fine-grained sediments in the East China sea over the past 200 kyr. Quat. Sci. Rev. 340, 108858. https://doi.org/10.1016/j.quascirev.2024.108858.

Siddall, M., Rohling, E.J., Thompson, W.G., Waelbroeck, C., 2008. Marine isotope stage 3 sea level fluctuations: data synthesis and new outlook. Rev. Geophys. 46. https://doi.org/10.1029/2007RG000226.

Sionneau, T., Bout-Roumazeilles, V., Biscaye, P.E., Van Vliet-Lanoe, B., Bory, A., 2008. Clay mineral distributions in and around the Mississippi River watershed and Northern Gulf of Mexico: sources and transport patterns. Quat. Sci. Rev. 27, 1740–1751. https://doi.org/10.1016/j.quascirev.2008.07.001.

Song, H., Liu, J., Yin, P., Zhang, Y., Chen, X., 2018. Characteristics of heavy minerals and quantitative provenance identification of sediments from the Muddy Area outside the Oujiang Estuary Since 5.8 kyr. J. Ocean Univ. China 17, 1325–1335. https://doi.org/10.1007/s11802-018-3684-6.

Steinke, S., Hanebuth, T.J.J., Vogt, C., Stattegger, K., 2008. Sea level induced variations in clay mineral composition in the southwestern South China Sea over the past 17,000 yr. Mar. Geol. 250, 199–210. https://doi.org/10.1016/j.margeo.2008.01.005.

Steudel, A., Batenburg, L.F., Fischer, H.R., Weidler, P.G., Emmerich, K., 2009. Alteration of swelling clay minerals by acid activation. Appl. Clay Sci. 44, 105–115. https://doi.org/10.1016/j.clay.2009.02.002.

Su, N., Yang, S., Guo, Y., Yue, W., Wang, X., Yin, P., Huang, X., 2017. Revisit of rare earth element fractionation during chemical weathering and river sediment transport. Geochem. Geophys. Geosyst. 18, 935–955. https://doi.org/10.1002/2016GC006659.

Su, N., Yang, S., Xie, X., 2018. Typhoon-enhanced silicon and nitrogen exports in a mountainous catchment. J. Geophys. Res. Biogeosci. 123, 2270–2286. https://doi.org/10.1029/2018JG004389.

Sun, B., Liu, S., Seddique, A.A., Wu, K., Qi, W., Zhang, H., Cao, P., Liu, J., Shi, X., 2024a. Clay mineral composition and transport pattern of surface sediments in the Ganges Submarine Delta. Cont. Shelf Res. 282, 105333. https://doi.org/10.1016/j.csr.2024.105333.

Sun, Y., Zhang, Y., Lv, D., Ruan, W., Zhuang, Z., Zhang, L., 2024b. Spatial and temporal variations of sediment flux entering into the South China Sea from 2001 to 2020. Haiyang Xuebao 46, 98–113 (in Chinese). 10.12284/hyxb2024061.

Suo, Y.H., Li, S.Z., Zhao, S.J., Somerville, I.D., Yu, S., Dai, L.M., Xu, L.Q., Cao, X.Z., Wang, P.C., 2015. Continental margin basins in East Asia: tectonic implications of the Meso-Cenozoic East China Sea pull-apart basins. Geol. J. 50, 139–156. https://doi.org/10.1002/gj.2535.

Tan, P., Oberhardt, N., Dypvik, H., Riber, L., Ferrell, R.E., 2017. Weathering profiles and clay mineralogical developments, Bornholm, Denmark. Mar. Pet. Geol. 80, 32–48. https://doi.org/10.1016/j.marpetgeo.2016.11.017.

Tazaki, K., 2013. Clays, micro-organisms and biomineralization. In: Developments in Clay Science. Elsevier, pp. 613–653. https://doi.org/10.1016/B978-0-08-098258-8.00019-5.

Tian, S., Li, Z., Wang, Z., Jiang, E., Wang, W., Sun, M., 2021. Mineral composition and particle size distribution of river sediment and loess in the middle and lower Yellow River. Int. J. Sediment Re. 36, 392–400. https://doi.org/10.1016/j.ijsrc.2020.07.008.

Tu, J., Fan, D., Shang, S., Chen, L., Zhang, Y., 2014. Evolution and sedimentary sequence of tidal channel-flat system at bore-affected reach of the Qiantang Estuary. Earth Sci. J. China Univ. Geosci. 39, 261–270 (in Chinese).

Uehara, K., Saito, Y., 2003. Late Quaternary evolution of the Yellow/East China Sea tidal regime and its impacts on sediments dispersal and seafloor morphology. Sediment. Geol. Clim. Impact Sediment. Syst. 162, 25–38. https://doi.org/10.1016/S0037-0738(03)00234-3.

Um, I.K., Choi, M.S., Lee, G.S., Chang, T.S., 2015. Origin and depositional environment of fine-grained sediments since the last glacial maximum in the southeastern Yellow

Sea: evidence from rare earth elements. Geo-Mar. Lett. 35, 421–431. https://doi.org/10.1007/s00367-015-0416-4.
Wang, P., 2004. Cenozoic deformation and the history of sea-land interactions in Asia. In: Continent-Ocean Interactions within East Asian Marginal Seas. American Geophysical Union (AGU), pp. 1–22. https://doi.org/10.1029/149GM01.
Wang, Z., Chen, Z., Tao, J., 2006. Clay mineral analysis of sediments in the Changjiang Delta Plain and its application to the late quaternary variations of sea level and sediment provenance. J. Coast. Res. 223, 683–691. https://doi.org/10.2112/03-0120.1.
Wang, H., Yang, Z., Wang, Y., Saito, Y., Liu, J.P., 2008. Reconstruction of sediment flux from the Changjiang (Yangtze River) to the sea since the 1860s. J. Hydrol. 349, 318–332. https://doi.org/10.1016/j.jhydrol.2007.11.005.
Wang, S., Rao, W., Qian, J., He, M., Mao, C., Li, K., Feng, Y., Zhao, J., 2021. Clay mineralogy of surface sediments in the three gorges reservoir: implications for sediment provenances and weathering regimes. Clays Clay Miner. 69, 52–67. https://doi.org/10.1007/s42860-020-00106-5.
Wang, H., Saito, Y., Zhang, Y., Bi, N., Sun, X., Yang, Z., 2011. Recent changes of sediment flux to the western Pacific Ocean from major rivers in East and Southeast Asia. Earth Sci. Rev. 108, 80–100. https://doi.org/10.1016/j.earscirev.2011.06.003.
Wang, H., Zhou, Z., Wang, L., Yuan, L., An, J., Huang, B., 2015a. Calibration of illite crystallinity Kübler index and determination of Anchizone. Acta Geol. Sin. 89, 406–411.
Wang, B., Lei, H., Huang, F., Kong, Y., Pan, F., Cheng, W., Chen, Y., Guo, L., 2020. Effect of sea-level change on deep-sea sedimentary records in the Northeastern South China Sea over the past 42 kyr. Geofluids 2020, 8814545. https://doi.org/10.1155/2020/8814545.
Wang, J., Li, A., Xu, K., Zheng, X., Huang, J., 2015b. Clay mineral and grain size studies of sediment provenances and paleoenvironment evolution in the middle Okinawa Trough since 17 ka. Mar. Geol. 366, 49–61. https://doi.org/10.1016/j.margeo.2015.04.007.
Wang, Y.J., Cheng, H., Edwards, R.L., An, Z.S., Wu, J.Y., Shen, C.-C., Dorale, J.A., 2001. A high-resolution absolute-dated late pleistocene monsoon record from Hulu Cave, China. Science 294, 2345–2348. https://doi.org/10.1126/science.1064618.
Wang, Y., Fan, D., Liu, J.T., Chang, Y., 2016. Clay-mineral compositions of sediments in the Gaoping River-Sea system: implications for weathering, sedimentary routing and carbon cycling. Chem. Geol. 447, 11–26. https://doi.org/10.1016/j.chemgeo.2016.10.024.
Wang, R.-M., You, C.-F., Chung, C.-H., Huang, K.-F., Hsu, Y.-J., 2022a. Uranium isotopes in a subtropical mountainous river of Taiwan: insight into physical and chemical weathering processes. J. Hydrol. 607, 127481. https://doi.org/10.1016/j.jhydrol.2022.127481.
Wang, Z., Yang, S., Tang, H., Zheng, Y., Wang, H., Zhang, Z., Zhang, Y., Mei, X., Wang, Q., Lai, Z., 2022b. Revisit the sedimentary stratigraphic evolution and environmental changes on the outer shelf of the East China Sea Since MIS 5. Front. Mar. Sci. 9. https://doi.org/10.3389/fmars.2022.863245.
Wang, L., Jian, X., Fu, H., Zhang, W., Shang, F., Fu, L., 2023. Decoupled local climate and chemical weathering intensity of fine-grained siliciclastic sediments from a paleo-megalake: an example from the Qaidam basin, northern Tibetan Plateau. Sediment. Geol. 454, 106462. https://doi.org/10.1016/j.sedgeo.2023.106462.
Wang, L., Jian, X., Mei, H., Shen, X., Fu, H., 2024. Clay composition heterogeneity in sediments from mountainous catchments with contrasting bedrock lithology in SE China coast. CATENA 247, 108470. https://doi.org/10.1016/j.catena.2024.108470.
Warr, L.N., 2022. Earth's clay mineral inventory and its climate interaction: a quantitative assessment. Earth Sci. Rev. 234, 104198. https://doi.org/10.1016/j.earscirev.2022.104198.
Warr, L.N., Grathoff, G.H., Haberzettl, T., 2024. The Clay Mineral Alteration Index (CMAI) as an improved indicator of climate change. Appl. Clay Sci. 256, 107419. https://doi.org/10.1016/j.clay.2024.107419.
Wei, G., Liu, Y., Ma, J., Xie, L., Chen, J., Deng, W., Tang, S., 2012. Nd, Sr isotopes and elemental geochemistry of surface sediments from the South China Sea: implications for provenance tracing. Mar. Geol. 319–322, 21–34. https://doi.org/10.1016/j.margeo.2012.05.007.
Wei, X., Liang, Y., Liu, T., Ma, Z., Ma, X., Ji, S., Lin, F., Xu, H., Wang, Z., 2025. Hydrodynamic processes and extreme events recognized from the sedimentary records at ancient Port Shuomen in the Oujiang River mouth, Southeast China. Mar. Geol. 486, 107562. https://doi.org/10.1016/j.margeo.2025.107562.
Weight, R.W.R., Anderson, J.B., Fernandez, R., 2011. Rapid mud accumulation on the Central Texas shelf linked to climate change and sea-level rise. J. Sediment. Res. 81, 743–764. https://doi.org/10.2110/jsr.2011.57.
Weymer, B.A., Everett, M.E., Haroon, A., Jegen-Kulcsar, M., Micallef, A., Berndt, C., Michael, H.A., Evans, R.L., Post, V., 2022. The coastal transition zone is an underexplored frontier in hydrology and geoscience. Commun. Earth Environ. 3, 1–8. https://doi.org/10.1038/s43247-022-00655-8.
Wu, T., 2019. Quaternary Strata and Paleoenvironmental Evolution in Coastal Plain of Wenzhou (master's thesis). Chengdu University of Technology (in Chinese).
Wu, T., Wang, P., Yang, Z., Wang, Y., Cang, F., Fang, L., 2017. Sediment particle size and sedimentary environment analysis of the Early Pleistocene Epoch (1.072∼1.778 Ma BP) in the Oujiang River in Wenzhou. J. Eng. Geol. 25, 38–44 (in Chinese). 10.13544/j.cnki.jeg.2017.s1.083.
Wu, T., Yang, Z., Wang, Y., Wang, P., Peng, P., Zhang, P., Cang, F., 2019. Marine stratigraphy since Late Pleistocene on Wenzhou coastal plain and its depositional environment. Mar. Geol. Quat. Geol. 39, 148–162 (in Chinese). 10.16562/j.cnki.0256-1492.2019010703.
Wu, X., Xu, J., Wang, H., Shi, X., 2023. The transport and deposition processes of shelf sediments along the coast of China. Cont. Shelf Res. 257, 104962. https://doi.org/10.1016/j.csr.2023.104962.
Xiao, S., Li, A., Chen, M., Liu, J., Jiang, F., Li, T., Xie, Q., Xiang, R., Chen, Z., 2005. Recent 8 ka mud records of the East Asian Winter Monsoon from the inner shelf of the East China Sea. Earth Sci. J. China Univ. Geosci. 30, 573–581 (in Chinese).
Xu, X., O'Reilly, S.Y., Griffin, W.L., Wang, X., Pearson, N.J., He, Z., 2007. The crust of Cathaysia: age, assembly and reworking of two terranes. Precambrian Res. 158, 51–78. https://doi.org/10.1016/j.precamres.2007.04.010.
Xu, K., Milliman, J.D., Li, A., Paul Liu, J., Kao, S.-J., Wan, S., 2009. Yangtze- and Taiwan-derived sediments on the inner shelf of East China Sea. Cont. Shelf Res. 29, 2240–2256. https://doi.org/10.1016/j.csr.2009.08.017.
Xu, K., Li, A., Liu, J.P., Milliman, J.D., Yang, Z., Liu, C.-S., Kao, S.-J., Wan, S., Xu, F., 2012. Provenance, structure, and formation of the mud wedge along inner continental shelf of the East China Sea: a synthesis of the Yangtze dispersal system. Mar. Geol. 291–294, 176–191. https://doi.org/10.1016/j.margeo.2011.06.003.
Xu, T., Shi, X., Wang, G., Qiao, S., Yang, G., Liu, S., Wang, X., Zhao, Q., 2013. Sedimentary facies of the subaqueous Changjiang River delta since the late Pleistocene. Chin. J. Oceanol. Limnol. 31, 1107–1119. https://doi.org/10.1007/s00343-013-2281-1.
Xu, G., Liu, J., Liu, S., Wang, Z., Hu, G., Kong, X., 2016. Modern muddy deposit along the Zhejiang coast in the East China Sea: response to large-scale human projects. Cont. Shelf Res. 130, 68–78. https://doi.org/10.1016/j.csr.2016.10.007.
Xu, Z., Lim, D., Li, T., Kim, S., Jung, H., Wan, S., Chang, F., Cai, M., 2019. REEs and Sr-Nd isotope variations in a 20 ky-sediment core from the middle Okinawa Trough, East China Sea: an in-depth provenance analysis of siliciclastic components. Mar. Geol. 415, 105970. https://doi.org/10.1016/j.margeo.2019.105970.
Xu, G., Bi, S., Gugliotta, M., Liu, J., Liu, J.P., 2023a. Dispersal mechanism of fine-grained sediment in the modern mud belt of the East China Sea. Earth Sci. Rev. 240, 104388. https://doi.org/10.1016/j.earscirev.2023.104388.
Xu, C., Wang, H., Mou, X., Wu, X., Wang, Y, Li, X., Zhang, Y., Kong, X., Cong, J., Ning, Z., 2022. Sea level change determined paleochannel development on the continental shelf of the southern East China Sea since MIS 5. Palaeogeogr. Palaeoclimatol. Palaeoecol. 606, 111242. https://doi.org/10.1016/j.palaeo.2022.111242.
Xu, X., Zhang, Y., Dou, Y., Cong, J., Mi, B., Chen, X., Li, X., Xu, C., Ye, Y., 2023b. Clay minerals and elemental composition of sediments on different sedimentary units in the northern East China Sea shelf: provenance tracing and genetic mechanism analysis. Acta Oceanol. Sin. 42, 19–34. https://doi.org/10.1007/s13131-023-2168-8.
Xu, T., Liu, X., Fang, X., Zhu, A., He, L., Wang, H., Chen, J., Xiong, Z., Liu, Y., Shi, X., 2024. Sedimentary evolution of the Holocene subaqueous Changjiang Delta, with an emphasis on contributions of the two major Rivers, the Changjiang and Yellow Rivers. Palaeogeogr. Palaeoclimatol. Palaeoecol. 655, 112501. https://doi.org/10.1016/j.palaeo.2024.112501.
Xue, C., Jia, J., Gao, S., Cai, T., Chao, H., Li, J., Chen, Y., Xia, X., 2018a. The contribution of middle and small rivers to the distal mud of subaqueous Changjiang Delta: results from Jiaojiang River and Oujiang River. Haiyang Xuebao 40, 75–89 (in Chinese).
Xue, C., Qin, Y., Ye, S., Laws, E.A., Wang, Z., 2018b. Evolution of Holocene ebb-tidal clinoform off the Shandong Peninsula on East China Sea shelf. Earth Sci. Rev. 177, 478–496. https://doi.org/10.1016/j.earscirev.2017.12.012.
Yan, L.-L., He, Z.-Y., Jahn, B., Zhao, Z.-D., 2016. Formation of the Yandangshan volcanic–plutonic complex (SE China) by melt extraction and crystal accumulation. Lithos 266–267, 287–308. https://doi.org/10.1016/j.lithos.2016.10.029.
Yang, X., 1995. Clay minerals of suspended sediments in Oujiang River. Mar. Sci. Bull. 14, 86–92 (in Chinese).
Yang, S., Wang, Z., Dou, Y., Shi, X., 2014. A review of sedimentation since the Last Glacial Maximum on the continental shelf of eastern China. In: Chiocci, F.L., Chivas, A.R. (Eds.), Continental Shelves of the World: Their Evolution During the Last Glacio-Eustatic Cycle. Geological Society of London. https://doi.org/10.1144/M41.21.
Yang, S., Wei, G., Shi, X.-F., 2015. Geochemical approaches of tracing source-to-sink sediment processes and environmental changes at the east asian continental margin. Bull. Mineral. Petrol. Geochem. 34, 902–910. https://doi.org/10.3969/j.issn.1007-2802.2015.05.003.
Yang, R.J., Liu, J.T., Fan, D., Burr, G.S., Lin, H.-L., Chen, T.-T., 2017. Land-sea duel in the late Quaternary at the mouth of a small river with high sediment yield. J. Asian Earth Sci. 143, 59–76. https://doi.org/10.1016/j.jseaes.2017.03.028.
Yang, S.-Y., Liang, J.-P., Jiang, S.-Y., Zhang, X., Zhang, R.-X., 2021. Late Jurassic–Early Cretaceous irregular slab rollback of paleo-Pacific plate beneath southeastern China: insights from the petrogenesis of volcanic rocks of Moshishan Group in Dazhou volcanic basin, Gan-Hang Belt. Lithos 392–393, 106137. https://doi.org/10.1016/j.lithos.2021.106137.
Yang, J., Chen, X., Liu, R., Xu, Z., Song, W., Wang, S., Hu, K., Lin, Z., Li, A., Zheng, H., 2022. Acoustic stratigraphy of the Quaternary in the south of the Oujiang River Estuary. Mar. Geol. Front. 38, 11–19 (in Chinese). 10.16028/j.1009-2722.2021.204.
Yao, Z., Shi, X., Qiao, S., Liu, Q., Kandasamy, S., Liu, J., Liu, Y., Liu, J., Fang, X., Gao, J., Dou, Y., 2017. Persistent effects of the Yellow River on the Chinese marginal seas began at least ∼880 ka ago. Sci. Rep. 7, 2827. https://doi.org/10.1038/s41598-017-03140-x.
Ye, W., Liu, S., Fan, D., Zhang, H., Cao, P., Pan, H.-J., Li, J., Li, X., Fang, X., Khokiattiwong, S., Kornkanitnan, N., Shi, X., 2022. Evolution of sediment provenances and transport processes in the central Bay of Bengal since the Last Glacial Maximum. In: Quaternary International, Understanding the Late Quaternary Paleomonsoon and Paleoenvironmental Shifts of Asia, 629, pp. 27–35. https://doi.org/10.1016/j.quaint.2020.12.007.
Yoshimura, T., Araoka, D., Kawahata, H., Hossain, H.M.Z., Ohkouchi, N., 2021. The influence of weathering, water sources, and hydrological cycles on lithium isotopic compositions in river water and groundwater of the Ganges–Brahmaputra–Meghna

River system in Bangladesh. Front. Earth Sci. 9. https://doi.org/10.3389/feart.2021.668757.
Yu, S., Zheng, Z., Chen, F., Jing, X., Kershaw, P., Moss, P., Peng, X., Zhang, X., Chen, C., Zhou, Y., Huang, K., Gan, H., 2017. A last glacial and deglacial pollen record from the northern South China Sea: new insight into coastal-shelf paleoenvironment. Quat. Sci. Rev. 157, 114–128. https://doi.org/10.1016/j.quascirev.2016.12.012.
Youn, J., Yang, S., Park, Y.A., 2007. Clay minerals and geochemistry of the bottom sediments in the northwestern East China Sea. Chin. J. Oceanol. Limnol. 25, 235–246. https://doi.org/10.1007/s00343-007-0235-1.
Yu, Z., Colin, C., Bassinot, F., Wan, S., Bayon, G., 2020. Climate-driven weathering shifts between highlands and floodplains. Geochem. Geophys. Geosyst. 21, e2020GC008936. https://doi.org/10.1029/2020GC008936.
Yuan, G.D., Theng, B.K.G., Churchman, G.J., Gates, W.P., 2013. Clays and clay minerals for pollution control. In: Developments in Clay Science. Elsevier, pp. 587–644. https://doi.org/10.1016/B978-0-08-098259-5.00021-4.
Yuan, J., Ye, F., Wang, Y., Huang, J., Ye, W., 2023. Quaternary stratigraphy and sedimentary environment evolution of the Ruian Plain in Wenzhou, China revealed by cores of hole QTZ4. Bull. Mineral. Petrol. Geochem. 42, 98–106 (in Chinese). 10.19658/j.issn.1007-2802.2022.41.102.
Zhang, Y., 1991. The evolution of holocene sedimentary environment in Wenzhou Bay. J. Northwest Normal Univ. (Nat. Sci.) 71–77 (in Chinese). 10.16783/j.cnki.nwnuz.1991.04.018.
Zhang, Z., Chu, Z., 2018. Modern variations in clay minerals in mud deposits of the Yellow and East China Seas and their geological significance. The Holocene 28, 386–395. https://doi.org/10.1177/0959683617729446.
Zhang, X., Yu, X., Wu, S., Wei, T., Zhang, X., 2006. Effect of forest vegetation on runoff and sediment production in sloping lands of Loess area. Front. Forest. China 1, 336–342. https://doi.org/10.1007/s11461-006-0038-0.
Zhang, J., Liu, J., Kong, X., Xue, C., Liu, X., Sun, L., Yue, B., Wen, C., 2011. Clay mineral assemblage of sediments from middle reach of Huaihe River. Mar. Geol. Quat. Geol. 31, 21–29 (in Chinese). https://doi.org/10.3724/SP.J.1140.2011.01021.
Zhang, L., Song, X., Xia, J., Yuan, R., Zhang, Y., Liu, X., Han, D., 2011b. Major element chemistry of the Huai River basin, China. Appl. Geochem. 26, 293–300. https://doi.org/10.1016/j.apgeochem.2010.12.002.
Zhang, M., Fan, D., Wu, G., Shang, S., Chen, L., 2012. Palynological characters of late quaternary in the South Flank of the Oujiang River delta and their paleoclimate implication. Quat. Sci. 32, 1234–1247 (in Chinese).
Zhang, X., Lin, C.-M., Dalrymple, R.W., Gao, S., Li, Y.-L., 2014. Facies architecture and depositional model of a macrotidal incised-valley succession (Qiantang River estuary, eastern China), and differences from other macrotidal systems. GSA Bull. 126, 499–522. https://doi.org/10.1130/B30835.1.
Zhang, L., Qin, X., Liu, J., Sun, C., Mu, Y., Gao, J., Guo, W., An, S., Lu, C., 2016. Geochemistry of sediments from the Huaibei Plain (east China): implications for provenance, weathering, and invasion of the Yellow River into the Huaihe River. J. Asian Earth Sci. 121, 72–83. https://doi.org/10.1016/j.jseaes.2016.02.008.
Zhang, X., Huang, C., Wang, Y., Clift, P.D., Yan, Y., Fu, X., Chen, D., 2017. Evolving Yangtze River reconstructed by detrital zircon U-Pb dating and petrographic analysis of Miocene marginal Sea sedimentary rocks of the Western Foothills and Hengchun Peninsula, Taiwan. Tectonics 36, 634–651. https://doi.org/10.1002/2016TC004357.
Zhang, L., Liu, J., Qin, X., 2018. The environmental effects and mechanism of the Yellow River flooding into the Huaibei Plain during Quaternary: a brief review. Quatern. Sci. 38, 441–453 (in Chinese). 10.11928/j.issn.1001-7410.2018.02.15.
Zhang, J., Wan, S., Clift, P.D., Huang, J., Yu, Z., Zhang, K., Mei, X., Liu, J., Han, Z., Nan, Q., Zhao, D., Li, A., Chen, L., Zheng, H., Yang, S., Li, T., Zhang, X., 2019. History of Yellow River and Yangtze River delivering sediment to the Yellow Sea since 3.5 Ma: tectonic or climate forcing? Quat. Sci. Rev. 216, 74–88. https://doi.org/10.1016/j.quascirev.2019.06.002.
Zhang, K., Li, A., Zhang, J., Lu, J., Wang, H., 2020. Seasonal variations in the surficial sediment grain size in the East China Sea continental shelf and their implications for terrigenous sediment transport. J. Oceanogr. 76, 1–14. https://doi.org/10.1007/s10872-019-00523-8.
Zhang, F., Li, S., Sun, C., Li, W., Zhao, X., Chen, Z., Nie, T., Chen, Y., Li, X., 2022a. Human impacts overwhelmed hydroclimate control of soil erosion in China 5,000 years ago. Geophys. Res. Lett. 49, e2021GL096983. https://doi.org/10.1029/2021GL096983.
Zhang, S., Jian, X., Liu, J.T., Wang, P., Chang, Y.-P., Zhang, W., 2022b. Climate-driven drainage reorganization of small mountainous rivers in Taiwan (East Asia) since the last glaciation: the Zhuoshui River example. Palaeogeogr. Palaeoclimatol. Palaeoecol. 586, 110759. https://doi.org/10.1016/j.palaeo.2021.110759.
Zhang, S., Liu, S., Shu, Z., Xu, X., Lv, J., Shi, Y., Gao, J., 2022c. Climate-driven provenance variation and sedimentary system evolution at the Changjiang distal mud since the mid-Holocene. Mar. Geol. 452, 106902. https://doi.org/10.1016/j.margeo.2022.106902.
Zhang, J., Liu, P., Liu, Y., Jiang, F., Sun, Q., Miao, B., Chen, J., 2023. Avulsion of the Yellow River into the South Yellow Sea during the early to middle Holocene: evidence from Clay Provenance of the Yangtze Paleovalley. Palaeogeogr. Palaeoclimatol. Palaeoecol. 625, 111694. https://doi.org/10.1016/j.palaeo.2023.111694.
Zhao, D., Wan, S., Toucanne, S., Clift, P.D., Tada, R., Révillon, S., Kubota, Y., Zheng, X., Yu, Z., Huang, J., Jiang, H., Xu, Z., Shi, X., Li, A., 2017. Distinct control mechanism of fine-grained sediments from Yellow River and Kyushu supply in the northern Okinawa Trough since the last glacial. Geochem. Geophys. Geosyst. 18, 2949–2969. https://doi.org/10.1002/2016GC006764.
Zhao, B., Yan, X., Wang, Z., Shi, Y., Chen, Z., Xie, J., Chen, J., He, Z., Zhan, Q., Li, X., 2018a. Sedimentary evolution of the Yangtze River mouth (East China Sea) over the past 19,000 years, with emphasis on the Holocene variations in coastal currents. Palaeogeogr. Palaeoclimatol. Palaeoecol. 490, 431–449. https://doi.org/10.1016/j.palaeo.2017.11.023.
Zhao, D., Wan, S., Clift, P.D., Tada, R., Huang, J., Yin, X., Liao, R., Shen, X., Shi, X., Li, A., 2018b. Provenance, sea-level and monsoon climate controls on silicate weathering of Yellow River sediment in the northern Okinawa Trough during late last glaciation. Palaeogeogr. Palaeoclimatol. Palaeoecol. 490, 227–239. https://doi.org/10.1016/j.palaeo.2017.11.002.
Zhao, Y., Zou, X., Gao, J., Wang, C., Li, Y., Yao, Y., Zhao, W., Xu, M., 2018c. Clay mineralogy and source-to-sink transport processes of Changjiang River sediments in the estuarine and inner shelf areas of the East China Sea. J. Asian Earth Sci. 152, 91–102. https://doi.org/10.1016/j.jseaes.2017.11.038.
Zhejiang Water Resources Department, 2020. General Annals of Zhejiang: Water Conservancy Annals. Zhejiang People's Publishing House, Hangzhou.
Zheng, X., Li, A., Wan, S., Jiang, F., Yin, X., Lu, J., 2015. Formation of the modern current system in the East China Sea since the early Holocene and its relationship with sea level and the monsoon system. Chin. J. Oceanol. Limnol. 33, 1062–1071. https://doi.org/10.1007/s00343-015-4089-7.
Zhou, X., Gao, S., Jia, J., 2003. Preliminary evaluation of the stability of Changjiang clay minerals as fingerprints for material source tracing. Oceanol. Limnol. Sin. 34, 683–692 (in Chinese).
Zhou, X., Sun, T., Shen, W., Shu, L., Niu, Y., 2006. Petrogenesis of Mesozoic granitoids and volcanic rocks in South China: a response to tectonic evolution. Episodes J. Intern. Geosci. 29, 26–33. https://doi.org/10.18814/epiiugs/2006/v29i1/004.
Zhu, X., Huang, X., Liu, M., Yang, S., Zhao, X., Jin, G., 2025. Characteristics of detrital zircon U-Pb age distribution and influencing factors in the rivers of Zhejiang and Fujian Provinces, China. Mar. Geol. Quat. Geol. 45, 1–16 (in Chinese). 10.16562/j.cnki.0256-1492.2025052601.
Zielinski, O., Pieck, D., Schulz, J., Thölen, C., Wollschläger, J., Albinus, M., Badewien, T. H., Braun, A., Engelen, B., Feenders, C., Fock, S., Lehners, C., Lõhmus, K., Lübben, A., Massmann, G., Meyerjürgens, J., Nicolai, H., Pollmann, T., Schwalfenberg, K., Stone, J., Waska, H., Winkler, H., 2022. The Spiekeroog coastal observatory: a scientific infrastructure at the land-sea transition zone (Southern North Sea). Front. Mar. Sci. 8. https://doi.org/10.3389/fmars.2021.754905.